WIND-WAVE CHARACTERISTICS GENERATED BY TROPICAL CYCLONE ACTIVITY IN THE GULF OF THAILAND

WATTANA KANBUA

A THESIS SUBMITTED IN PARTIAL FULFILLMENT
OF THE REQUIREMENTS FOR
THE DEGREE OF DOCTOR OF PHILOSOPHY
(MATHEMATICS)
FACULTY OF GRADUATE STUDIES
MAHIDOL UNIVERSITY
2004

ISBN 974-04-5336-8

Thesis
entitled

WIND-WAVE CHARACTERISTICS GENERATED BY TROPICAL CYCLONE ACTIVITY IN THE GULF OF THAILAND

.....
Mr. Wattana Kanbua
Candidate

.....
Prof. I-Ming Tang,
Ph.D. (Physics)
Major-Advisor

.....
Asst. Prof. Seree Sutharatid,
Ph.D. (Engineering)
Co-Advisor

……
Assoc. Prof. Benchawan Wiwatanapataphee,
Ph.D. (Applied Mathematics)
Co-Advisor

.....
Assoc.Prof. Rassmidara Hoonsawat,
Ph.D.
Dean
Faculty of Graduate Studies

.....
Assoc.Prof. Montip Tiensuwan,
Ph.D. (Applied Statistics)
Chair
Doctor of Philosophy Programme
in Mathematics
Faculty of Science

Thesis
entitled

WIND-WAVE CHARACTERISTICS GENERATED BY TROPICAL CYCLONE ACTIVITY IN THE GULF OF THAILAND

was submitted to the Faculty of Graduate Studies, Mahidol University
for the degree of Doctor of Philosophy (Mathematics)

on

September 24, 2004

.....
Mr. Wattana Kanbua
Candidate

.....
Prof. I-Ming Tang,
Ph.D. (Physics)
Chair

.....
Asst. Prof. Seree Sutharatid,
Ph.D. (Engineering)
Member

.....
Dr. Nawarat Krairapanond,
Ph.D. (Marine Science)
Member

.....
Assoc. Prof. Benchawan Wiwatanapataphee,
Ph.D. (Applied Mathematics)
Member

.....
Assoc.Prof. Rassmidara Hoonsawat,
Ph.D.
Dean
Faculty of Graduate Studies
Mahidol University

.....
Prof. Prasert Sobhon,
Ph.D. (Microbiology),
Dean
Faculty of Science
Mahidol University

ACKNOWLEDGMENTS

I would like to express my sincere gratitude and deep appreciation to Professor I-Ming Tang, my Principal Supervisor for his guidance, invaluable advice, supervision and encouragement throughout this research which enabled me to complete this thesis successfully. He was never lacking in kindness and support. I am also grateful to Assistant Professor Seree Sutharatid, Associate Professor Benchawan Wiwatanapataphee, Associate Professor George Kallos and Dr. Nawarat Krairapanond, my Associate Supervisors for their helpful comments, guidance and advice about this thesis.

I owe unending gratitude to my family and all my teachers who filled in the knowledge and whose support and encouragement helped me to finish my education.

Finally, I am particularly indebted to the Royal Golden Jubilee Ph.D. Program for the financial support (contract numbers PHD/0100/2544) which has enabled me to undertake my study.

Wattana Kanbua

WIND-WAVE CHARACTERISTICS GENERATED BY TROPICAL CYCLONE ACTIVITY IN THE GULF OF THAILAND

WATTANA KANBUA 4436661 SCMA/D

Ph.D. (MATHEMATICS)

THESIS ADVISORS : I-MING TANG, Ph.D., SEREE SUTHARATID, Ph.D., BENCHAWAN WIWATANAPATAPHEE, Ph.D.

ABSTRACT

A typhoon is a tropical cyclone, which may generate strong wind and huge waves. Wind waves are one of the important phenomena in the ocean. They influence the design of maritime structures. Understanding their characteristics leads to an appropriate means to prevent casualty, loss and damages. We are interested in two techniques for studying typhoon waves, one using hard computing techniques, the other using soft computing of techniques. In this research, the hard computing technique employed a numerical wave model, namely WAM (WAve Model). In its computations, the WAM takes into account most factors affecting tropical seas and shallow water areas. The Gulf of Thailand is such an area, the area of our interest in this research. For the soft computing technique we used the artificial neural network (ANN), specifically GRNN (General Regression Neural Network) to forecast waves. The results indicated that the developed model was the best method of prediction of wave height. The adjusted parameter model predicted better than WAM model. However, the prediction by the artificial neural network was best in both wave periods and wave heights.

This study focuses on the turbulent effect of typhoon LINDA in 1997 on the wave field in the Gulf of Thailand. The investigation was based on two well known models, WAM and GRNN models. A comparison of the results using the two models was done. The proposed model and computational technique was verified by using data from the 4 wave stations. The wave hindcast results of WAM model underestimates the wave heights when compared with GRNN. The prediction accuracy of the GRNN is quite high. The magnitude and phase of wave heights and wave periods can be simulated reasonably well. This indicates that for wave prediction, the GRNN should be viewed as a strong alternative in operational forecasting.

KEY WORDS : WAM MODEL/ SIGNIFICANT WAVE HEIGHT/ HINDCAST/ TROPICAL CYCLONE/ TYPHOON LINDA/ ANN/ GRNN

132 P. ISBN 974-04-5336-8

ลักษณะของคลื่นลมซึ่งเกิดมาจากอิทธิพลของพายุหมุนเขตร้อนในอ่าวไทย(WIND-WAVE CHARACTERISTICS GENERATED BY TROPICAL CYCLONE ACTIVITY IN THE GULF OF THAILAND)

วัฒนา กันบัว 4436661 SCMA/D

ปร.ด. (คณิตศาสตร์)

คณะกรรมการควบคุมวิทยานิพนธ์ : ไอมิง ถัง, Ph.D., เสรี ศุภราทิตย์, Ph.D.,
เบญจวรรณ วิวัฒนปฐพี, Ph.D.

บทคัดย่อ

พายุไต้ฝุ่นเป็นพายุหมุนเขตร้อนที่มีกำลังแรงที่สุด ซึ่งจะทำให้เกิดลมแรงมาก และก่อให้เกิดคลื่นขนาดใหญ่ คลื่นลมเป็นปรากฏการณ์ทางธรรมชาติที่สำคัญอย่างหนึ่ง ที่มีอิทธิพลต่อสิ่งปลูกสร้างในทะเลและมหาสมุทร เทคนิคในการจำลองการพยากรณ์คลื่นลม มีสองวิธี คือ 1. วิธีการคำนวณแบบแข็ง (hard computing) และ 2. วิธีการคำนวณแบบอ่อน (soft computing) ในการวิจัยนี้ใช้วิธีการคำนวณแบบแข็ง ซึ่งได้แก่การพยากรณ์คลื่นจากแบบจำลองการพยากรณ์คลื่นลมเชิงตัวเลขที่ชื่อว่าแบบจำลองแวม (WAM) เนื่องจากในแบบจำลองแวมได้รวบรวมผลกระทบต่างๆ ที่เป็นปัจจัยที่เกี่ยวข้องกับการพยากรณ์คลื่นลมในเขตร้อนอย่างอ่าวไทย ซึ่งเป็นบริเวณศึกษา ส่วนการคำนวณแบบอ่อนในการวิจัยนี้ใช้วิธีโครงข่ายประสาทเทียม เพื่อพยากรณ์คลื่นลม พบว่า แบบจำลองที่ถูกพัฒนาขึ้นสามารถพยากรณ์ความสูงคลื่นนัยสำคัญได้ดี อย่างไรก็ตามการพยากรณ์คลื่นลมโดยใช้โครงข่ายประสาทเทียม ให้ผลการพยากรณ์ทั้งคาบคลื่น และความสูงคลื่นอย่างมีนัยสำคัญได้ผลดี

การวิจัยนี้จะเน้นในผลกระทบอันเนื่องมาจากพายุไต้ฝุ่นลินดา ปี พ.ศ. 2540 ที่เกิดขึ้นบริเวณอ่าวไทย โดยใช้แบบจำลองคลื่นคือ แบบจำลองแวม (WAM) และ แบบจำลองโครงข่ายใยประสาทเทียมแบบถดถอย (GRNN) ผลการพยากรณ์ความสูงคลื่นจากทั้งสองแบบจำลอง เมื่อเปรียบเทียบกับสถานีตรวจวัดคลื่นลมในอ่าวไทย 4 แห่ง ปรากฏว่า แบบจำลองโครงข่ายใยประสาทเทียมแบบถดถอย ให้ผลการพยากรณ์คลื่นที่ดีกว่าแบบจำลองแวม ดังนั้น แบบจำลองโครงข่ายใยประสาทเทียมแบบถดถอยน่าจะเป็นแบบจำลองฯ ที่ใช้ในอ่าวไทยต่อไป

132 หน้า ISBN 974-04-5336-8

CONTENTS

CONTENTS (Continued)

LIST OF TABLES

LIST OF FIGURES

LIST OF FIGURES (Continued)

LIST OF ABBREVIATIONS

GISTDA	Geo-Informatics and Space Technology Development Agency (Public Organization)
ETOPO5	Earth Topography - 5 Minute
NOGAPS	Navy Operational Global Atmospheric Prediction System
NRLMRY	The Naval Research Laboratory at Monterey
WAM	Wave Model
HHN	Hua-Hin buoy
CHN	Chang buoy
KSI	Sichang buoy
UNC	Unocal platform marine station
ANN	Artificial Neural Networks
GRNN	General Regression Neural Networks
JONSWAP	Joint North Sea Wave Project
TC	Tropical Cyclones

CHAPTER I

INTRODUCTION

1.1 An Overview of the Tropical Cyclones

Tropical cyclone is the generic term used by the World Meteorological Organisation to define weather systems developing over tropical or subtropical waters. Tropical cyclones also have a definite organised surface circulation. The tropical cyclones are given names for easier identification and tracking. In the Atlantic and Eastern Pacific such spiral strong wind is called HURRICANE. In the Western Pacific, including the Philippines, it is called as TYPHOON, near Australia, it is called as WILLY WILLY and in the Indian Ocean, it is called as CYCLONES.

A tropical cyclone may occur under the following conditions :

- the warm sea temperature in excess of 26 degrees Celsius or 79 degrees Fahrenheit;
- high relative humidity (degree to which air is saturated by vapour);
- atmospheric instability;
- a location of at least 4 - 5 latitude degrees from the Equator.

Developmental phases of tropical cyclone may be classified into the following 4 stages associating to its wind intensity. The first stage is called as the tropical disturbance. The weather system in this stage gives rise to a specific area of cloudiness with embedded showers and thunderstorms. In the second stage, the tropical cyclone system circulates counter-clockwise with maximum speed of less than 38 mph (61 km/h) that such system is called as the tropical depression. If the maximum wind speed is greater than 38 mph (61 km/h), but less than 74 mph (119 km/h), the third stage will be developed and called as the tropical storm. The last stage is called as

typhoon. The wind speed is greater than 74 mph (119 km/h). The weather system in this stage is better organised and its eye is well defined as shown in figure 1.1.

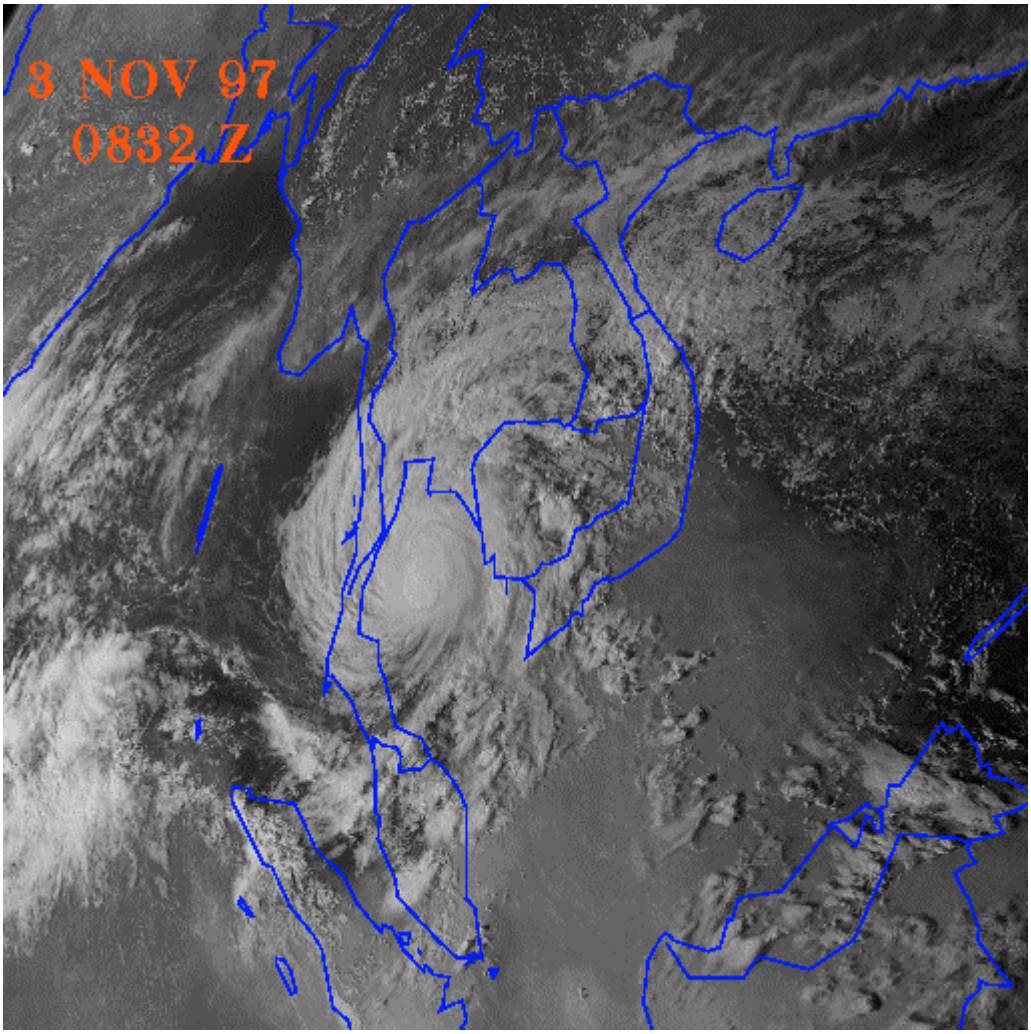

Figure 1.1 Visible meteorological satellite imagery

Characteristic of Tropical cyclone may be characterised by their destructive winds, storm surges and exceptional levels of rainfall. The strong winds generated by Tropical cyclones circulate clockwise in the Southern Hemisphere and counter clockwise in the Northern Hemisphere. It spirals inward and moves towards the cyclone centre. Wind speed progressively increases towards the core. As the eye arrives, wind falls off to become almost calm but rise again just as quickly as the eye passes. It is then replaced by hurricane force obtained from the reverse direction of those previously blowing.

As the cyclone approaches the coast, the friction of strong on-shore winds on the sea surface, plus the "suction effect" of reduced atmospheric pressure, can pile up sea water along a coastline near a cyclone's landfall well above the predicted tide level. In addition, the high humidity condenses into rain and giant cumulus clouds result in high precipitation rates when the cyclone reaches land. The rain rapidly saturates the ground and rapid run off will result in severe flooding.

To understand the interior dynamics of an ocean wave many researchers Komen *at al.* [77] have been proposed the models of wave propagation in the open ocean, where the seafloor is not a factor. In addition, large-scale motions such as the earth’s rotation, Coriolis force, and tides will not be taken into consideration. Their models can describe the wave interaction with the shoreline and the end of the life cycle of wave. Using a perspective of fixed position, a two-dimensional sine wave function undulating across a coordinate axis gives the perspective necessary to describe an idealized ocean wave. The vertical axis is large enough to show the full positive and negative amplitude of the sine wave function. The horizontal axis extends from the origin so that one minimum and one maximum of the wave can be seen. Smith [111] Taking an instance in time along this prescribed coordinate system allows the characteristics of the wave to be individually defined.

The period of a wave (T) is defined as the time it takes any point on the wave’s surface to complete a full cycle, in terms of an ocean wave, the period denotes the time lapse between two maximums. The maximum of an ocean wave is the crest, where the minimum is the trough. The wavelength (L) is the horizontal distance between two consecutive crests. The wave height (H) is the vertical distance between a crest and trough Wave speed is determined by dividing wavelength by the period. Wave speed (C) is dependent on wavelength but not on height Bowden [11]. The steepness is the wave height divided by the wave length (H/L) and is not the same thing as the slope between a wave crest and its adjacent trough.

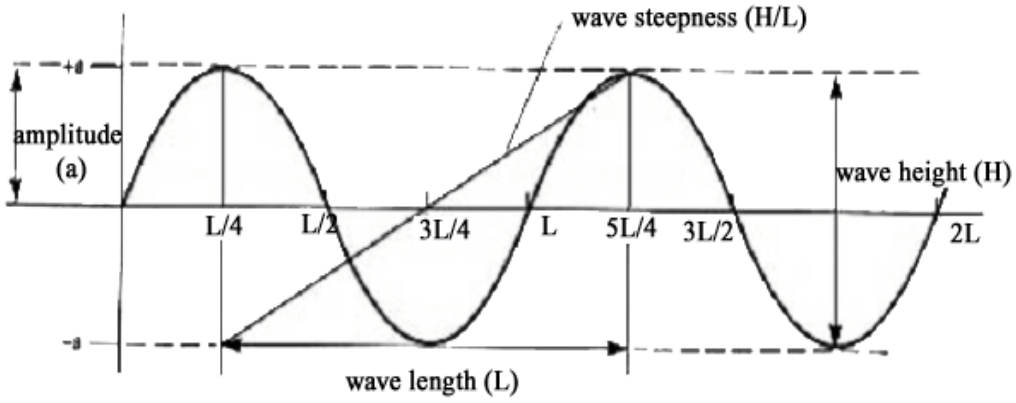

Figure 1.2 Wave parameters

In the open ocean, water does not move forward along at speed of a wave set. Each parcel rotates in an orbit as the wave passes. Only a slight displacement of the water particle in the direction of wave movement results. Upon initial inspection, particle motion appears only at the surface, yet it actually extends down vertically to a depth of half a wavelength. The orbital rotation directly beneath the surface has a diameter equal to its height. Past the depth of the first rotational orbit, the diameter of the preceding orbits decreases exponentially with depth. Any rotation of water particles due to the passing of a wave becomes negligible deeper than half a wavelength. This is defined as the rotational energy of the wave, which is restricted to a relatively shallow layer along the ocean surface.

1.2 Scope of Study

This research focused on the development of a mathematical to describe the wind propagation when the tropical cyclone occurs in the Gulf of Thailand. The hard computing and soft computing techniques are used to explain wind wave characteristics, in particular for the event of Typhoon Linda occurring during August to December in 1997. We compared results obtained from both techniques and also compared them with observing data such as moored buoy data in the Gulf of Thailand under GISTDA (Geo-Informatics and Space Technology Development Agency), and an automatics marine station at platform in the Gulf of Thailand under Unocal Thailand company.

1.3 Outline of the Thesis

This thesis comprises five chapters. In chapter 1, an overview of the tropical cyclone is presented. The scope and objectives are also given in this chapter.

In chapter 2, a brief theoretical background is summarized, Literature review, wave spectral analysis, numerical ocean wave modeling, the neural network model, and the hard and the soft computing approach are given in this chapter.

In chapter 3 concerns the mathematical model for studying the ocean wave of typhoon Linda in year 1997. The construction of mathematical model is presented and numerical algorithm based on finite difference method is developed to solve the problem.

In chapter 4, the parameter study and numerical simulation are presented.

The conclusions gained from this thesis are given in chapter 5, together with some suggestions for further research.

CHAPTER II

THEORETICAL BACKGROUND

2.1 Prior Studies

Over the past 40 years, spectral wave modeling has made significant advances, from the theoretical framework of Phillips [97] and Miles [86]. It was describing how waves develop and grow, through the era of hand calculations and nomograms where the engineer was able to estimate wave heights and periods for the project design. In the last 10 years, there have been numerous publications describing spectral models and their respective generation level, i.e. the first, the second, and more recently, the third generation. The first time user may be very confused and because those models are cumbersome. The aim of this section is to define, summarize, and identify the capabilities of the existing spectral wave modeling.

The evolution of spectral wave modeling began in the early 1940's with forecasting waves for planning and execution of military operations during World War II. Sverdrup and Munk [119] used physical arguments to approximate a generalized version of wind-wave growth. From a statistical basis related to the sea-state, the significant wave method was formed. Further theoretical work, using the energy balance equation and non-dimensional analysis, resulted in defining two wave parameters: the significant wave height H_s and significant period T_s. They determined that H_s and T_s could be directly related to the wind speed, a fetch length or duration. These curves and a parallel study, Bretschnider [12], provided the foundation for early wave forecasting methods. These methods were further refined into a spectral approach by Pierson, Neuman and James [102], where a series of nomograms describing a frequency spectrum could be constructed from various wind

speed, fetch lengths and durations. These techniques, which were strongly founded on empirical results, remained a basis for coastal design for nearly 20 years.

2.1.1 First-Generation Modeling

In the early 1960's, there were numerous groups developing what we would classify as first *generation wave models* (1G). The governing equation used for deep-water application is the energy balance or transport equation.

$$\frac{\partial E}{\partial t} + \vec{C}_g \cdot \vec{\nabla} E = \sum S_i \tag{2.1}$$

where E is the two-dimensional wave spectrum. The value of E depends on the spatial coordinates x and y, the temporal variable t, the frequency domain f, and the direction domain θ. The parameter $\vec{C}_g$ is the group velocity function of variables x, y, f and θ. The parameter S_i defines source/sink terms, such as the atmospheric input S_{in} the nonlinear wave-wave interaction S_{nl}, and the high frequency dissipation S_{ds}. The goal is to solve for the time rate of change in E, or the directional spectra in a prescribed gridded system.

Quantification of the source/sink terms in Equation (2.1) was initiated from theoretical considerations by Miles [86] and Phillips [97] termed as the Miles-Phillips Mechanisms for wind-wave growth. An energy source term transfers energy into the system, while an energy sink term removes energy from the system. In theory, the sum of all source/sink terms is balanced, or equal to zero. Miles' and Phillips' presumptions were that momentum was transferred from the winds to the free surface via an atmospheric input expression through two terms: an external turbulent pressure forcing mechanism, and a linear feedback mechanism, mathematically represented by the formula (2.2)

$$S_{in} = A + B \cdot E \tag{2.2}$$

The A term (Phillips' mechanism) initiates linear growth with respect to time; and the $B \cdot E$ term (Miles' instability mechanism) sustains an exponential growth over time. Based on this equation, wind- wave growth would never stop. However, additional work by Phillips [98] on the universal *equilibrium range* formed the foundation to control wind-wave growth. In the final growth stages, there is a weak coupling between the input of energy from the winds and the limit in relative steepness via the dissipation term. Later, Pierson and Moskowitz [101] formulated an assumed limit to the frequency spectrum described as fully developed conditions.

The Spectral Ocean Wave Model [100] and a more recent version Global Spectral Ocean Wave Model [22], used by the Fleet Numerical Meteorology and Oceanography Center (FNMOC, Monterey, CA), and also the Ocean Data Gathering Program model [19] are examples of first generation spectral wave models. For accurate representations of wind-wave growth in model simulations, the A term had to be set into several orders of magnitude greater than indicated in the turbulent pressure measurements. In addition, the A term had to be increased by an order of magnitude beyond theoretical limits set by Miles [86], as derived from work by Jeffreys [65]. Field measurements by Barnett and Wilkerson [5] observed a phenomenon called as *overshoot* in the frequency spectrum during wind-wave growth. The 1G models could not reproduce this property with only the Miles-Phillips mechanism. Although these models were simplistic, they produced reasonable results [135].

2.1.2 Second-Generation Modeling

While first generation wave modeling was being carried out, a major theoretical breakthrough was surfacing. Wind-wave growth based on the Miles-Phillips mechanisms assumed that physical processes were based on a coupled linear system between the atmospheric input and a dissipation term. It appeared that a coupled nonlinear process could explain transfers of energy between frequency bands, and the eventual migration of the spectral peak toward lower frequencies. Hasselmann [48, 49, 50] introduced the concept of the *nonlinear wave-wave interaction that*

seemed to define these processes rather well. Solution of the Boltzmann integrals [48] produced estimation of the nonlinear wave-wave interaction term. This contribution provided the foundation of the second-generation wave modeling. Many theoreticians debated the strength of S_{nl} in the evolution of ocean wave spectra. It was not until careful laboratory experiments [87], and field experiments (Joint North Sea Wave Project or JONSWAP [51] measuring winds and wave spectra that the effect of S_{nl} was generally accepted. Based on these experiments, new ideas of wave physics were developed, as well as formulations for fetch and duration growth rate expressions. More importantly, these measurements supported theoretical findings that the nonlinear wave-wave interaction mechanism had a significant impact in the physics of ocean wave spectra. The atmospheric input would transmit energy into the system, while the wave-wave interaction mechanism was responsible for the exchanging of energy between frequency bands. This allowed the migration of energy into the forward face (low frequencies) and high-frequency rear face of the spectrum. Coupling the nonlinear wave-wave interaction term and the atmospheric source input selectively reduced the contribution of the S_{in} winds by an order of magnitude, approaching the results envisioned by Miles [86] and Phillips [97].

The spectral shape based on historical [5], and more recently JONSWAP data [51] was found to be strongly influenced by the S_{nl} term. The overshoot-undershoot phenomenon was also characteristic of the generalized shape of S_{nl}. As indicated in the JONSWAP experiment [51], and its subsequent spectral shape, the peak in the spectral energy was nearly a factor of 3 greater than in fully developed conditions, a consequence of S_{nl}. Hence, on theoretical and also experimental grounds, wind-wave growth seemed to be well understood. The spectral energy balance was now linked to a nonlinear system with three terms (S_{in}, S_{nl} and S_{ds}) rather than two decoupled, linear processes (S_{in} and S_{ds}) described in the 1G models. Barnett [4] and Ewing [32] were credited with the development of initial spectral wave models containing the S_{nl} term. However, the relative strength of the nonlinear wave-wave interaction source

term was very weak, and the growth was essentially controlled by the S_{in} and S_{ds} terms.

The 2G models, although different in structure or numerical solution method, contain the terms of S_{in}, S_{nl} and S_{ds} relationships in one form or another. Terms for both the atmospheric input [113] and the dissipation sink [76] are well-posed, and can be applied to a discrete frequency direction space in a spectral wave model. The greatest problem to overcome in these models was how to evaluate the nonlinear wave-wave interaction term. The exact solution of the three-dimensional Boltzmann integral is computationally restrictive. Parameterizations of S_{nl} were also found to be restricted to very narrow banded spectra, like that proposed by Resio [103]. A database containing S_{nl} for a much larger class of spectra [54] would be nearly impossible to generate as indicated by Resio [104]. To mix integral parameterizations (i.e. total energy flux out of the rear face toward the forward face resulting from S_{nl}) with a discrete approximation to the S_{in} and S_{ds} could be considered technically incorrect. Thus, the only viable alternative solution method available is to formulate all source/sink terms as the net energy transfer.

The number of degrees of freedom between the description of the source/sink terms and the actual spectrum becomes a significant deficiency to overcome. Modeling the source/sink terms is carried out in the form of total energy (or momentum flux) into the system, and subsequent transfer and dissipation. The energy must then be redistributed into the discrete frequency/direction domain describing the spectrum. This can lead to the development of unrealistic spectral distributions that can only be controlled by restraining the spectrum to some predetermined level. Declaring a priori limit to the frequency spectrum is the greatest deficiency in the 2G modelling [122], [104]. Selection of an appropriate Limiting form of the spectrum has a certain degree of uncertainty. The slope of the rear face of a spectrum was initially defined by Phillips [98] as f^{-5}, and supported by the JONSWAP data [51]. Toba [126] found from his measurements that the slope of the rear face in spectra followed an f^{-4} shape, and was supported on theoretical grounds by Kitiagordskii [75], and

also Resio and Perrie [105]. Secondly, the construction of this spectral form requires as little as two arguments (the peak frequency, f_m, and a form of the Phillips' equilibrium constant, α), to as many as five in a JONSWAP-type spectrum [51]. Scaling of these parameters has not been shown to be consistent. From self-similarity principles [75], a given spectral shape is not completely in error, as long as the wave field is at or nearly at equilibrium conditions. Scaling of the energy levels below equilibrium conditions, or during complex meteorological situations as in rapidly changing wind fields (e.g. frontal passages, hurricanes) or mixed wind-sea/swell conditions may sufficiently diminish the accuracy level of the spectrum. Uncertainties in reconstructing a frequency/direction spectrum would, in turn, be reflected in the mean wave parameters such as height, period and the flow direction.

2.1.3 Third-Generation Modeling

One of the overriding conclusions by the SWAMP Group was the vast differences between individual 2G wave models. Academic tests performed as a first-order validation study. As the SWAMP Group convened, a new focus toward spectral modeling technology became evident. Two distinct recommendations were cited, the first was that none of the present (being the mid-1980's) 2G models were applicable for all wind conditions, and secondly, the restriction on the spectral shape severely hampered the final results. The European wave model community coordinated their efforts and embarked on the development of the third-generation spectral model. The work was carried within the framework of the WAM (Wave Modeling) program [133]. In the following years, a wave model called as 3GWAM (or sometimes referred to as WAM) was developed. Four other 3G models have been developed by various individuals that incorporate the 3G concepts. They are WAVEWATCH [127], Nedwam [16] OWI-3G [70] and the Full Boltzmann Model. They were developed under contract though the Coastal Research and Development Program [105], [106], [104]. Differences in these 3G models are generally found in the evaluation of the source/sink term expressions, and predominantly S_{nl}. The actual definition of the 3G model is a rather tenuous one and seems to vary from author to author. In general, 3G models have the following characteristics:

- Description and solution of the source/sink mechanisms are based on the first principles, defined discretely in the frequency/direction domain, and do not formulated in a parametric or empirical framework.
- There is no a priori limit on the spectral shape. The resulting spectrum is defined from the balance in the source/sink term specification.
- The nonlinear wave-wave interaction term is solved explicitly, and is consistent with the number of degrees of freedom contained in the description of the frequency/directional spectrum.

One has to realize that although technically 3G models are better posed in the evaluation of the physical processes, the physical processes dictated by equational formulations still may not be sufficiently adequate. Recent evidence from the Surface Wave Dynamics Experiment show that 3GWAM has produced extremely precise mean wave parameter estimation and frequency/directional estimation. Comparison with the measurements done by Graber *et al.* [43], Jensen *et al.* [67] and Cardone *et al.* [20]. In an operational mode at the European Centre for Medium Range Weather Forecasts, 3GWAM has, on a daily basis, provided very accurate wave forecasts [137], [46], [77].

2.2 Wave Spectral Analysis

In the period 1950-1960, Rice [107] work on signal processing was extended to ocean waves [72], [99]. In principle, the time-history of surface elevation (such as in Figures 2.1 and 2.2) was recognized to be similar to a noise record. By assuming that it is a discrete sample of a continuous process, the principles of Fourier analysis could be extended to describe these records. The power of Fourier representation is such that given a series of time snapshots of measurements of a three-dimensional surface, a full mathematical representation of the surface and its history may be obtained. However, the utility of the spectral analysis is using a reduced dimensional approach that is powerful and useful.

Considering a single-point time-history of surface elevation such as in Figures 2.1, and 2.2, spectral analysis proceeds from viewing the record as the variation of the surface from the mean and recognizes the variation that consists of several periodicities. In contrast to the wave-by-wave approach, which seeks to define individual waves, the spectral analysis seeks to describe the distribution of the variance with respect to the frequency of the signal. By convention, the distribution of the variance with frequency is written as $E(f)$ or $S(f)$ with the underlying assumption that the function is continuous in frequency space. The reason for this assumption is that all observations are discretely sampled in time, and thus, the analysis should produce estimation as discrete frequencies which are then statistically smoothed to estimate a continuum. Although $E(f)$ is actually a measurement of variance, it is often called as the one-dimensional or frequency energy spectrum because (assuming linear wave theory) the energy of the wave field may be estimated by multiplying $E(f)$ by ρg.

Figures 2.1 (a regular wave) and 2.2 (an irregular wave) show two wave records and their spectrum. One immediate value of the spectral approach gives information to the engineer and marine meteorologist about frequencies that have significant energy content and thus acts somewhat analogous to the height-period diagram. The primary disadvantage of spectral analysis is that information on individual waves is lost. If a specific record is analyzed, it is possible to retain information about the phases of the record.

The surface can be envisioned not as individual waves but as a three-dimensional surface. It represents a displacement from the mean and the variance to be periodic in time and space. The simplest spectral representation is to consider $E(f,\theta)$, which represents how the variance is distributed in frequency f and direction θ (Figure 2.4). $E(f,\theta)$ is called as the directional energy spectrum because it can be multiplied by ρg to obtain wave energy. The advantage of this representation is about the direction of the wave energy movement. A directional spectrum and its frequency are displayed in Figure 2.4.

The power of wave spectral analysis comes from three major factors. First, the approach is easily implemented on a microchip and packaged with the gauging instrument. Second, the principal successful theories for describing wave generation by the wind and modeling the evolution of natural sea states in coastal regions are based on spectral theory. Third, it is currently the only widely used approach for measuring wave direction. A final factor is that Fourier or spectral analysis of wave-like phenomena has an enormous technical literature and statistical basis that can be readily drawn upon.

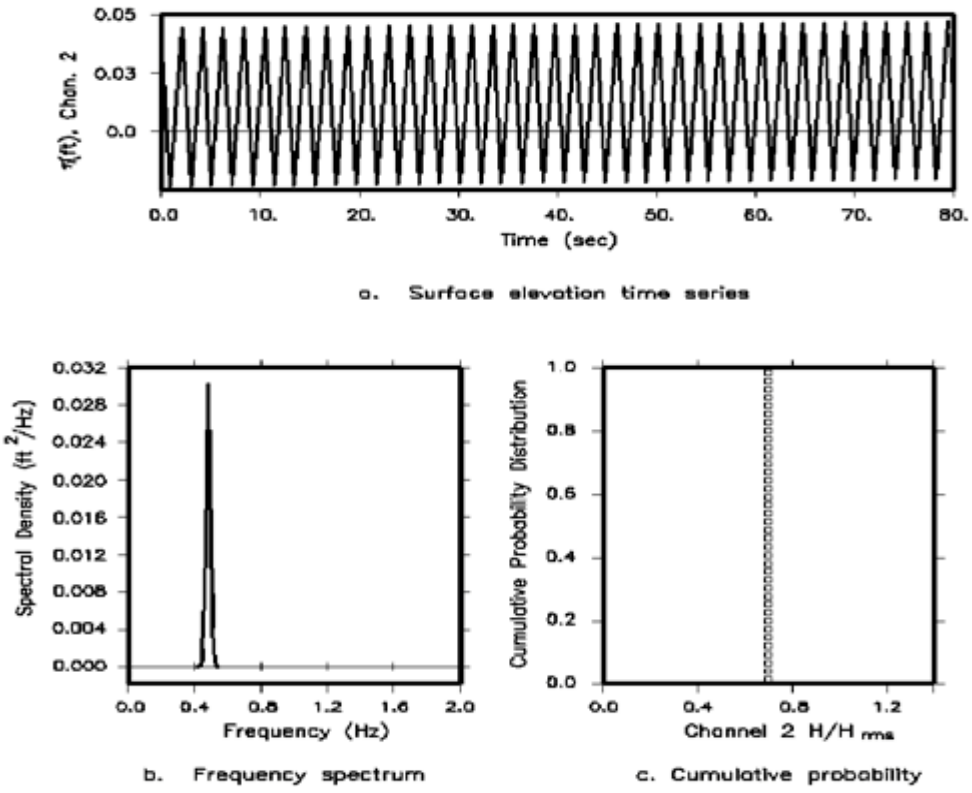

Figure 2.1 Surface elevation time series of a regular wave and its spectrum [15]

Before proceeding to the details of how a wave spectrum is derived from a record, it is important to touch upon some statistical assumptions that are important in analyzing a wave record spectrally. Many of these assumptions also hold for making a wave-by-wave analysis useful as well. First of all, wave records are finite in length (typically 17-68 min long) and are made up of samples of surface elevation at a discrete sampling interval (typically 0.5-2.0 sec). For the wave records to be of general

use, the general characteristics of the record should not be expected to change much if the record was a little shorter or longer, if the sampling was started some fraction of time earlier or later, or if the records were collected a short distance away. In addition, it is desirable that there may not be any underlying trend in the data.

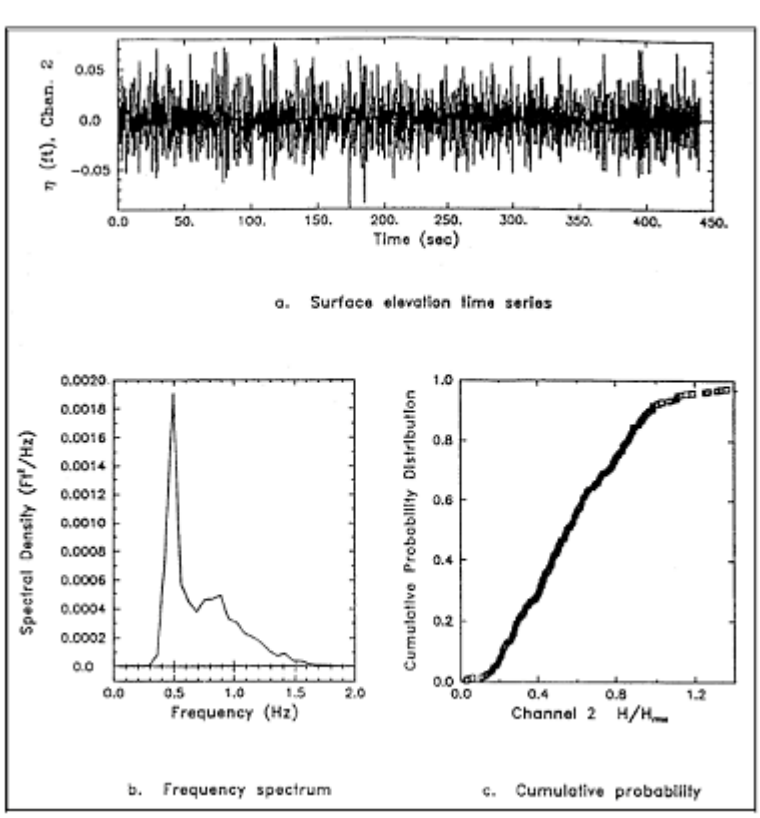

Figure 2.2 Surface elevation time series of an irregular wave and its spectrum [15]

If the above assumptions are not reasonably valid, it implies that the underlying process is unstable and may not be characterized by a simple statistical approach. Fortunately, most of the time in ocean and coastal areas, the underlying processes are not changing too fast and these assumptions reasonably hold. In principal the statistical goal is to assume that there is some underlying statistical

process for which we have obtained an observation. The observation is processed in such a way that the statistics of the underlying process are obtained.

2.2.1 Description of wave spectral analysis

Unlike the wave train or wave-by-wave analysis, the spectral analysis method determines the distribution of wave energy and average statistics for each wave frequency by converting time series of the wave record into a wave spectrum. This is essentially a transformation from time-domain to the frequency domain. It is accomplished most conveniently using a mathematical tool known as the Fast Fourier Transform (FFT) technique [23]. Here we will treat analysis of the time recording of the surface at a point, in order to obtain a frequency spectrum of the record. In a later section, we will describe how to obtain a frequency-directional spectrum.

The wave energy spectral density $E(f)$ or simply the wave spectrum may be obtained directly from a continuous time series of the surface $\eta(t)$. Using a Fourier analysis, the wave profile time trace can be written as an infinite sum of sinusoids of amplitude A_n, frequency ω_n , and relative phase ε_n, that is

$$\begin{aligned}\eta(t) &= \sum_{n=0}^{\infty} A_n \cos(\omega_n t - \varepsilon_n) \\ &= \sum_{n=0}^{\infty} a_n \cos n\omega t + b_n \sin n\omega t\end{aligned} \tag{2.3}$$

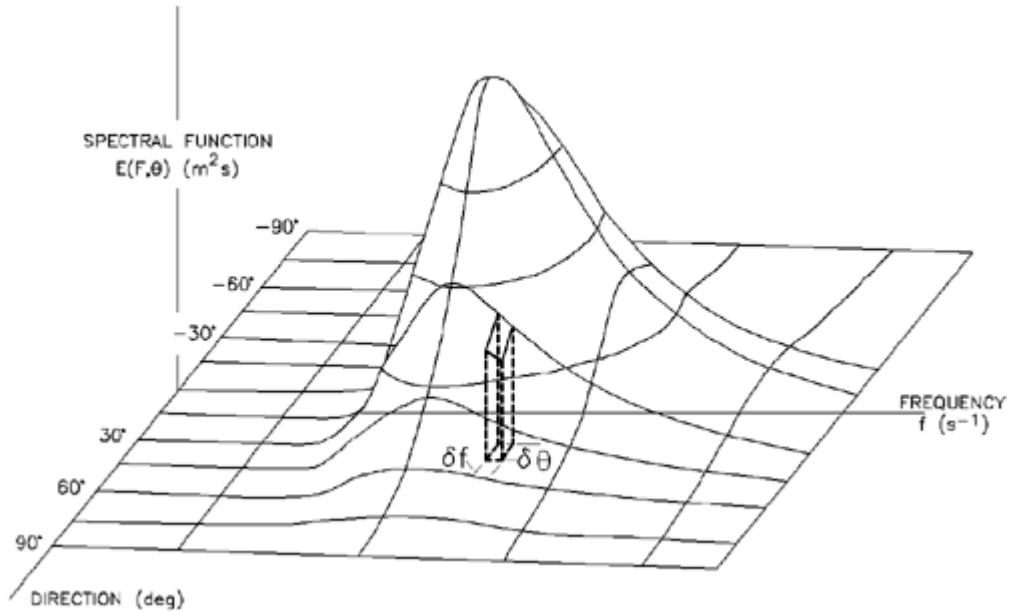

Figure 2.3 A schematic for a two-dimensional wave spectrum $E(f,\theta)$

The coefficients a_n and b_n in the above equation may be determined explicitly from the orthogonality properties of circular functions. Note that a0 is the mean of the record. Because real observations are of finite length, the finite Fourier transform is used and the number of terms in the summation is a finite value.

The covariance of $\eta(t)$ is related to the wave energy spectrum. This is defined in terms of the squares of component amplitudes as

$$\begin{aligned} \overline{\eta^2}(t) &= \sum_0^\infty A_n^2 \Delta f \\ A_n^2 &= \frac{1}{2}\sqrt{a_n^2 + b_n^2} \\ \varepsilon_n &= \tan^{-1}\frac{b_n}{a_n} \end{aligned} \tag{2.4}$$

By induction, an estimation of the continued energy spectrum of η(t) may be obtained by

$$E(f) = \frac{1}{T_r}\left[\sum_{n=0}^{N} \eta(n\Delta t)\, e^{2\pi i f(n\Delta t)} \Delta t\right]^2 \tag{2.5}$$

where T_r is the record length and Δt is the sampling interval.

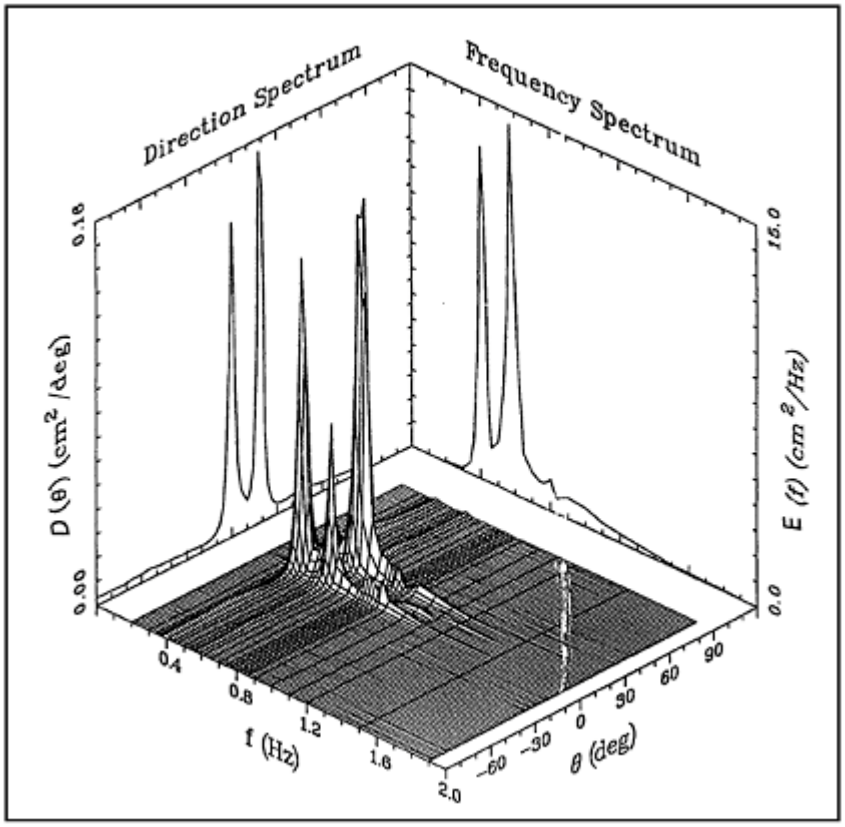

Figure 2.4 A directional spectrum, its frequency and direction spectrum [15]

There are numerous intricacies involved in the application of these discrete formulas, ranging from the length of time series necessary to digitizing frequency and many others. For unfamiliar users, most computer library systems now have FFT (Finite Fourier Transform) algorithms available to perform the computations.

In actual practice, the total data length is divided into M smaller segments with equal number of data points N. By letting N be a power of 2 for computational efficiency, the result then is averaged over the M sections. In an FFT, the variables M, N and Δt have to be independently selected, though T_r and Δt are fixed for a given record so that the total number of data points can be obtained. Therefore, the only choice that has to be made is the number of sections M. Traditionally, the most

common value of N is in the range of 512 to 2,048, while the value of M is usually 8 or greater. Since T_r is dependent on N, M and Δt as $T_r = MN\mathrm{H}\Delta t$, then higher values of N and M in general yield better resolution and high confidence in the estimation of spectra. The larger the N, the more spiky or irregular the spectrum, and the smaller the N, the smoother the spectrum [23], [21].

To better understand the wave spectrum by the FFT method, we consider the wave surface profile of a single-amplitude and frequency wave given by a sinusoidal function as

$$\eta(t) = a\sin\omega t \tag{2.6}$$

where a and ω are respectively the amplitude and frequency of the sine wave. The variance of this wave over the 2π period is

$$\begin{aligned}\sigma^2 = \overline{[\eta(t)]^2} &= \frac{1}{2\pi}\int_0^{2\pi} a^2 \sin^2 2\pi ft\, d(2\pi ft) \\ &= \frac{a^2}{2} = 2\int_0^{\infty} E^1(f)\, df = \int_{-\infty}^{\infty} E^2(f)\, df\end{aligned} \tag{2.7}$$

Thus the quantity $a^2/2$ represents the contribution to the variance σ^2 associated with the component frequency $\omega = 2\pi f$ (Figure 2.5). The connection between the variance, wave energy, and the spectrum is now more obvious since they are proportional to the wave amplitude (or height) squared. For consistency of units, an equality between these quantities requires the wave spectrum that does not include the ρg term.

Note that the two-sided spectrum is symmetric about the origin, covering both negative and positive frequencies to account for all wave energy from $-\infty$ to ∞. But, it is customary in ocean engineering to present the spectrum as a one-sided spectrum. This requires that the spectral density ordinates of E^2 be doubled in value if only the positive frequencies are considered. This is the reason for introducing a factor of two

in Equation (2.7). It is henceforth understood that $E(f)$ refers to E^1 (Figures 2.7 and 2.8).

By an intuitive extension of this simple wave, the variance of a random signal with zero mean may be considered to be made up of contributions with all possible frequencies. We thus can find a random signal as

$$\sigma_\eta^2 = \sum_{n=1}^{\infty} \frac{a_n^2}{2} = \int_0^{\infty} E(f)\,df = m_0 \tag{2.8}$$

where m_0 is the zero-th moment of the spectrum. Physically, m_0 represents the area under the curve of $E(f)$. The area under the spectral density represents the variance of a random signal whether the one-sided or two sided spectrum is used.

The moments of a spectrum can be obtained by

$$m_i = \int_0^{\infty} f^i E(t)\,df \qquad i = 0,1,2,... \tag{2.9}$$

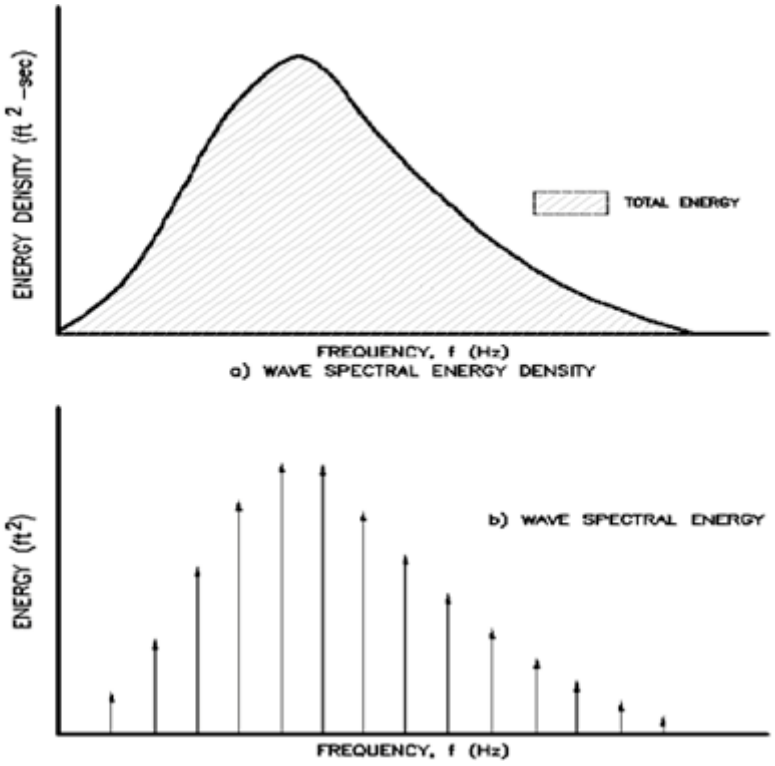

Figure 2.5 Sketches of wave spectral energy and energy density [21]

We now use the definition of the variance of a random signal (Equation (2.8)) to define the significant wave height. As stated earlier, this gives an estimation of the significant wave height using the wave spectrum. For Rayleigh distributed wave heights, H_s may be approximated [82] by

$$H_s = 3.8\sqrt{m_0} \approx 4\sqrt{m_0} \tag{2.10}$$

Therefore, the zero-th moment m_0, the total area under the wave energy density spectrum, determines the significant wave height for a given $E(f)$ (Figure 2.7).

2.2.2 Wave spectrum and its parameters

Two parameters are frequently used in the probability distribution for waves. These are the spectral width ν and the spectral bandwidth ε, and are used to determine the narrowness of a wave spectra. These parameters range from 0 to 1, and may be approximated in terms of spectral moments by

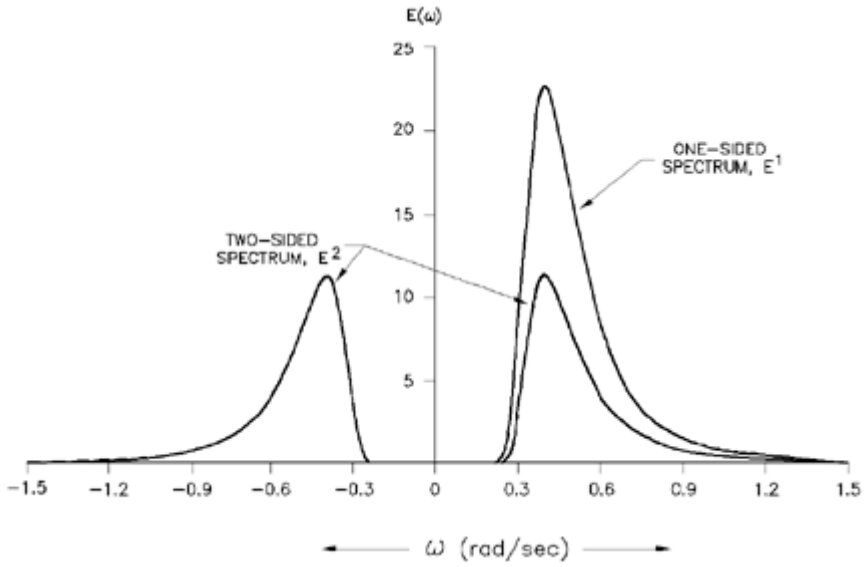

Figure 2.6 Definition of one- and two-side wave spectrum [21]

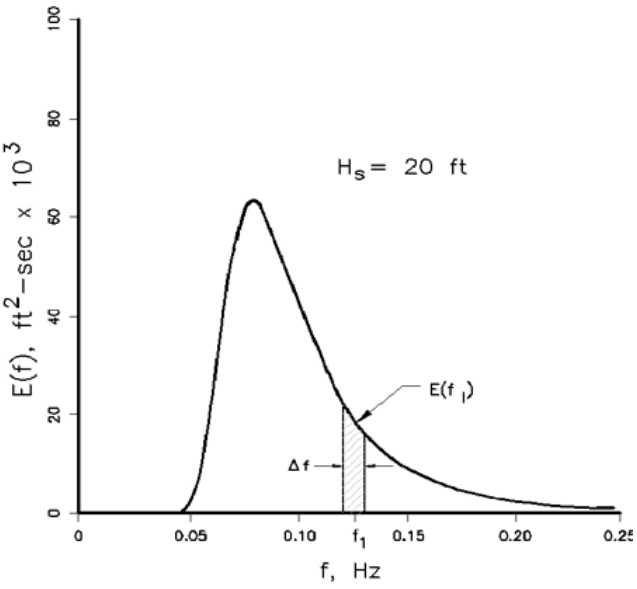

Figure 2.7 Energy density and frequency relationship [21]

$$\nu = \sqrt{\frac{m_0 m_2}{m_1} - 1}\,;$$

$$\varepsilon = \sqrt{1 - \frac{m_2^2}{m_0 m_4}} \tag{2.11}$$

For a narrow-band spectrum, both ν and ε must be close to 0 (Figure 2.8). For example, for the two most common empirical spectra, the Pierson-Moskowitz (PM) spectrum [101] and the JONSWAP spectrum [51], ν = 0.425 and 0.389, respectively, with $\varepsilon = 1$ for both. Natural ocean waves, therefore, have a broad-banded spectrum.

The values of ε obtained from a wave energy spectrum are generally not considered as the sole indication of how broad the spectra be. This is due to the amplification of the noise present in the wave energy spectral density at higher frequencies that enters into the calculation of the higher moments m_2 and m_4 in Equation (2.11) for ε. Goda [37] proposed a spectral parameter called Q_p defined as

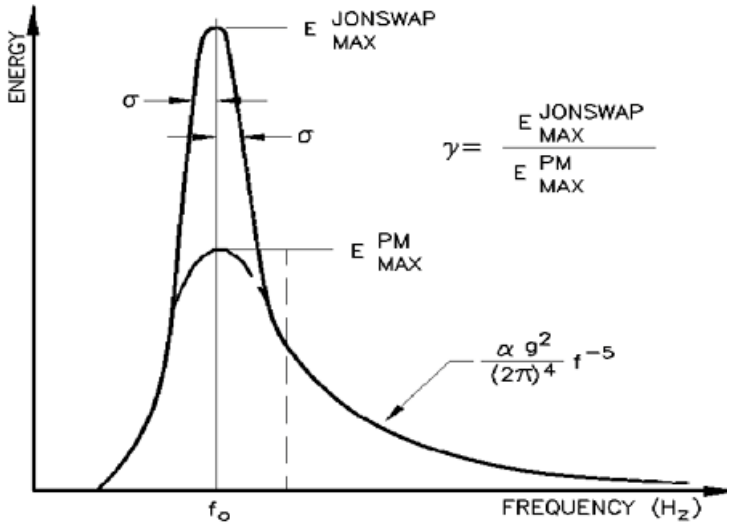

Figure 2.8 Comparison of the PM and JONSWAP spectra [21]

$$Q_p = \frac{2}{m_0^2} \int_0^\infty f\, E^2(f)\, df \tag{2.12}$$

which depends only on the first moment of the energy density spectrum, and is not directly related to ε. In general, a small ε implies that Q_p is large, and a large ε means that Q_p is small.

Approximating the relations for most common wave parameters using the statistical analysis, we obtain

$$\begin{aligned} H_s &= 4.0\sqrt{m_0} \quad ; \quad H_{1/10} = 5.1\sqrt{m_0} \\ T_z &= \sqrt{\frac{m_0}{m_2}} \quad ; \quad T_c = \sqrt{\frac{m_2}{m_4}} \\ \overline{\eta} &= \sqrt{m_0} \quad ; \quad \varepsilon = \sqrt{1 - \frac{m_2^2}{m_0 m_4}} \end{aligned} \tag{2.13}$$

In deep and intermediate water depths, the significant wave height obtained by the spectral analysis using Equation (2.13) is usually greater than that from the wave train analysis. The zero-crossing period from the spectral method is only an approximation, while the period associated with the largest wave energy known as the peak period T_p, can only be obtained via the spectral analysis. In the spectral representation of swell waves, there is a single value of the peak period and wave energy decays at frequencies to either side. The spectra of storm waves is sometimes multi-peaked. One peak (not always the highest) corresponds to the swell occurring at lower frequencies. These peaks are associated with storm waves occurring at comparatively higher frequencies. In a double-peaked spectra of storm waves, the zero-crossing period generally occurs at higher frequencies than the peak period. In a multi-peaked spectrum, the zero-crossing period is not a measure of the frequency where the peak energy occurs.

2.2.3 Relationships among $H_{1/3}$, H_s and H_{m0} in shallow water

By conception, significant height is the average height of the third-highest waves in a record of time period. By tradition, wave height is defined as the distance from crest to trough. Significant wave height H_s can be estimated from a wave-by-wave analysis in which case it is denoted by $H_{1/3}$, but more often is estimated from the variance of the record or the integral of the variance in the spectrum in which case it is denoted by H_{m0}. Therefore, H_s in Equation (2.13) should be replaced by H_{m0}. While $H_{1/3}$ is a direct measure of H_s, H_{m0} is only an accurate estimation of the significant wave height under some circumstances. In general in deep water, the values of $H_{1/3}$ and H_{m0} are almost the same and are both considered as the estimation of H_s. All modern wave forecast models predict H_{m0} which is the standard output of most wave gauge records. Few routine field gauging programs actually compute $H_{1/3}$ and report as H_s with no indication of how it was derived. Where $H_{1/3}$ and H_s are equivalent, this is of little concern.

Thompson and Vincent [125] investigated how $H_{1/3}$ and H_{m0} vary in the shallow water near breaking. They found that the ratio $H_{1/3}/H_{m0}$ varied systematically across the surf zone, approaching a maximum near breaking. Thompson and Vincent displayed the results in terms of a nomogram (Figure 2.10). For steep waves, $H_{1/3}/H_{m0}$ increased from 1 to about 1.1, then decreased to less than 1 after breaking. For low steepness waves, the ratio increased from 1 before breaking to as much as 1.3-1.4 at breaking, then decreased afterwards. Thompson and Vincent explained this systematic variation in the following way. As low steepness waves shoal prior to breaking, the wave shape systematically changes from being near sinusoidal to a wave shape that has a very flat trough with a very pronounced crest. Although the shape of the wave is significantly different from the sine wave in shallow water, the variance of the surface elevation is about the same, it is just arranged over the wave length differently from a sine wave. After breaking, the wave is more like a bore and $H_{1/3}$ can be smaller (by about 10 percent) than H_{m0}.

The critical importance of Thompson and Vincent's work is in interpreting wave data near the surf zone. It is of fundamental importance for the engineer. As an example, if the data from a gauge is actually H_{m0} and the waves are near breaking, the proper estimation of H_s is given by $H_{1/3}$. Given the steepness and relative depth, $H_{1/3}$ may be estimated from H_{m0} as shown in Figure 2.10. Numerically modeled waves near the surf zone are frequently equivalent to H_{m0}. In this case, H_s will be closer to $H_{1/3}$ and the nomogram should be used to estimate H_s.

2.2.4 Parametric spectrum models

In general, the spectrum of the sea surface does not follow any specific mathematical form. However, under certain wind conditions the spectrum does have a specific shape. A series of empirical expressions have been found which can be fit to the spectrum of the sea surface elevation. These are called parametric spectrum models which are useful for routine engineering applications.

There are many forms of wave energy spectra used in practice, which are based on one or more parameters such as wind speed, significant wave height, wave period, shape factors, etc. Phillips [98] proposed an equation for the equilibrium range of the spectrum for a fully-developed sea in deep water. His work is the basis of most subsequent developments. Phillips' equilibrium range is often written in terms of the angular frequency ω and is of the form

$$E(\omega) = \alpha g^2 \omega^{-5} \tag{2.14}$$

where α is the Phillips' constant (= .0081) and g the gravitational acceleration.

In wave hindcasting and forecasting projects, the single-parameter spectrum of Pierson-Moskowitz PM [101] is commonly used. An extension of the PM spectrum is the JONSWAP spectrum [51, 53]; there is a five-parameter spectrum, although three of these parameters are usually held constant. The relationship between PM and

JONSWAP spectra is shown in Figure 2.8. Other commonly used two-parameter wave spectra forms, including those proposed by Bretschneider [13], ISSC [61], Scott [110], ITTC [62], Liu [80], Mitsuyasu [89], Goda [40] and Bouws *et al.* [10] are essentially derivatives of the PM and JONSWAP spectra. A six-parameter wave spectrum has been developed by Ochi and Hubble [93]. The utility of this spectrum can describe multi-peaks in the energy spectrum in a sea state mixed with swell (Figure 2.9). Next, we will describe the parametric wave spectra forms, that is often used in coastal engineering.

The equilibrium form of the PM spectrum for fully-developed seas may be expressed in terms of wave frequency f and wind speed U_w as

$$E(f) = \frac{0.0081 g^2}{(2\pi)^4 f^5} \exp\left(-0.24 \left[\frac{2\pi U_w f}{g} \right]^{-4} \right) \tag{2.15}$$

where U_w is the wind speed at 19.5 meters above mean sea level. The PM spectrum describes a fully-developed sea with one parameter, the wind speed, and assumes that both the fetch and duration are infinite. This idealization is justified when wind blows over a large area at a constant speed without substantial change in its direction for tens of hours.

The JONSWAP spectrum for fetch-limited seas was obtained from the Joint North Sea Wave Project - JONSWAP [51] and may be expressed as

$$E(f) = \frac{\alpha g^2}{(2\pi)^4 f^5} \exp\left(-1.25 \left[\frac{f}{f_p} \right]^{-4} \right) \gamma^{\exp\left[-\frac{\left(\frac{f}{f_p} - 1 \right)^2}{2\sigma^2} \right]}$$

$$\text{where } f_p = 3.5 \left[\frac{g^2 F}{U_{10}^3} \right]^{-0.33} \quad ; \quad \alpha = 0.076 \left[\frac{gF}{U_{10}^2} \right]^{-0.22} \quad ; 1 \le \gamma \le 7 \tag{2.16}$$

$$\sigma = 0.07 \; for \; f \le f_p \quad and \quad \sigma = 0.09 \; for \; f > f_p$$

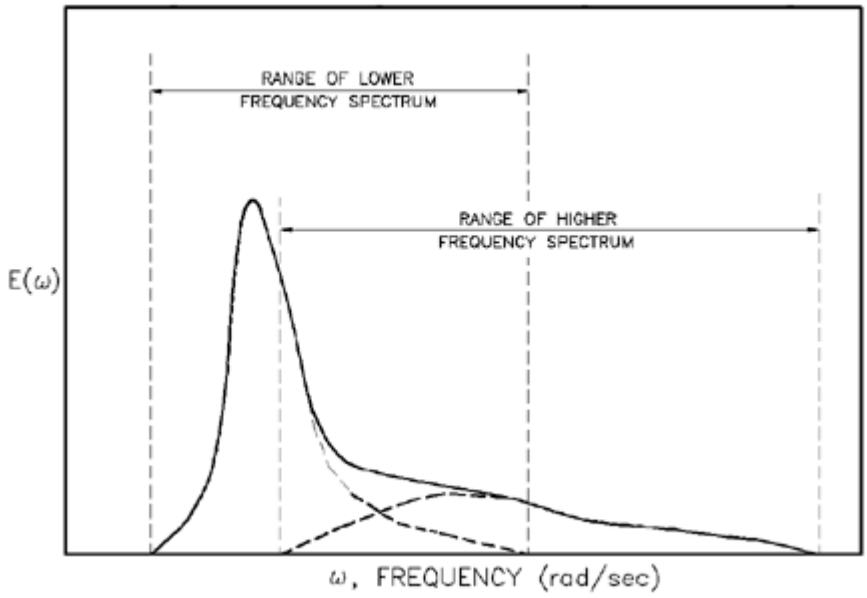

Figure 2.9 Definition sketch for Ochi-Hubble spectrum [93]

In Equation (2.16), α is the scaling parameter, γ the peak enhancement factor, f_p the frequency at the spectral peak, U_{10} the wind speed at the elevation 10 meters above the sea surface, F the fetch length. Figure 2.8 qualitatively illustrates the relationship between JONSWAP and PM spectra. The JONSWAP spectrum can also be fitted mathematically to observed spectra by iteratively solving for d, γ, f_m *and* σ.

A six-parameter spectrum developed by Ochi and Hubble [93] is the only wave spectrum which exhibits two peaks (Figure 2.9). One associated with underlying swell (lower frequency components) and the other with locally generated waves (higher frequency components). It is defined as

$$E(\omega) = \frac{1}{4}\sum_{j=1}^{2} \frac{\left(\frac{4\lambda_j + 1}{4}\omega_{0j}^4\right)^{\lambda_j}}{\Gamma(\lambda_j)} \frac{H_{sj}^2}{\omega^{4\lambda_j+1}} \exp\left[-\frac{4\lambda_j+1}{4}\left(\frac{\omega_{0j}}{\omega}\right)^4\right] \qquad (2.17)$$

where H_{s1}, ω_{01} and λ_1 are respectively the significant wave height, modal frequency, and shape factor for the lower frequency components while H_{s2}, ω_{02} and λ_2 correspond to the higher frequency components (Figure 2.9). The value of λ_1 is usually much higher than λ_2. For the most probable value of ω_{01}, it can be shown that $\lambda_1 = 2.72$, while λ_2 is related to H_s in feet as

$$\lambda_2 = 1.82\, e^{(-0.027 H_s)} \tag{2.18}$$

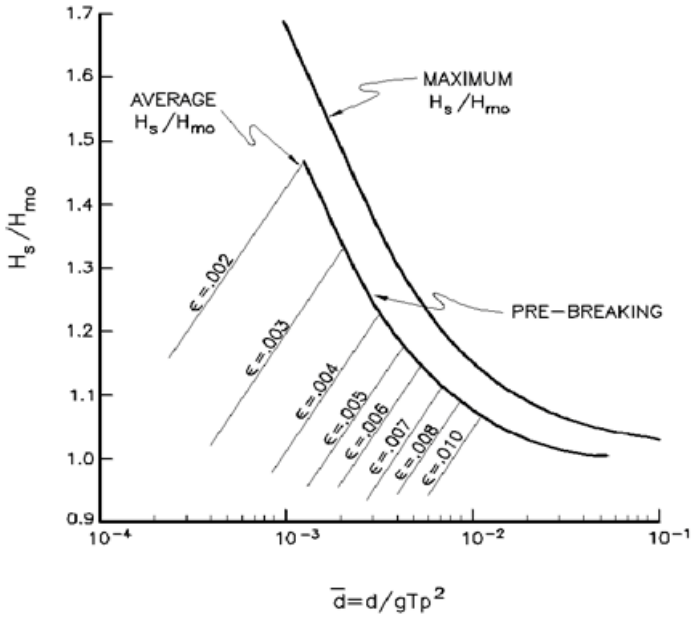

Figure 2.10 Variation of H_s / H_{m0} as a function of relative depth $\bar{d}$ and significant steepness [125]

The parameters λ_j control the shape and the sharpness of the spectral peak of the Ochi-Hubble spectral model if in either spectral component (i.e., sea or swell) the values of H_{sj} and ω_{0j} are held constant. Therefore, λ_1 and λ_2 are called the spectral shape parameters. On the assumption of a narrow-bandedness of the entire Ochi-Hubble spectrum, an equivalent significant wave height may be calculated by Ochi and Hubble [93].

$$H_s = \sqrt{H_{s1}^2 + H_{s2}^2}\,, \tag{2.19}$$

in which for λ_1 = 1 and λ_2 = 0, the PM spectra may be recovered.

In shallow water, the wave spectrum deviates from the standard spectra forms presented so far, and at frequencies above the peak, the spectrum no longer decays as f^{-5}. Kitaigorodoskii *et al.* [74] showed that the equilibrium range is proportional to -3 power of the wave number, and thus, the form of the spectrum is of f^{-3} in the high-frequency range. This change is attributed to the effect of water depth on wave spectrum and to the interaction between spectral components. Bouws *et al.* [9] proposed a variation to the JONSWAP energy spectrum for representing wave spectra in finite-depth water. The spectrum so obtained, the product of JONSWAP and the Kitaigorodoskii depth function accounting for the influence of the water depth, is called the TMA spectrum after the names of three sources of data used in its development [10].

Kitaigorodoskii *et al.* [74] obtained the form of depth dependence as

$$\Phi(\omega, d) = \frac{\left[k^{-3}\dfrac{\partial k}{\partial \omega}\right]_{d=finite}}{\left[k^{-3}\dfrac{\partial k}{\partial \omega}\right]_{d=\infty}} S\,, \tag{2.20}$$

where k denotes wave number (= $2\pi/L$ = $2\pi/CT$) [length-1], S is Dimensionless controlling parameter for the angular distribution that determines the peakedness of the directional spreading.

Thus, Φ is a weighing factor of the quantity in the bracket, which is determined from the ratio of the quantity evaluated for finite and infinite water depth cases. Using the linear wave theory, the above equation has been approximated by Kitaigorodoskii *et al.* [74] as

$$\Phi(\omega,d)=\begin{bmatrix} \frac{1}{2}\omega^2 & for\ \omega\le 1 \\ 1-\frac{1}{2}(2-\omega)^2 & for\ \omega>1 \end{bmatrix} \tag{2.21}$$

The TMA spectrum was intended for wave hindcasting and forecasting in water of finite depth. This spectrum is a modification of the JONSWAP spectrum simply by substituting Kitaigorodoskii's expression for effects of the finite depth equilibrium function. By using the linear wave theory, we find the following complete form of the TMA spectrum:

$$S_{TMA}(\omega,d)=S_{JONSWAP}(\omega)\Phi(\omega^*,d)$$

$$\Phi(\omega^*,d)=\frac{1}{f(\omega^*)}\left[1+\frac{K}{\sinh K}\right];\quad \omega^*=\omega\sqrt{\frac{d}{g}}; \tag{2.22}$$

$$f(\omega^*)=\tanh^{-1}[k(\omega^*)d];\quad K=2\omega^{*2}f(\omega^*)$$

The substitution (2.22) transforms the decay or slope of the spectral density function of the JONSWAP spectrum in the high-frequency side from ω^{-5} to ω^{-3} type dependence during the shoaling process approximated by linear wave theory. Bouws *et al.* [9] presented equations for α, γ, and σ. As with the JONSWAP, the equation may be iteratively fit to an observed spectrum and α, γ, f_m and σ may be estimated.

The PM, JONSWAP and TMA spectra can be estimated if something about the wind, depth and fetch are known. Furthermore, these spectral equations can be used as target spectra whose parameters can be varied to fit observed spectra which may have been measured. In the first situation, the value of the parameterization is in making an educated guess at what the spectrum may have looked like. The value in the second case is for ease of analytical representation. However, today engineering analyses are made on the basis of numerical simulations of a specific event by using a numerical model. In this case, the model estimates the spectrum and a parametric form is not required.

2.2.5 Directional spectra

The wave spectra described so far have been one-dimensional frequency spectra. Wave direction does not appear in these representations, and thus variation of wave energy with wave direction was not considered. However, the sea surface is often composed of many waves coming from different directions. In addition to wave frequency, the mathematical form of the sea state spectrum corresponding to this situation should therefore include the wave direction θ. Each wave frequency may then consist of waves from different directions θ. The wave spectra so obtained are two-dimensional, and are denoted by $E(f,\theta)$. Figures 2.3 and 2.4 display directional spectra.

Measurement of a directional spectrum typically involves measurement of either the same hydrodynamic parameter (such as surface elevation or pressure) at a series of nearby locations (within one to tens meters) or different parameters (such as pressure and two components of horizontal velocity) at the same point. These records are then cross-correlated through a cross-spectral analysis and a directional spectrum is estimated. In general, the more parameters or more locations involved, the higher the quality of the directional spectrum obtained.

The major systems that are routinely employed at the present time for measuring directional spectra include directional buoys, arrays of pressure or velocity gauges, and the p-U-V technique. With directional buoys, pitch-roll-and-heave or heave-and-tilt methods are used. Most directional buoys are emplaced in deeper water. Arrays of pressure gauges or velocity gauges arranged in a variety of shapes (linear, cross, star, pentagon, triangle, rectangle, etc.) are also used, but these are usually restricted to shallower water. The p-UV technique uses a pressure gauge and a horizontal component current meter almost co-located to measure the wave field. This can be used in shallow or in deeper water if there is something to attach it to near the surface. Other techniques include arrays of surface-piercing wires, triaxial current meters, acoustic doppler current meters and radars.

A mathematical description of the directional sea `state is feasible by assuming that the sea state can be considered as a superposition of a large number of regular sinusoidal wave components with different frequencies and directions. With this assumption, the representation of a spectrum in frequency and direction becomes a direct extension of the frequency spectrum alone, allowing the use of Fast Fourier Transform (FFT) method. It is often convenient to express the wave spectrum $E(f,\theta)$ describing the angular distribution of wave energy at respective frequencies by

$$E(f,\theta) = E(f)\,G(f,\theta)\,, \tag{2.23}$$

where the function $G(f,\theta)$ is a dimensionless quantity, and is known as the directional spreading function. Other acronyms for $G(f,\theta)$ are the spreading function, angular distribution function and the directional distribution.

The one-dimensional spectra may be obtained by integrating the associated directional spectra over θ as

$$E(f) = \int_{-\pi}^{\pi} E(f,\theta)\,d\theta \tag{2.24}$$

From Equation (2.23) and (2.24), $G(f,\theta)$ must satisfy the condition (2.25)

$$\int_{-\pi}^{\pi} G(f,\theta)\,d\theta = 1 \tag{2.25}$$

The functional form of $G(f,\theta)$ has no universal shape and several proposed formulas are available. In the most convenient simplification of $G(f,\theta)$, it is customary to consider G to be independent of frequency f such that we have

$$G(\theta) = \frac{2}{\pi}\cos^2\theta \quad for \quad \left|\theta < 90^\circ\right| \tag{2.26}$$

This cosine-squared distribution is due to St. Denis and Pierson [116], and testing with field data shows that it reproduces the directional distribution of wave energy. Longuet-Higgins [83] found the cosine-power forms of $G(\theta)$ and $C(s)$ as follows :

$$G(\theta) = C(s)\cos^{2s}\frac{\theta-\bar{\theta}}{2}$$
$$C(s) = \frac{\sqrt{\pi}}{2\pi}\frac{\Gamma(s+1)}{\Gamma\left(s+\frac{1}{2}\right)} \tag{2.27}$$

where θ is the principal (central) direction for the spectrum, s is a controlling parameter for the angular distribution that determines the peakedness of the directional spreading, $C(s)$ is a constant satisfying the normalization condition, θ is a counterclockwise measured angle from the principal wave direction and Γ is the Gamma function.

Mitsuyasu *at al.* [88], Goda and Suzuki [39] and Holthuijsen [57] have shown that for wind waves, the parameter s varies with wave frequency and is related to the stage of wave development (i.e., wind speed and fetch).

$$s = \begin{cases} s_{\max}\left(\frac{f}{f_p}\right)^{5} & for \quad f \le f_p \\ s_{\max}\left(\frac{f}{f_p}\right)^{-2.5} & for \quad f > f_p \end{cases} \tag{2.28}$$

where $s_{\max}$ and f_p are defined as

$$s_{\max} = 11.5\left(\frac{2\pi f_p U}{g}\right)^{-2.5}$$

$$\frac{2\pi f_p U}{g} = 18.8\left(\frac{gF}{U^2}\right)^{-0.33} \tag{2.29}$$

U in Equation (2.29) is the wind speed at the 10-m elevation above the sea surface and F is the fetch length. These equations remain to be validated with field data for wind waves. The parameter s for shallow-water waves may also vary spatially during wave transformation. This is due to refraction. A large value of s is greater than 50. It may be necessary if the dependence of $s_{\max}$ on refraction is of concern. For deepwater applications where wind waves are jointly presented with swells in deep water, Goda and Suzuki [39] proposed the following values of $s_{\max}$ to be 10 for wind waves and 25 for swells with wind waves of relatively large steepness and 75 for swells with wind waves of small steepness. Under simple wind wave conditions, the spreading function may be approximated by the equations provided. They are typical of deepwater wind seas for which the wind has been constant.

2.2.6 Wave groups and groupiness factors

Measurements of waves usually show a tendency of grouping between waves that is; high waves; often seem to be grouped together. Examination of the sea surface profile records indicates that wave heights are not uniform and they occur in successive groups of higher or lower waves. The interest in wave groups is stimulated by the fact that wave grouping and associated nonlinear effects play an important role in the long-period oscillation of moored vessels [27, 28], [33], surf beats, irregular wave runup, resonant interaction between structures [25], [26], and other irregular fluctuations of the mean water level nearshore [40,42]. Unfortunately there is no way to predict grouping.

Wave grouping is an important research topic and there are several ways to quantify wave grouping. These include the smoothed instantaneous wave energy

history analysis [36], the concept of the run of wave heights [38], and the Hilbert transform. A short exposition of the wave grouping analysis is provided here.

The length of wave grouping can be described by counting the number of waves exceeding a specified value of the wave height which could be the significant, mean, or other wave height. The succession of high wave heights is called a run or a run length with an associated wave number j_1. The definition sketch for two wave groups is shown in Figure 2.11 with the threshold wave height limit set at $H = H_c$. The recurrence interval or repetition length above the threshold value of wave height is called the total run denoted by j_2.

The group occurrence for N waves with k number of lags between waves in a sequence in a record may be defined in terms of a correlation coefficient. The correlation coefficient R_H so defined will describe the correlation between wave heights as a function of the mean μ and standard deviation σ and is given by

$$R_H = \frac{1}{\sigma_0}\frac{1}{N-k}\sum_{i=1}^{N-k}(H_i - \mu)(H_{i+k} - \mu)$$

$$\sigma_0 = \frac{1}{N}\sum_{i=1}^{N}(H_i - \mu)^2 \qquad (2.30)$$

Thus, R_H varies with the number of lags k between waves. If the succeeding waves are uncorrelated, then $R_H \to 0 \, as \, N \to \infty$. Real wave data indicate that $R_H(1) \approx 0.20 \, to \, 0.40$ while $R_H(k) \approx 0$ for k > 1. Furthermore, a positive value of R_H suggests that large waves tend to be succeeded by large waves, and small waves by other small waves.

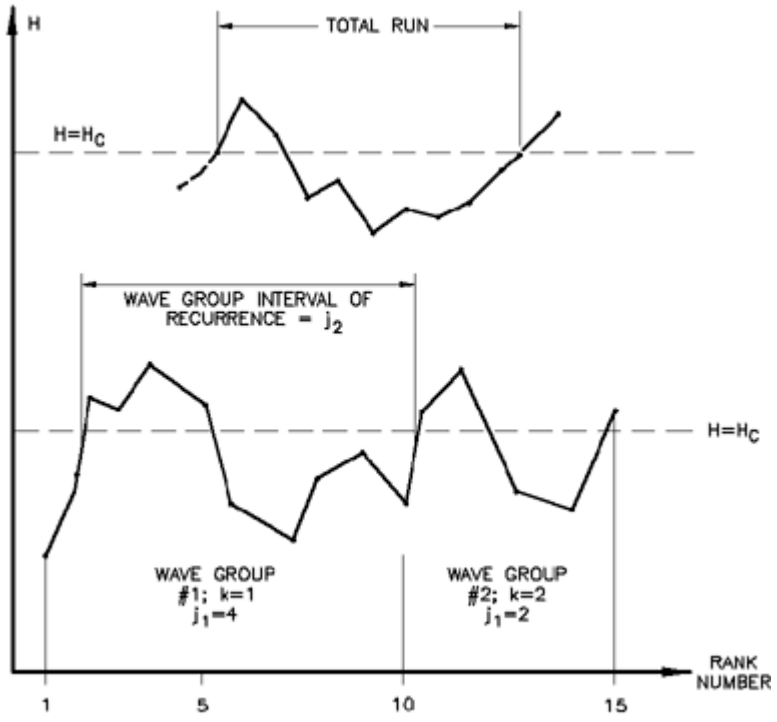

Figure 2.11 Identification and description of wave groups through ordered statistics [38]

Assuming that successive wave heights are uncorrelated, the probability of a run length j_1 is [38]

$$P(j_1) = P^{(j_1-1)}(1-p) \tag{2.31}$$

in which p is the occurrence probability for $H > H_c$. The mean and standard deviation of j_1 are

$$\mu_{j_1} = \frac{1}{q} \quad ; \quad q = 1-p \quad ; \quad \sigma_{j_1} = \frac{\sqrt{1-q}}{q}$$

$$p = p(H > H_c) = \exp\left[-\frac{1}{8}\eta_c^2\right] \quad ; \quad \eta_c = \frac{H_c}{\sigma_\eta} \tag{2.32}$$

The probability of a total run with the length j_2 can be derived by mathematical induction as

$$\mu_{j_2} = \frac{1}{p} + \frac{1}{q} \quad ; \quad \sigma_{j_2} = \sqrt{\frac{p}{q^2} + \frac{q}{p^2}} \tag{2.33}$$

where it has been assumed that successive wave heights are uncorrelated. Successive wave heights of the real ocean waves are mutually correlated, and the degree of correlation depends on the sharpness of the spectral peak. The effect of spectral bandwidth on wave height distribution has been considered by Kimura [71], Tayfun [120] and Longuet-Higgins [84]. Tayfun has shown that the parameter that best describes the spectral peakedness is the correlation coefficient of the wave envelope, relating wave height variation between successive wave heights. This coefficient R_{HH} may be calculated as [120]

$$R_{HH} = \frac{E(\lambda) - (1-\lambda^2)\dfrac{K(\lambda)}{2} - \dfrac{\pi}{4}}{1 - \dfrac{\pi}{4}}$$

$$\lambda(\overline{T}) = \frac{1}{m_0}\sqrt{A^2 + B^2} \tag{2.34}$$

$$A = \int_0^\infty E(f)\cos 2\pi f \overline{T}\, df \quad ; \quad B = \int_0^\infty E(f)\sin 2\pi f \overline{T}\, df$$

By further assuming that Rayleigh distribution is suitable for the consecutive wave heights, the joint probability density function $p(H_1, H_2)$ for two successive wave heights H_1 and H_2 in the wave group may then be established.

The correlation coefficient R_{HH} takes a value of about 0.2 for wind waves and 0.6 or greater for swells [38], a clear indication that wind waves rarely develop significant grouping of high waves. Su [117] has shown that the wave group containing the highest wave in a record is often longer than the ordinary groups of

high waves, and that the extreme wave usually consists of three high waves with the highest greater than the significant wave height. Wave groups and their characteristics have been investigated by analyzing the successive wave groups [38] and [71].

Wave grouping and its consequences are of significant concern, but there is little guidance and few practical formulae for use in practical engineering. The engineer needs to be aware of its existence and, for designs that would be sensitive to grouping-related phenomena, attempt to evaluate its importance to the problem of concern. This may involve performing numerical simulations or physical model simulations in which a wide variety of wave conditions are tested and are designed to include those with high levels of groupiness.

2.2.7 Random wave simulation

Given a one-dimensional parametric spectrum model or an actual wave energy density spectrum, it is sometimes necessary to use these quantities to calculate the height, period, and phase angle of a wave at a particular frequency. Such an approach for simulating random waves from a known wave spectra is sometimes termed the deterministic spectral amplitude method, since individual wave components in this superposition method are deterministic [6]. The method is also called the random phase method because the phases of individual components are randomly chosen [7]. Random waves simulated by this approach may not satisfy the condition of a Gaussian sea unless $N \to \infty$ in the limit. In practice, for $200 \le N \le 1200$ components, the spectrum can be duplicated accurately.

The wave profile generated by simulation methods is used in a number of engineering applications in spite of requiring a large number of components and considerable computer time. For example, random wave simulation is frequently used during modeling studies in a wave tank for duplicating a required target wave energy density spectrum. Random wave profiles are also extensively used in numerical models for calculating structural loads and responses due to a random sea. The simulation method permits direct prediction of the wave particle kinematics at any

location in a specified water depth for given wave height period pair and random phase angle.

There are two methods for simulating wave surface profiles from known wave spectra. They are deterministic and non-deterministic spectral amplitude methods. In the deterministic spectral simulation method, the wave height, period and phase angle associated with a frequency f_1 whose corresponding energy density is $E(f_1)$ and it may be obtained from the following formulas

$$H(f_1) = H\Big|_{f_1} = 2\sqrt{2E(f_1)\Delta f}$$

$$T(f_1) = T\Big|_{f_1} = \frac{1}{f_1} \tag{2.35}$$

$$\varepsilon(f_1) = \varepsilon\Big|_{f_1} = 2\pi r_N$$

where the phase angle ε is arbitrary since r_N is a random number between zero and one. The time series of the wave profile at a point x and time t may be computed by [131]

$$\eta(x,t) = \sum_{n=1}^{N} H(n)\cos[k(n)x - 2\pi f(n)t + \varepsilon(n)], \tag{2.36}$$

where $k(n) = 2\pi / L(n)$, and $L(n)$ is the wavelength corresponding to the nth frequency $f(n)$; N the total number of frequency bands of width Δf. It is not required to divide the spectrum curve equally, except that doing so greatly facilitates computations. The value of wave height is sensitive to the choice of Δf, but as long as Δf is small, this method produces a satisfactory random wave profile. The use of the equal increments, Δf, requires N to be greater than 50 to assure randomness and duplicating the spectrum accurately.

For the non-deterministic spectral amplitude method, the wave surface profile is represented in terms of two independent Fourier coefficients. These Gaussian distributed random variables a_n and b_n with zero mean and variance of $E(f)\Delta f$ are then obtained from

$$\eta(x,t) = \sum_{n=1}^{N} a_n \cos[k(n)x - 2\pi f(n)t] + \sum_{n=1}^{N} b_n \sin[k(n)x - 2\pi f(n)t] \tag{2.37}$$

In essence, an amplitude and a phase for individual components are replaced by two amplitudes, the coefficients of cosine and sine terms in the wave profile. This random coefficient scheme may yield a realistic representation of a Gaussian sea, provided that N is large for a true random sea. This method differs from the deterministic spectral amplitude approach by ensuring that sea state is Gaussian. Elgar [31]have considered simultaneous simulation of both narrow and broad-banded spectra using more than 1000 Fourier components, and concluded that both simulation methods yield similar statistics. These approaches may be extended to the two-dimensional case.

2.2.8 Kinematics and dynamics of irregular waves

Firstly, an individual wave is measured by either a wave-by-wave analysis or constructed synthetically (such as choosing, H_s, T_z, and a direction) and monochromatic theory is used to estimate the desired quantities at a given wave phase [33]. Next, pressure, velocity, and acceleration spectra are estimated by applying linear theory to translate the surface elevation spectra to the desired parameter [24]. Finally, the random wave simulation technique may be used to synthetically generate a surface time history and corresponding kinematic and dynamic properties [8]. Of the three methods, the last may provide the most realistic results, but it is also the most complex approach.

2.3 Numerical Ocean Wave Modeling

The basic theory of wave modeling is given in this section. The waves, considered in numerical wave prediction, is assumed to be "short" in the sense that they are not affected by the rotation of the earth. Also the effects of density stratification of the ocean is assumed to have no impact of the ocean waves. Description of the basic laws of wave motion in fluids, and an interpretation of the individual terms in the wave energy equation are presented.

2.3.1 Wave propagation

Considering the propagation of waves on the surface of a fluid, it is important to recognize the difference between the velocity of one individual wave and the group velocity, which expresses the velocity of the wave energy for a particular wave length. The surface elevation caused by one Fourier component may be expressed as (for simplicity we assume only one dimension of propagation)

$$\eta = \sin(kx - \omega t) \tag{2.36}$$

where $k = 2\pi / \lambda$ is the wave number and λ is the wave length. $\omega = 2\pi / T$ is the angular frequency and T is the wave period. The speed of one individual wave is

$$C = \frac{\omega}{k} \tag{2.37}$$

while the group velocity is defined as the rate of change of angular frequency to the wave number

$$C_g = \frac{d\omega}{dk} \tag{2.38}$$

For deep water waves, the dispersion relation yields

$$\omega = \sqrt{g\,k} \tag{2.39}$$

where g is the acceleration of gravity. In this case the relation between the wave speed and the group velocity becomes

$$C_g = \frac{1}{2}C \tag{2.40}$$

In deep water the wave energy may propagates with half the wave speed of the individual waves. However, for waves that are long compared with the ocean dept., the wave propagation speed will be independent of the wave length. In this case the relation between group and wave velocity will be

$$C = C_g = \sqrt{g\,H} \tag{2.41}$$

i.e. the wave energy will propagate with the same speed as the individual wave modes.

2.3.2 Swell

Definition: Swell is waves generated outside the area where they are observed. Generally, wave energy enters the ocean as short waves and ripples. Through the process of non-linear interaction between the wave modes in the spectrum, the wave energy will be transferred to longer waves, finally ending up as long swells at the shore. The frictional dissipation of energy in long waves (the order of 100 m and more) is extremely small, and wave energy generated in one part of the ocean may easily travel across the world oceans, ending up as swells at the shore on a different continent. When considering such waves one must take into account how waves behave on a globe. Generally, deep water wave propagation on a sphere will be along a great circle path. If the wave length is comparable with the ocean depth, waves propagating over a sloping bottom will be bent toward shallow areas. Long waves, compared to the ocean depth, will always be bent toward shallow areas when they

propagate over a sloping bottom. The modeling of swells propagating over large distances is difficult in numerical wave prediction models.

2.3.3 Conservation of wave energy

The wave energy spectrum

The main outcome of any wave prediction model is the energy spectrum. As mentioned, it is based upon the idea that the ocean surface could be represented by a series of harmonic functions with different angles and frequencies. As an example for one dimensional motion

$$\eta = \sum_{i}^{n} a_i \sin(k_i x + \omega_i t) + b_i \cos(k_i x + \omega_i t) \tag{2.42}$$

Here, the mean wave energy in one single frequency interval `df` will in this case be

$$dE_i = \frac{a_i^2 + b_i^2}{2} \tag{2.43}$$

The spectral energy pr. Frequency interval is then defined as

$$F(f, \theta, x, y, t) = \frac{dE_i}{df} \tag{2.44}$$

$F(f, \theta, x, y, t)$ must be interpreted as the mean energy in one place (x, y) of a Fourier component with one particular frequency, propagating in one particular direction. When the equation for the development of the wave spectrum, the basic assumption is that in absence of frictional dissipation, wind, bottom variation and nonlinear interaction, the wave spectrum will change according to

$$\frac{\partial F}{\partial t} + \nabla \cdot (C_g F) = 0 \tag{2.45}$$

which simply is an advection equation describing the change of the energy spectrum because of advection of wave energy with the group velocity (c_g). The effects of wind, friction and non-linear interaction are now introduced as source/sink terms in this equation

$$\frac{\partial \quad F}{\partial \quad t} + \nabla \cdot (C_g \quad F) = S_{in} + S_{ds} + S_{nl} + S_{bt} \tag{2.46}$$

A brief description of these sink and source terms will be given below

Wind input

The wind input source term represents the work done by the wind on the ocean surface to produce waves. The wind generation of waves takes place in the high frequency part of the spectrum, i.e. it produces the relatively short waves (the order of a few meters and less) which can be observed when wind is blowing on the surface. The basic theory behind wind input term was developed by Miles [86]. And it assumes a linear relationship between wave energy and the rate of change of energy,

$$\frac{\partial F}{\partial t} = S_{in} = \gamma \quad F \tag{2.47}$$

which gives an exponential growth of wave energy with time

$$F \approx F_0 e^{\gamma t}$$

A realistic parametrization of the interaction between wind and wave was given by Janssen [64], a summary of which is given below. The basic assumption Janssen [64] made, which was corroborated by his numerical results of 1989, was that even for

young wind sea the wind profile has a logarithmic shape, though with a roughness length that depends on the wave-induced stress. As shown by Miles [86], the growth rate of gravity waves due to wind then only depends on two parameters, namely

$$x = \frac{u_*}{C}\cos(\theta - \phi)$$
$$\Omega_m = \frac{g z_0}{u_*^2} \tag{2.48}$$

with u_* the friction velocity, θ the direction in which the waves propagate, ϕ the wind direction, C the phase speed of the waves and z_0 the roughness length. Thus, through Ω_m the growth rate depends on the roughness, which on its turn depends on the sea state. The growth rate, normalised by angular frequency ω, is given as

$$\frac{\gamma}{\omega} = \varepsilon \quad \beta x^2 \tag{2.49}$$

where γ is the growth rate, ω the angular frequency, ε the air-water density ratio and β the so-called Miles' parameter. In terms of the dimensionless critical height $\mu = kz_c$ (with k the wave number and z_c the critical height defined by $u_0(z = z_c) = c$) Miles' parameter becomes

$$\beta = \frac{\beta_m}{\kappa^2}\mu \ln^4(\mu), \ \mu \le 1 \tag{2.50}$$

where κ is the von Kármán constant and β_m a constant. In terms of wave and wind quantities μ is given as

$$\mu = (\frac{u_*}{kc})^2 \Omega_m \exp(\frac{k}{x}) \tag{2.51}$$

For positive values of the growth rate the wind will give at net input of wave energy to the ocean. In the wave model WAM this growth rate is always either positive or zero. It is important to note that in the real world, the growth rate may also have negative values. This means that the flow of energy is from the waves to the wind, i.e. that waves may generate wind. An example of this is very long waves or wind blowing in the opposite direction of the wind.

Dissipation of energy

Wave energy may be lost from the ocean in two different ways; wave breaking and frictional dissipation caused by velocity differences. White capping and breaking of waves takes energy from the waves and transfer some of it into current, the rest is dissipated, which means that mechanical energy is lost and water is heated up. The physical processes that takes place during wave breaking and white capping is extremely difficult to model. And in wave models these processes are parametrized by using data from several measurements. The dissipation source term is based on K. Hasselmanns [51] white capping theory according to Komen et al. [77]. In order to obtain a proper energy balance at high-frequencies the dissipation by white capping was extended by adding a k^2 term, thus

$$S_{ds} = (-\gamma_d)F \tag{2.52}$$

$$\gamma_d = \frac{1}{2} C_{ds} <\omega> (<k>^2 m_0)^2 \left(\frac{k}{<k>} + \left(\frac{k}{<k>}\right)^2\right) \tag{2.53}$$

where C_{ds} is constants, m_0 is the total wave variance per square meters, k the wavenumber and $<\omega>$ and $<k>$ are the mean angular frequency and mean wavenumber, respectively.

On the other hand, the dissipation of energy that takes place within the fluid because of velocity differences may by modeled in a way similar to that of wind input, as a linear relationship between the wave energy and the rate of change of energy.

Non-linear interaction

If wind input and frictional dissipation was the only processes that was acting to change the energy spectrum, ocean waves would consist of only short surface waves. Apparently, the ocean also consist of long swells which could not be generated by the wind directly. Such long waves are the result of energy cascades that takes energy from the short wind waves and feeds the longer waves with energy. When the wave amplitude becomes large, three waves with different wave lengths may interact through mechanical resonance and create a fourth wave length. Only a limited combination of waves makes this possible.

Evaluating the functional derivative of the energy of the wave F with respect to a^* then gives the deterministic evolution equation for a.

$$\begin{aligned}\frac{\partial}{\partial t}(a_1 + i\omega_1 a_1) &= -i\int d\ k_2\ \ d\ k_3\ \ V_{1,2,3}\, a_2 a_3 \delta\ (k_1 - k_2 - k_3) \\ +...+\ -i\int d\ k_2 d\ k_3 d\ k_4\, W_{1,2,3,4}\delta\ (k_1 + k_2 - k_3 - k_4)\, a_2^* a_3 a_4\end{aligned} \tag{2.54}$$

Where V and W are known functions of wavenumber.

To summarise, the evolution equation allows both three- and four-wave interactions, where for three-wave processes the resonance conditions

$$\omega_1 \pm \omega_2 \pm \omega_3 = 0,\ k_1 \pm k_2 \pm k_3 = 0 \tag{2.55}$$

should be satisfied simultaneously, and for four wave processes the resonance conditions

$$\omega_1 + \omega_2 - \omega_3 - \omega_4 = 0,\ k_1 + k_2 = k_3 + k_4 \tag{2.56}$$

where the components 1, 2 and 3 exchange energy with component 1. Expressions for the exchange of energy due to this mechanism. Pierson-Moskowitz spectrum is applied. This is a narrow-banded wave superposed on a Pierson-Moskowitz wave with the same peak frequency. As a representation of the JONSWAP spectrum however, this model is crude and the results are approximate only.

Bottom friction

The bottom may induce wave energy dissipation in various ways : e.g. friction, percolation (water penetrating the bottom) wave induced bottom motion and breaking. Outside the surf zone, bottom friction is usually the most relevant. It is essentially nothing but the effort of the waves to maintain a turbulent boundary layer just above the bottom.

Several formulation have been suggested for the bottom friction. A fairly simple expression, in terms of the energy balance is due to Hasselmann *at al.* [51] in the JONSWAP project:

$$S_{bl}(\omega,\theta) = -\Gamma \frac{\omega^2}{g^2 \sinh\ kd} F(\omega,\theta) \tag{2.57}$$

Where Γ is an empirically determined coefficient. Tolman [129] shows that this expression is very similar in its effects to more complex expressions that have been proposed.

2.4 The Neural Network Model

2.4.1 Artificial Neuron Model

The most commonly used neuron model, based on the model proposed by McCulloch and Pitts [85], [94] consisted of inputs, a bias, weights, an activation function and an output. Each neuron input, x_1, x_2, …, x_n, is weighted by the values w_1, w_2, …, w_n respectively. A bias is assigned by a constant input of 1 weighted by the value w_0. The out put, y, is obtained by summing the weighted inputs to the neuron an passing the result through an activation function, f, as shown in Figure 2.12.

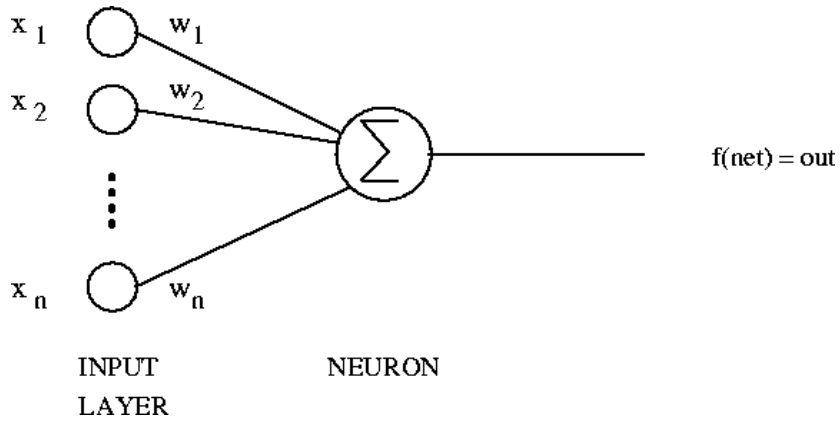

Figure 2.12 An Artificial Neuron

Various types of activation functions are possible such as linear, theshold, sigmoidal and herperbolic tangent functions.

2.4.2 Single Layer of Neuron

A single layer of neurons consists of *I* inputs and H neurons, each of all inputs is weighted to each of all neurons.

2.4.3 Multilayer Neural Network

A multilayer neural network consists of several single layer of neurons. The inputs of the network are the inputs of the first layer of neurons and the outputs of the network are the outputs of the last layer of neurons. The layer of neurons is called that the output layer and the other layers are called the hidden layers. A two-layer neural network is shown in Figure 2.13.

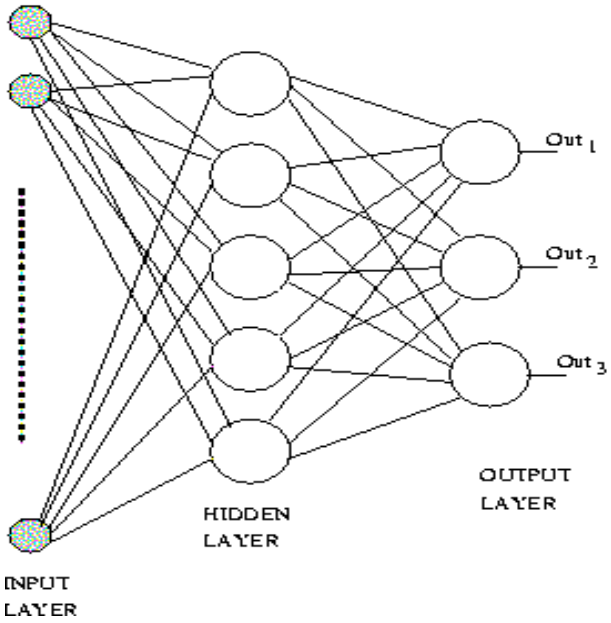

Figure 2.13 Two-layer neural network

The basic idea of training (Schmidt, 1996) is to present the input to the network; calculate in the forward direction the output of each layers and the final output of the network. For the output layer the desired values are known and therefore the weights can be adjusted as for each layer of neurons. One of the most popular training algorithms for multilayer neural network is backpropagation algorithm.

2.5 Hard and Soft Computing Approach

Physical systems described by multiple variable and multiple parameter models such as WAM model having non-linear coupling, frequently occur in the fields of marine meteorology. The conventional approaches (hard computing) for understanding and predicting the behaviour of such systems based on analytical techniques can prove to be very difficult, even at the initial stages of establishing an appropriate mathematical model. The computational environment used in such an analytical approach is perhaps too categoric and inflexible in order to cope with the intricacy and the complexity of the real world physical systems. It turns out that in dealing with such systems, one has to face a high degree of uncertainty and tolerate imprecision. Trying to increase precision can be very costly.

Soft Computing (SC) is a consortium of methodologies which provide a foundation for the conception, design and deployment of intelligent systems. The essence of soft computing is that unlike the traditional, hard computing, soft computing is aimed at an accommodation with the pervasive imprecision of the real world. Thus, the guiding principle of soft computing is: Exploit the tolerance for imprecision, uncertainty and partial truth to achieve tractability, robustness, low solution cost and better rapport with reality.

2.5.1 Hard computing approaches

The WAM model, which was developed by WAMDI-group (WAMDI group, 1988) and improved by Komen et al. (1994), is one of the best-tested wave models. It is widely used for global and regional operational wave forecasting in many marine and meteorological centers around the world, such as global operational wave forecasting at the European Centre for Medium-Range Weather Forecast (ECMWF). The model runs for any given regional and global grid with a prescribed topographic dataset. The grid resolution can be arbitrary in space and time. The computation can be done on a latitudinal-longitudinal or on a carthesian grid. The model outputs are significant wave height, mean wave direction and frequency, wind stress fields

including the wave induced stress, the drag coefficient and 2D wave spectrum at any selected grid points and time.

The model was continually updated to incorporate the latest results of research. The further development of the model is decided by the WAM model development group (WAMDI group, 1988). The WAM model is available to the entire research and forecasting community. It is expected that results achieved with the model are made available in return to the wave modeling group. So far four cycles of the model have been issued. The last cycle 4 (technically enhanced version of cycle 3) was carried out by Gunther et al. (1991) and using addition new wind inputs developed by Janssen (1991).

The WAM model solves the wave action density transport equation without predefined spectral constraints. The model is applicable in a broad range of wave conditions, ranging from quite daily to tropical cyclone wave conditions. As described in Komen et al. (1994) this wave model solves the transport equation of the directional wave spectrum (Eq. (2.58)).

$$\frac{dF}{dt} + \frac{\partial(\dot{\phi}F)}{\partial\phi} + \frac{\partial(\dot{\lambda}F)}{\partial\lambda} + \frac{\partial(\dot{\theta}F)}{\partial\theta} = S \tag{2.58}$$

where F represents the spectral density with respect to $(f, \theta, \phi, \lambda)$, f denotes frequencies, θ is the wave direction, ϕ and λ are the latitude and longitude, respectively, and $\dot{\phi}$, $\dot{\lambda}$, $\dot{\theta}$ are the rate of change of the position and propagation direction of a wave packet traveling along a great circle path. The source terms, S represents a superposition of the wind input, S_{in} white capping dissipation, S_{dis} and nonlinear transfer function, S_{nl} (see Eq. (2.59)).

$$S = S_{in} + S_{dis} + S_{nl} \tag{2.59}$$

The wind input term was adopted from Snyder et al. (1981). Wind input and dissipation terms of the present cycle 4 of the wave model are a further development

based on Janssen's quasi-linear theory of wind-wave generation (Janssen 1989, 1991). The dissipation source term is based on Hasselmann et al. (1974) white capping theory. The nonlinear source term is a parameterization of the exact nonlinear interactions as proposed by Hasselmann et al. (1985). The basic form of the exact nonlinear expression is retained. However the five-dimensional continuum of all resonant quadruplets is reduced to a two-dimensional continuum by considering only a pair of discrete interaction configurations.

The WAM model can be used, in principle, for deep and shallow water conditions, considering (or not) depth and current refraction. Extensively applied and tested for different meteorological conditions, it has a well establish performance envelope. However, one of the limitations of WAM appears when the propagation time step is larger that the source term integration time step (usually for high spatial resolutions in shallow waters). The small time step for propagation, requires a small time step for the source term integration and is consequently excessive and impractical (Monbaliu et al. 1998). Another limitation is that typical physical processes of shallow water waves are not considered in WAM cycle 4.0 (Diffraction, triad-wave interactions, depth-induced wave breaking, etc).

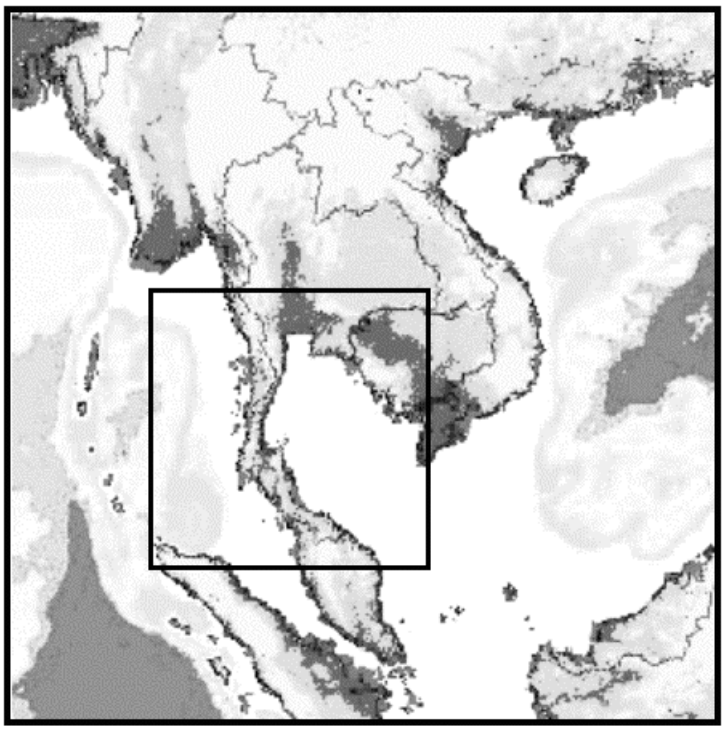

Figure 2.14 Boundary of coarse grid

A high grid-resolution third generation wave forecasting system has been developed for the east coast of southern part of Thailand and the Gulf of Thailand. The general objective of this system is to complement predictions of the present operational global wave model for the Gulf of Thailand coastal areas and to replace the operational wave model for the Gulf of Thailand. Since the present global model has a grid resolution of 1 deg. by 1 deg., the resulting predictions can not describe wave conditions over the coastal areas with sufficient detail. Because the present Gulf of Thailand model is a second generation model and does not consider waves propagating into the gulf from south China sea (It assumes the gulf is a closed basin.), it cannot predict realistic typhoon wave conditions in the gulf. A particular objective is to use the East Coast of southern part and Gulf of Thailand model as a basis to provide forecast guidance for selected locations along the east coast and the gulf coast where detailed description of wave fields are required.

In order to satisfy the above-mentioned objectives within the constraints of computational economy and computer memory, a model which is capable of handling

multiple grids must used. Furthermore, in view of the frequent occurrence of typhoons and extra-tropical cyclones which affect the east coast and the gulf areas, the wave model must also provide adequate descriptions of the sea state under rapidly varying weather conditions. In addition, consideration has to be given to the effects of water depth and ocean currents on the transformation of surface waves. At present, the WAM model readily meets these requirements. The capabilities of the WAM model have been assessed in SWAMP (1985), WAMDI (1988) and Komen et al (1994).

The system employs the WAM model Cycle-4 version software package (Gunther, Hasselmann and Janssen, 1991). The model solves the energy balance equation for the frequency-direction surface wave spectrum. We have assumed that the water surface elevation is not a function of time, and there are no currents involved. Thus, the physics of the energy balance equation involves mainly spherical propagation, shoaling and depth refraction, bottom dissipation, wind forcing, white capping, and wave-wave interactions.

The system consists of two grids named coarse (Fig. 2.14) and fine (Fig. 2.15). The coarse grid has a grid size of 0.5 deg. by 0.5 deg. It covers from latitude 0 deg. N to 25 deg. N and from longitude 90 deg. E to 115 deg. E. The purpose of this grid is to simulate swell which may propagate to the area of interest from far north and far south in the model domain. It also provides boundary conditions for the fine grid. The fine grid extends from 95 deg. E to 105 deg. E and from 5 deg. N to 15 deg. N. It covers the east coast and the Gulf of Thailand. The purpose of the Gulf of Thailand is to simulate typhoon waves generated in the region entering the gulf through the Vietnam Cape. The grid size is 1/4 deg. by 1/4 deg..

The prognostic part of the wave spectrum has 25 frequencies and 12 directions for all grids. The frequency is determined according to the logarithmic scale: f (m)=1.1f(m-1), where f, is the frequency, and m is the band number of the frequency. The minimum frequency (corresponding to the first frequency band, f(1)) is given to be 0.042 Hz. While the maximum frequency is 0.411 Hz. The computational time step

for the source term is the same as the propagation term; for coarse grid, the time step is 20 minutes, for fine grid, 5 minutes is used.

The required input data includes water depth and wind fields. The gridded depth fields are derived from bathymetry data of 5-minute grid-spacing obtained from the National Geophysical Data Center. Input wind fields, at 10 meters above the mean sea level, are obtained from NRLMRY's operational atmospheric models: the Global Atmospheric Spectral Model – NOGAPS specified at one degree intervals for coarse grid and fine grid. Wind data are given at three hour intervals up to 24 hours.

The system runs twice daily using wind data from NOGAPS run at 00Z (and 12Z). Each cycle produces up to 24 hour forecasts at three hour intervals. For coarse grid, a 12 hour hindcast is performed by using analyzed wind fields to provide initial wave fields for the forecast.

The source terms integration was performed with an implicit scheme while the propagation term was done by the first order upwind flux scheme. The CPU time and memory usage depended on the region of interest and the grid resolution. In this study 20 hrs. CPU time is needed for a 5 months simulation using a Pentium IV 2.6GHz on Linux system and resolution of grid at 0.25 by 0.25 degree lat-long grid (for fine grid), 25 frequencies, and 12 directions.

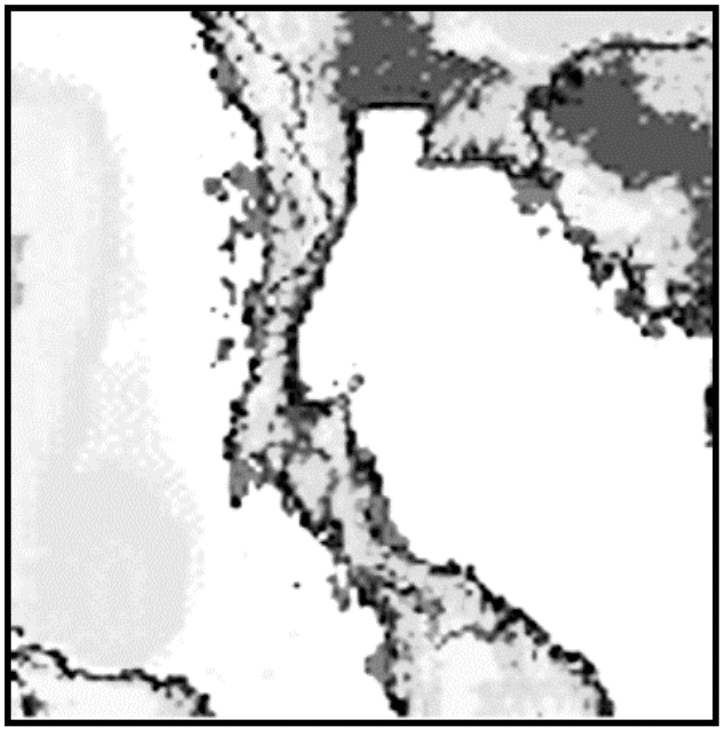

Figure 2.15 Boundary of nested grid

They can then be interpolated in space and time to the boundary points of the fine subgrid and the model can be rerun on the fine mesh grid at resolutions are 0.25 x 0.25 degree latitude-longitude.

The model results are saved in four files,

1) gridded output fields of significant wave height, mean wave direction, mean frequency (inverse of mean period), friction velocity, wind direction, wave peak frequency, drag coefficient and normalized wave stress,
2) swell gridded output fields of swell wave height, mean swell direction, mean wind wave direction and mean swell frequency,
3) spectra at selected grid points,
4) swell spectra at selected grid points.

2.5.2 Soft computing approaches

Use of neural network (NN) techniques to solve problems in civil engineering began in the late 1980s [34]. Their applications to simulating and forecasting problems in water resources are few and relatively recent [35, 59, 123, 18, 2, 3, 79, 60]. The NN modeling techniques used to solve oceanographic problems are also a relatively new area of research [132, 29, 130, 58, 78, 118]. Unlike other conventional-based models, NN model is able to solve problems without any prior assumptions. As long as enough data are available, a neural network will extract any regularities or patterns that may exist and use it to form a relationship between input and output. Additional benefits include data error tolerance and the characteristic of being data-driven, thereby providing a capacity to learn and generalize patterns in noisy and ambiguous input data.

Theorem of GRNN

Let x be a vector of random variables and y a scalar random variable. Let X be a particular measured value of x. In other words, X is the finite vector of noisy measurements of x, and y represents the associated scalar value. The conditional mean of y given X is defined by

$$E[y \mid X] = \frac{\int_{-\infty}^{\infty} y f(X, y) dy}{\int_{-\infty}^{\infty} f(X, y) dy} \tag{2.60}$$

where $f(X, y)$ denotes the joint continuous probability density function (pdf) of a vector random variable X and a scalar random variable y. If $f(X, y)$ is not known, an estimate $\hat{f}(X, y)$ must be used. Parzen [95] proposed a class of consistent estimators for $f(X, y)$. Using window estimation, $\hat{f}(X, y)$ can be written as

$$\hat{f}(X,y)=\frac{1}{(2\pi)^{p+1}\sigma^{p+1}}\cdot\frac{1}{n}\sum e^{(-(x-x^i)^T(x-x^i))/2\sigma^2}\cdot e^{(-(y-y^i))/2\sigma^2} \tag{2.61}$$

where $x\in R^p$ and n is the number of sample observations. Using (2.60), (2.61) becomes

$$\hat{y}=\frac{\sum_{i=1}^{n} e^{(-(x-x^i)^T(x-x^i))/2\sigma^2}\int_{-\infty}^{\infty} ye^{-(y-y^i)^2/2\sigma^2}dy}{\sum_{i=1}^{n} e^{(-(x-x^i)^T(x-x^i))/2\sigma^2}\int_{-\infty}^{\infty} e^{-(y-y^i)^2/2\sigma^2}dy} \tag{2.62}$$

Let $D_i^2=(X-X^i)^T(X-X^i)$; then the estimate of the expected value $\hat{y}$ becomes

$$\hat{y}=\frac{\sum_{i=1}^{n} y^i e^{-D_i^2/2\sigma^2}}{\sum_{i=1}^{n} e^{-D_i^2/2\sigma^2}} \tag{2.63}$$

These density estimators are consistent; i.e., they asymptotically converge to the underlying joint pdf f(x,y) at all points (x,y) provided that $\sigma=\sigma(n)$ is chosen such that

$$\lim_{n\to\infty}\sigma(n)=0 \text{ and } \lim_{n\to\infty}n\sigma^p(n)=\infty$$

Here σ can be visualized as a smoothing parameter. That is, if σ is made large, the estimated density is forced to be smooth and the limit becomes a multivariable Gaussian with covariance $\sigma^2 I$. On the other hand, a smaller value of σ allows the estimated density to assume non-Gaussian shapes. In such case, wild points may have too great an effect on the estimate.

Thus, given the joint pdf of X and y, the conditional pdf can be determined and, hence the expected value can be computed. Cacoullos [17] extended Parzen's method to the multivariable case. The resulting regression procedure is implemented via three layers of parallel neural network architecture [114, 115], where it called a general regression neural network.

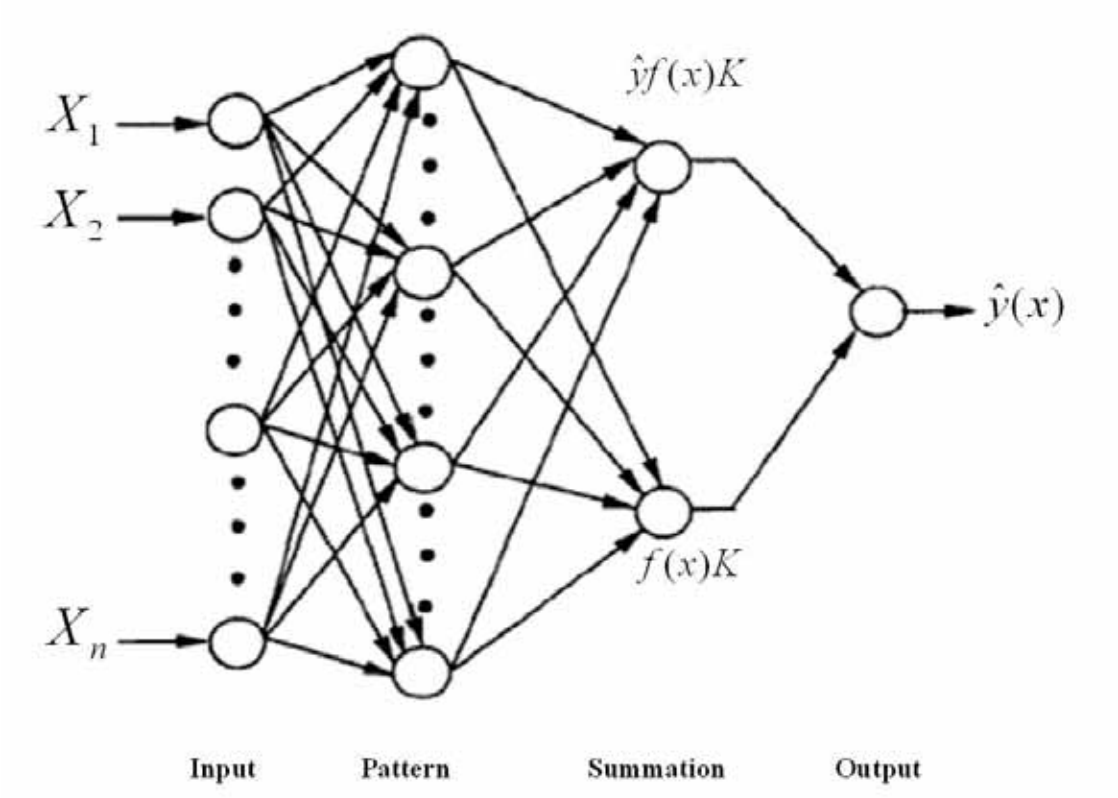

Figure 2.16 GRNN Block Diagram

Figure 2.16 show a feed forward network that that can be used to estimate a vector Y from a measurement vector X. The input units are merely distribution units, which provide all of the (scaled) measurements variables X to all of the neurons on the second layer (the pattern unit). Each pattern unit is dedicated to one exemplar or one cluster center.

Ocean wave model by GRNN

The GRNN is a neural network architecture that can solve any function approximation problems in the sense of estimating a probability distribution function. The network was firstly developed by Specht [115]. The learning process is equivalent to finding a surface in a multidimensional space that provides a best fit being measured by some statistical parameters. In GRNN, nearer projected state is weighted heavier than the remotely projected state in the phase space, which is a reasonable approximation.

The GRNN is a three-layer network with one hidden layer described in Figure 3.4. Each layer has entirely different roles:

- The input layer, where the inputs are applied.
- The hidden layer, where a nonlinear transformation is applied on the data from the input space to the hidden space, in most applications the hidden space is of high dimensionality.
- The linear output layer, where the outputs are produced.

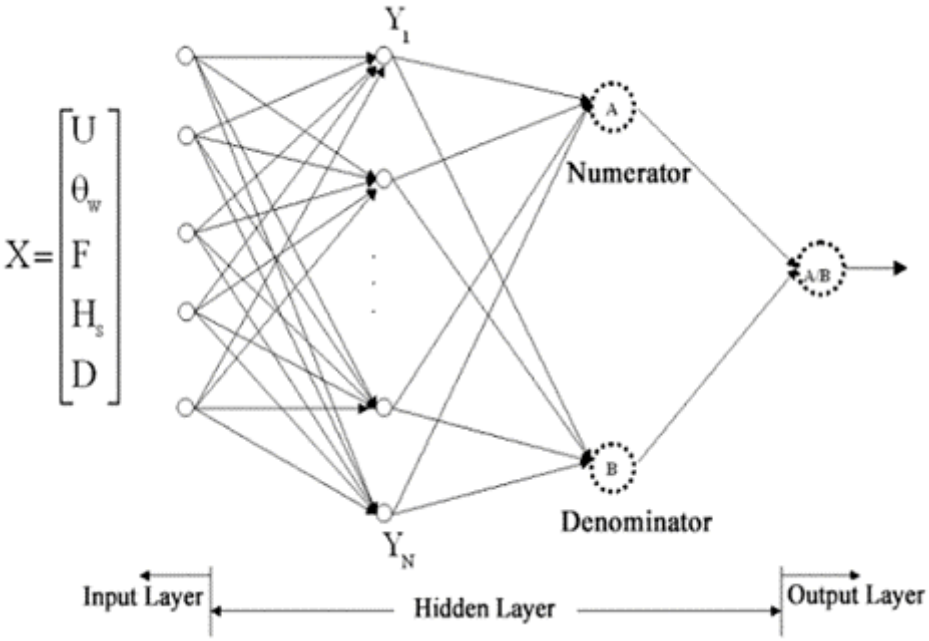

Figure 2.17 GRNN architecture of ocean wave forecast model

The input is a state space denoted by X_t (U_{10} = wind velocity at 10 m above the mean sea level, θ_w : wind direction, F_L : fetch length, H_s : significant wave height, D_w : sea depth) and the desired output is the future value, i.e. Y_{t+T}. The future prediction value (O_{t+T}) is calculated by Eq. (2.64).

$$O_{t+T} = \frac{\sum_{i=1}^{N} Y_{t+T} \exp(-\frac{D_i^2}{2\sigma^2})}{\sum_{i=1}^{N} \exp(-\frac{D_i^2}{2\sigma^2})} \tag{2.64}$$

where N is the number of input patterns, D_i^2 is a scalar function representing the Euclidean square from the new input pattern to the training input pattern, and σ is a single smoothing parameter which determines how tightly the network matches its predictions to the data in the training patterns.

CHAPTER III

MATHEMATICAL MODEL

3.1 Construction of Model

The mathematical description of surface waves has a large random element, which requires a statistical description with the statistical parameters. These parameters represent the wave field characterizing the conditions over a certain time period and spatial extent. Based on the assumption that the system is stationarity (steadiness in time) and spatial homogeneity, of these scales (time step or grid length) must be small enough to resolve the wave evolution. It must also be recognized that in time or space there are always going to be smaller-scale events which have to be overlooked.

In this thesis, our model is the spectral energy balance equation with unknown function of the energy density spectrum. It is a function of frequency and direction of wave propagation. This representation is particularly useful because it can interpret the wave physics with a sinusoidal wave in terms of the spectral components, $E(f,\theta)$. Using this spectrum, we obtain the parameters such as the significant wave height, the frequency spectrum, the peak frequency and secondary frequency maxima, the directional spectrum, the primary wave direction, any secondary wave directions and the zero-crossing period.

There is a reasonable conception of the physical processes, which are thought to control wave fields. Here, these processes are described by the response of wave ensembles, which can be translated into terms of useful statistical quantities such as the wave spectrum. Because all the processes are not yet fully understood, empirical results have been used to various degrees in the models.

3.1.1 The wave energy balance equation.

The concepts described in this chapter concern the development of wave models that suitable for the Gulf of Thailand. The formulation of numerical models is based on the elements as shown in Figure 3.1 and involves the following spectral energy balance equation.

$$\frac{\partial E}{\partial t} + c_g \cdot \nabla E = S \qquad (3.1)$$

where $E = E(f, \theta, x, t)$ is the two-dimensional wave spectrum (surface variance spectrum) depending on frequency, f, and direction of propagation, θ;

$c_g = c_g(f, \theta)$ is the deep-water group velocity.

The net source function S on the right hand side of equation (3.1) is the sum of energy input by the wind, S_{in}, the non-linear energy transfer by wave-wave interactions, S_{nl} and the dissipation, S_{ds}.

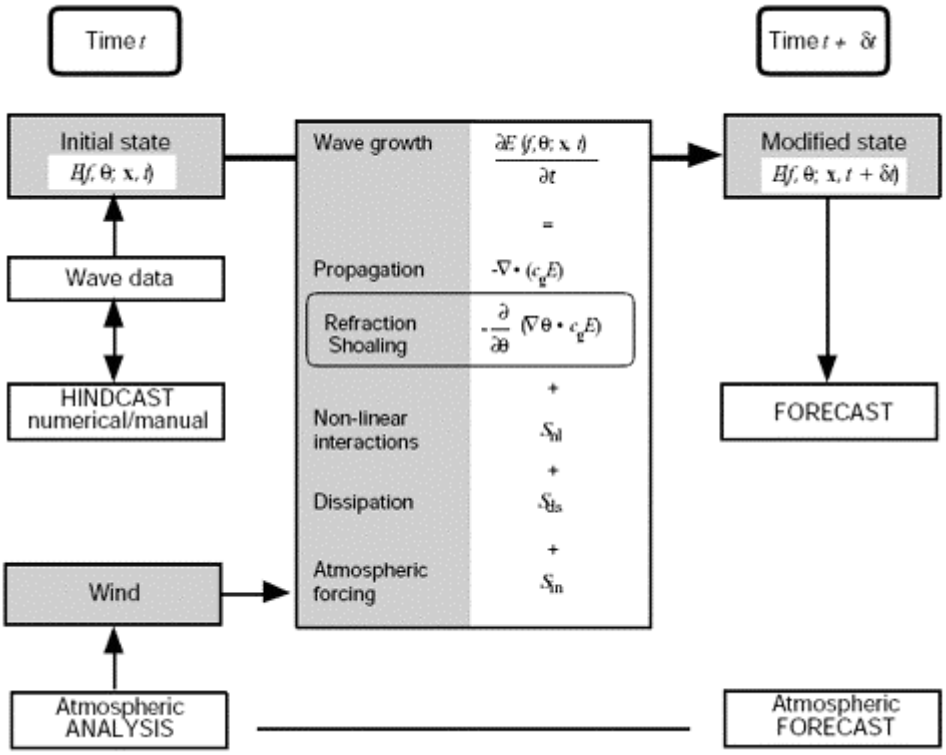

Figure 3.1 The elements of wave modelling [44]

3.1.2 Elements of wave modelling

The essence of wave modelling is to solve the energy balance equation (3.1). We then need to define an initial condition of energy.

Moreover, we also need to define the source terms on the right hand side of equation 3.1. These source terms correspond to the conditions in the Gulf of Thailand.

Initial conditions and Boundary conditions

Firstly, we start with a flat sea and then ‘spin up” the model with the winds from a period of several days prior to the period of interest. We then have a hindcast derived for the initial time.

The most important element in wave modelling is the motion of the atmosphere above the sea surface. We then consider the wind as an input of energy to the sea surface over the time scales. The energy transfer to the wave field is achieved through the surface stress applied by the wind, which varies roughly as the square of the wind speed.

It is known well that the atmosphere has a complex interaction among the wave field, wind speeds, wind profile and influence of the waves themselves on the atmospheric boundary layer.

In this study, a wind history or prognosis is given by supplying the wind field and its fetch at a series of time steps to the model. The wind field specification and the boundary configuration are then used in the propagation scheme.

Since the atmospheric boundary layer is not completely independent of the wave field, the wind input is dominated by a feedback mechanism depending on the energy in the wave field. The rate at which energy is fed into the wave field is designated by S_{in} which can be expressed as

$$S_{in} = A(f,\theta) + B(f,\theta)\,E(f,\theta), \tag{3.2}$$

where on the right hand side $A(f,\theta)$ is the resonant interaction between waves and turbulent pressure patterns in the air suggested by Phillips [97] and the second term represents the feedback between growing waves and induced turbulent pressure patterns as suggested by Miles [86] as

$$B(f,\theta) = \max\left[0, K_1 \frac{\rho_a}{\rho_w}\left(K_2 \frac{U_5}{g} f\cos\theta - 1\right) 2\pi f\right] \tag{3.3}$$

where ρ_a and ρ_w are the densities of air and water respectively; K_1 and K_2 are constants; and U_5 is the wind speed at 5 meters.

Equation (3.3) may be redefined in terms of the friction velocity $u_* = \sqrt{\tau / \rho_a}$, where τ is the wind shear stress. From a physical point of view, scaling wave growth to u_*, would be preferable to scaling with wind speed U_z at level z [76] U_z and u_* do not appear to be linearly related and the drag coefficient, C_d, used to determine τ, ($\tau = C_d U_z^2$) appears to be an increasing function of U_z.

In the case of a fully developed sea as given by the Pierson-Moskowitz spectrum E_{PM} [101], it is generally accepted that the dimensionless energy, ε,

$$\varepsilon = \frac{g^2 \int E_{PM}(f)\, d\, f}{u_*^4} = \frac{g^2 E_{total}}{u_*^4}$$

is a universal constant. If C_d is a function of U_{10} and ε is scaled in terms of U_{10}, this saturation limit then vary significantly with wind speed. Neither equation (3.3) nor the dependence of C_d on U_z are well documented in strong wind.

The term S_{ds} describes the rate at which energy is lost from the wave field. In deep water, this is mainly through wave breaking (whitecapping). In shallow water it may also be dissipated through interaction with the sea bed (bottom friction). In this study, we define S_{ds} as

$$S_{ds}(f,\theta) = -\psi(E)\frac{f^2}{\overline{f}} E(f,\theta), \qquad (3.4)$$

where $\psi(E)$ is a property of the integrated spectrum, E. ψ may be formulated as a function of a wave steepness parameter ($\xi = E\overline{f}^4 / g^2$, where $\overline{f}$ is the mean frequency). Forms for ψ have been suggested by Hasselmann [52] and Komen *at al.* [76].

The term S_{nl} describes the nonlinear interactions between the wave components. Its effect in the dominant region of the spectrum near the peak is greater than the dissipation. The excess energy is transferred by the non-linear interactions towards higher and lower frequencies. At the higher frequencies the energy is dissipated, whereas the transfer to lower frequencies leads to growth of new wave components on the forward side of the spectrum. This results in migration of the spectral peak towards lower frequencies. The non-linear wave-wave interactions preserve the spectral shape and can be calculated exactly. Here, we define S_{nl} as

$$S_{nl}(f,\theta) = f\iiint dk_1 dk_2 dk_3 \delta(k_1 + k_2 - k_3 - k)\delta(f_1 + f_2 - f_3 - f) \\ \left[n_1 n_2 (n_3 + n) - n_3 n (n_1 + n_2)\right] K(k_1, k_2, k_3, k) \tag{3.5}$$

In this integral, the delta functions, δ, enforce the resonance conditions, the (f_i, k_i) for i = 1, 2, 3 are the frequency and wavenumber pairs for the interacting wave components, the $n_i = E(f_i, \theta_i)/f_i$, are the wave action densities, and the Kernel function, *K*, gives the magnitude of the energy transfer to the component k, (or (f, θ)) from each combination of interacting wave components.

It is noted that wave energy propagates not at the velocity of the waves or wave crests but at the group velocity. In our modelling, we are dealing with the important descriptors such as the energy density and so it is the group velocity, which is important.

3.2 Finite Difference Method

The energy balance equation (3.1) can be solved numerically using finite difference schemes on a discrete grid as exemplified in Figure 3.2. Let Δx_i, (i=l,2) be the grid spacing in the two horizontal directions, Equation 3.1 may take such a form as

$$E(x,t+\Delta t) = E(x,t) - \Delta t \sum \left[\frac{(c_{gi}E)_x - (c_{gi}E)_{x-\Delta x_i}}{\Delta x_i} \right] + \Delta t \; S(x,t), \qquad (3.6)$$

where Δt is the time step, E and S are functions of wavenumber (k), or frequency and direction (f, θ).

Using the representation $E = E(f, \theta)$ we have energy density as an array of frequency direction bins (f, θ). The above approach collects a continuum of wave components travelling at slightly different group velocities into a single frequency bin. Due to the dispersive character of ocean waves, the area of a bin containing components within $(\Delta f, \Delta \theta)$ should increase with time as the waves propagate away from the origin. In the finite difference approach, all components propagate at the mean group velocity of the bin so that the energy field acquires a spotty appearance in contrast to the continuous distribution of the real world.

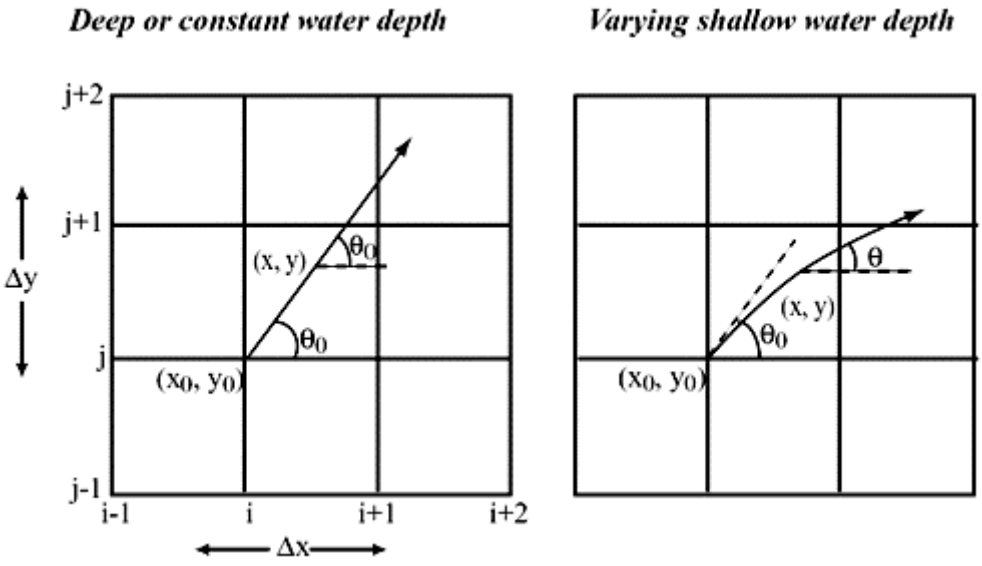

Figure 3.2 - Typical grid for numerical wave models (x stands for x_1 and y for x_2). In grid-type models the energy in (f, θ) bins is propagated between points according to the equation (3.6). In ray models the energy is followed along characteristic lines.

The discrete grid models calculate the complete (f, θ) spectrum at all sea

points of the grid at each time step.

In this thesis, we also used the Ray tracing method to solve the energy balance (3.1) along characteristics or rays. The time integration is still performed. but the spatial integration is not needed and the effect of discrete grids is avoided. The number of output points is thus reduced for reasons of computational costs.

For ocean waves there is a dispersion relation, relating the wave frequency to the wavenumber, of the form

$$f(x,t) = \sigma[k(x,t), \Psi(x,t)] \tag{3.7}$$

Here, σ denotes the particular frequency associated with wavenumber k, and the property of the medium, Ψ, which in this context will be the bottom depth and/or currents. Characteristic curves are then obtained by integration of

$$\frac{d\ x}{d\ t} = c_g = \frac{\partial\ \sigma}{\partial\ k} \tag{3.8}$$

and in an ocean with steady currents these curves need only be obtained once.

Thus, starting from the required point of interest, rays or characteristics are calculated to the boundary of the area considered necessary to obtain reliable wave energy at the selected point. Since we are considering the history of a particular wave frequency, our reference frame moves with the component. We then express the source function along the rays.

$$\frac{\partial\ E}{\partial\ t} = S \tag{3.9}$$

Rays are calculated according to the required directional resolution at the point

of interest; along each ray, equation (3.9) may be solved either for each frequency separately or for the total energy. The interactions in frequency domain are included but the directions are uncoupled.

Since the ray approach has been extensively used in models where wind-sea and swell are treated separately. In such cases, swell is propagated along the rays subjected only to frictional damping and geometric spread. Interactions with the wind-sea may take place where the peak frequency of the Pierson-Moskowitz spectrum ($\approx 0.13 \quad g/U_{10}$) is less than the swell frequency.

3.3 Numerical Implementation

Many of the differences between numerical wave models result from the way in which they cater for the weakly nonlinear wave-wave interactions (S_{nl}). The differences are particularly noticeable in the case of non-homogeneous and/or non-stationary wind fields. When the wind direction changes, existing wind-sea becomes partly swell and a new wind-sea develops. The time evolution of these components results in a relaxation of the wave field towards a new steady state that eventually approaches a fully developed sea in the new wind direction.

Three mechanisms contribute to the directional relaxation. There are (1) energy input by the wind to the new wind-sea (2) attenuation of the swell and (3) weak non-linear interactions, resulting in energy transfer from swell to wind-sea.

The way these mechanisms are modelled may yield significant deviations between models. The third mechanism appears to be dominant in this respect.

Water depth can considerably affect the properties of waves and how we model them. We know that waves “feel” the sea bed and are changed significantly by it at depths less than about one-quarter of the deep-water wavelength. In a sea with a wide spectrum, the longer waves may be influenced by the depth without much effect on the short waves. In absolute terms, a useful rule of thumb is to disregard the effects of

depth greater than about 40 m unless the waves are very long, i.e. if a large portion of the wave energy is in waves with periods greater than 10 seconds.

A major effect of depth is on the propagation characteristics. Waves are slowed down and, if the seabed is not flat, may be refracted. Also, the non-linear interactions tend to be enhanced and; of course, there are more dissipative processes involved through interaction with the sea bed. The framework we are describing for wave modelling is broad enough in its concept to be able to cope with depth-related effects without drastic alterations to the form of the model outlined in Figure 3.1.

The most existing wave models have an open ocean boundary. Wave energy may then enter the modelled area. The best solution is to obtain boundary data from a model operating over a larger area such as coarse grid model. If there is no knowledge of the wave energy entering the model area, a possible boundary condition is to let the energy be zero at the boundaries at all times. Another solution may be to specify zero flux of energy through the boundary. In either case it will be difficult to get a true representation of distantly generated swell. The area should therefore be sufficiently large to catch all significant swell that affects the region of interest.

In this thesis, we set up WAM models, with coarse grid resolution is 0.5 by 0.5 deg, it is difficult to get a true representation of coastlines and islands. A coarse resolution will strongly affect the shadowing effects of islands and capes. To obtain a faithful representation of the sea-state near such a feature we will require special precautions. One solution may be to use a finer grid for certain areas, a so-called “nested” model, where results from the coarse grid are used as boundary input to the fine grid. It is 0.25 by 0.25 deg. Another way may be to evaluate the effects of the topographic feature for affected wave directions at a certain number of grid points and tabulate these as “fudge factors” in the model.

The wave models are implemented on the Gulf of Thailand consists of two grids named coarse and fine. The coarse grid has a grid size of 0.5 deg. by 0.5 deg. It covers from latitude 0 deg. N to 25 deg. N and from longitude 90 deg. E to 115 deg.

E. The purpose of this grid is to simulate swell which may propagate to the area of interest from far north and far south in the model domain. It also provides boundary conditions for the fine grid. The fine grid extends from 95 deg. E to 105 deg. E and from 5 deg. N to 15 deg. N. It covers the east coast and the Gulf of Thailand. The purpose of the Gulf of Thailand is to simulate typhoon waves generated in the region entering the Gulf through the Vietnam Cape. The fine grid size is 1/4 deg. by 1/4 deg..

CHAPTER IV

NUMERICAL RESULTS

4.1 Parameter Study

Data

Bathymetry grid is taken from ETOPO5 covering the region 95°E to 105°E and 5°N to 15°N (see Figure 4.1) with 0.25 degree resolution in both latitude and longitude (41 x 41 grids). The initially employed wind data (from NOGAPS Model archives) were provided by the NRLMRY. The winds are from the period 00Z 1-8-97 to 00Z 31-12-97, with 1.0° resolution and are linearly interpolated to specify wind components at each wave grid point. During 1^{st} – 4^{th} November, 1997, strong northeasterly winds associated with a significant tropical cyclone activity were observed in the Gulf of Thailand. The wind speed reached up to 22 m/s over the area of study. Wave data were obtained from 3 moored buoys of GISTDA (HHN, KCH, and KSI stations) and 1 automatic marine meteorological station (UNC station).

Experiments

In this study we are interested ocean wave forecasting in the Gulf of Thailand by hard computing as WAM and soft computing as GRNN model. In order to forecast significant wave height in period such as 01 August – 31 December 1997, it was tropical cyclone case and make comparison of WAM and GRNN with observing data.

The tropical disturbance that would become Typhoon Linda (30W) formed within an area of convection east of the Philippine Islands near 10N 130E on 26 October 1997. The disturbance was mentioned in the Significant Tropical Weather Advisory (ABPW) as it tracked westward over the next several days under the

subtropical ridge to the north. Convection began to increase over the disturbance as it entered the Sulu Sea on 30 October 1997. At 0730Z on the 31st, a Tropical Cyclone Formation Alert (TCFA) was issued as deep convection continued to organize about the disturbance's center. The first warning on Tropical Depression (TD) 30W was issued approximately 12 hours later.

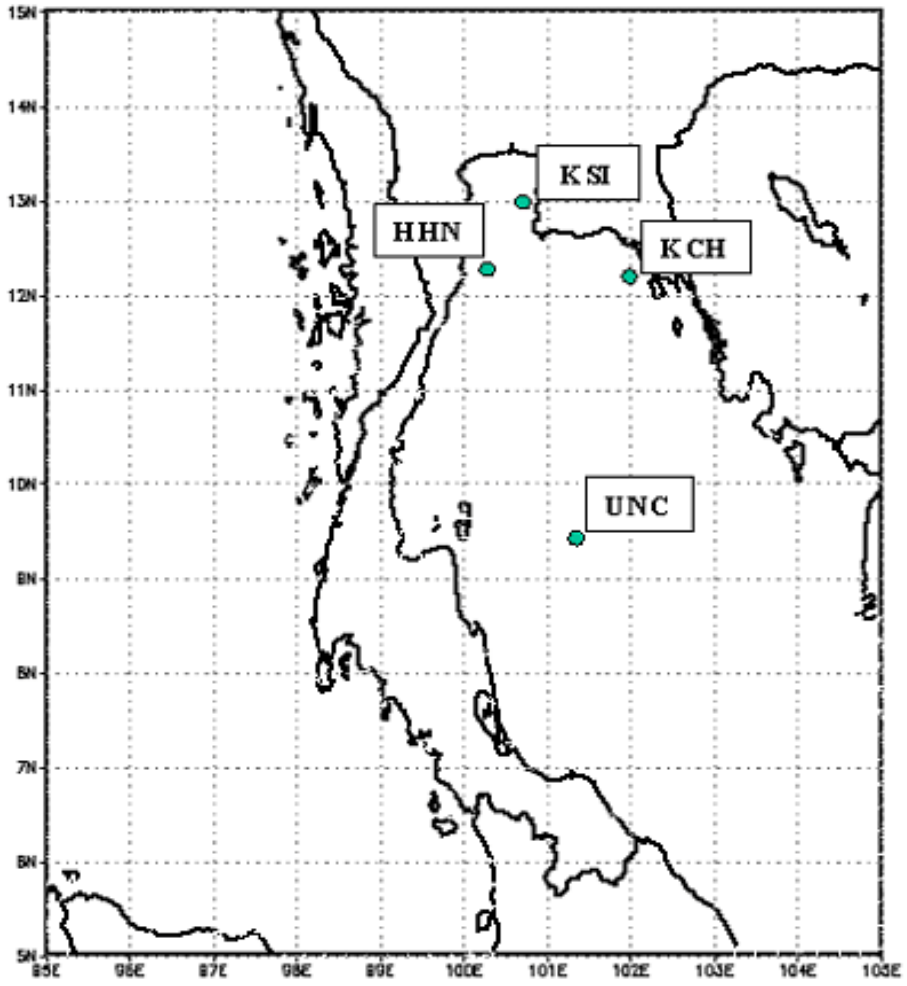

Figure 4.1 Study area

The newly formed tropical cyclone reached tropical storm intensity within 24 hours as it tracked over the South China Sea. At this point, Tropical Storm Linda (30W) accelerated westward toward the southern tip of Vietnam. It tracked over the

Vietnamese province of Ca Mau at 0900Z on the 2nd November 1997 with an intensity of 55 kt (28 m/sec).

Linda reached typhoon intensity shortly after entering the Gulf of Thailand. The cyclone turned northwestward following steering from the subtropical ridge. The system weakened slightly to 55 kt (28 m/sec) prior to striking the Malay Peninsula at 1600Z on 03 November. Crossing the Malay Peninsula, Linda further weakened as it encountered the region's 3000 ft (914 m) to 5000 ft (1524 m) mountains. However, once over the warm waters of the Andaman Sea, the system began to reconsolidate. This was the first tropical cyclone since Typhoon Forrest (30W) in 1992 to cross from the Western North Pacific to the North Indian Ocean.

4.2 Numerical Simulation

Using WAM model the wave hindcasting was carried out using 12 directional bands, 25 frequency bands and frequency interval extending from 0.042 to 0.41 Hz. A 5 minutes time step has been used for the integration of advection and source terms, considering depth refraction. The output time step was 6 hours and a JONSWAP spectrum was selected as an initial condition. The wind data during November 1st – 4th, 1997 was used to investigate the generated wave fields under the typhoon event. Wind fields, significant wave heights and peak wave periods are shown every 6 hours from Figure 4.3 to 4.5. The wind and wave directions are plotted using the meteorological convention with arrows every 10 grid points.

Figure 4.3 shows the wind input (NOGAPS), characterized by the speed and direction. On November 3rd, 1997, the wind field at 00 UTC was uniform along the shoreline with speeds approximately 10 m/s. The simultaneous wave fields displayed 2.0 m height with the maximum of 3.6 m near the storm center. Six hours later (at 06 UTC), the wind fields became more well organized with a speed of 12 m/s and 18 m/s along the shoreline and near the storm center, respectively. The storm still kept moving to the west and hit the landfall at 18 UTC. The wave of about 4.5 m height was observed near the shoreline. Generally, the wave fields follow the wind patterns

rather well. Comparing the wind fields from Figure 4.3 and wave fields from Figure 4.4 indicates that the spatial variability is closely related. The maximums of H_s are associated with the maximums wind speeds.

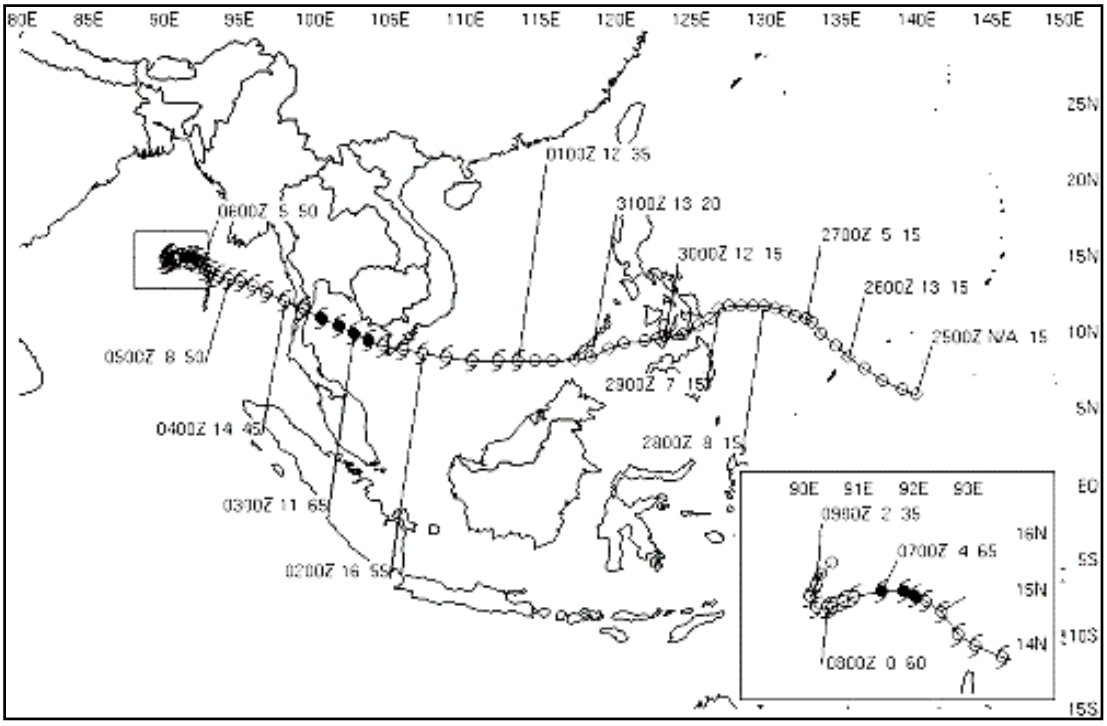

Figure 4.2 Best track of Typhoon Linda 1997

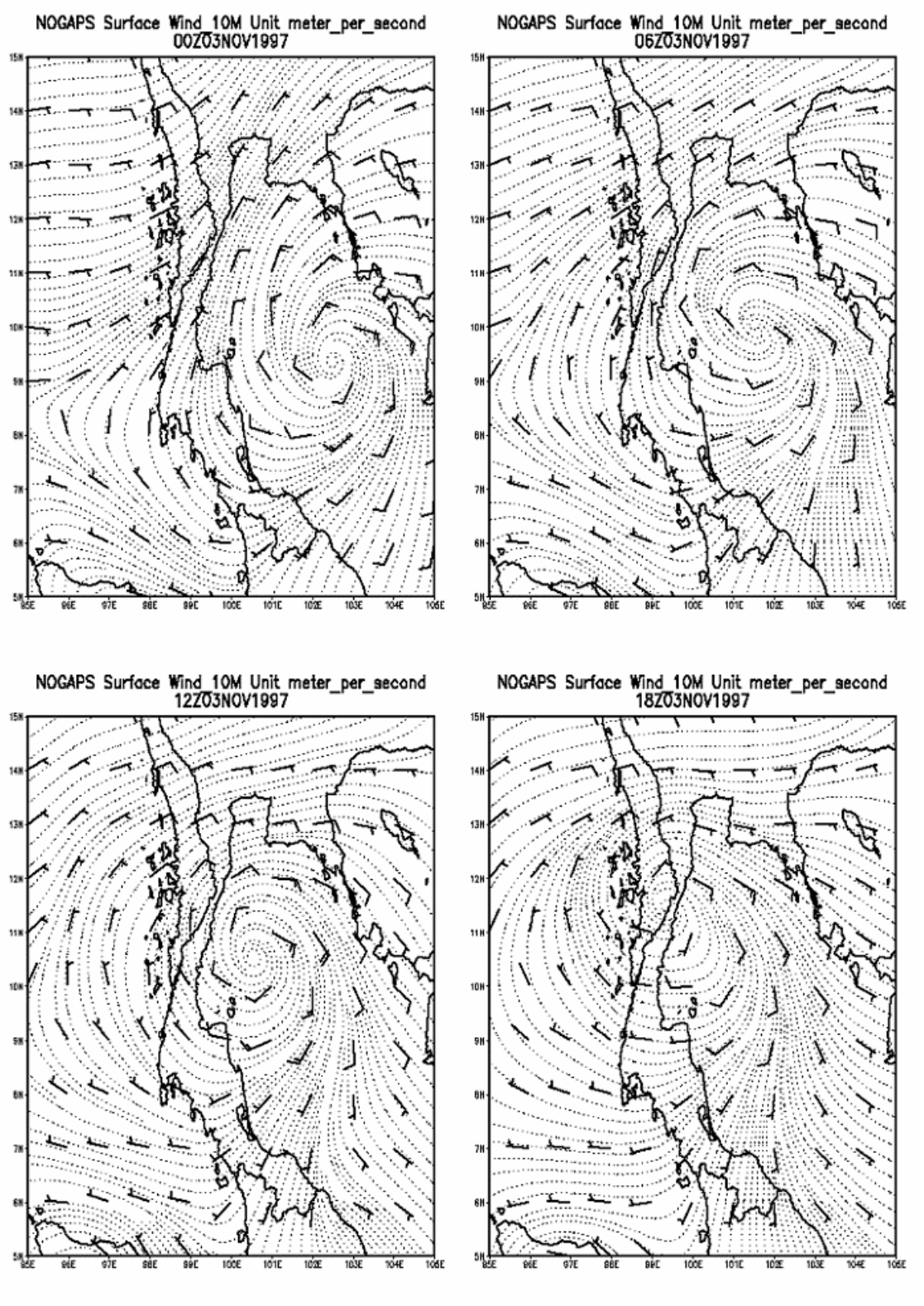

Figure 4.3 Wind fields on November 3rd, 1997 every 6 hours (NOGAPS)

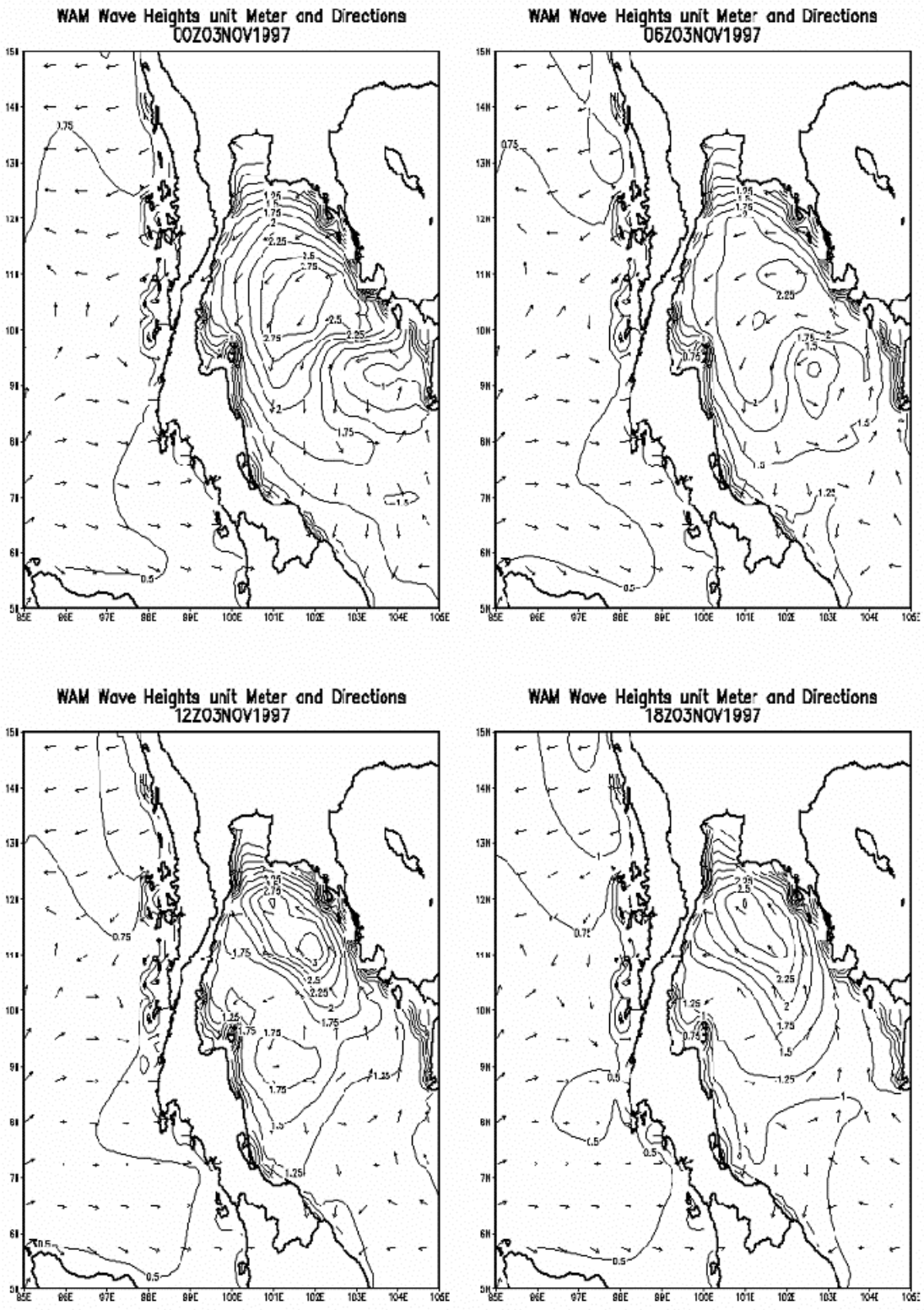

Figure 4.4 Wave fields on November 3rd, 1997 every 6 hours (WAM output)

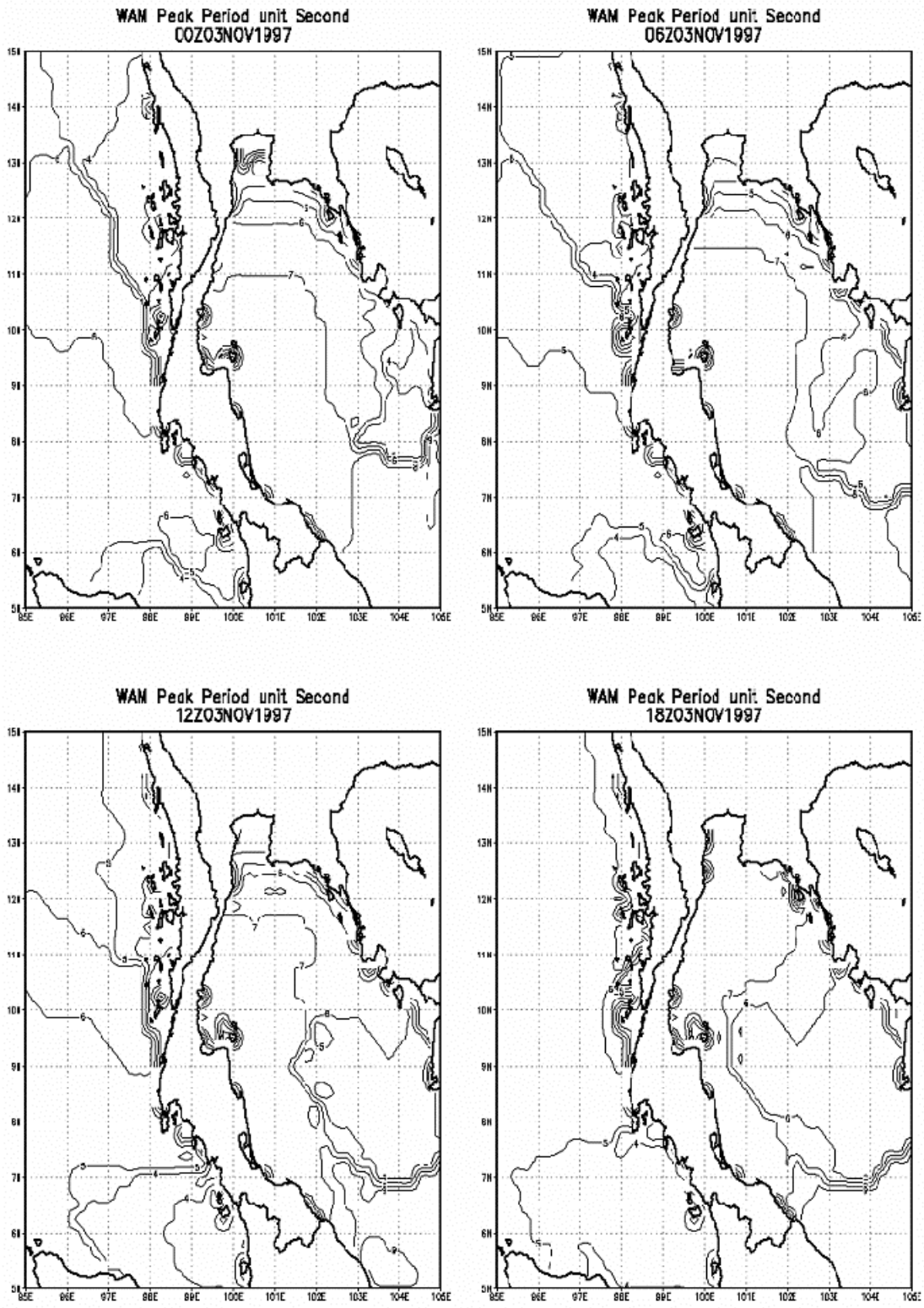

Figure 4.5 Peak period maps on November 3rd, 1997 (WAM output)

A sequence of peak wave period is shown in Figure 4.5. On November 3rd, during the first 6 hours, the region of simulation was characterized by mainly sea waves. Under the strong north-easterly winds a 9 seconds swell was generated and distributed along the south coast. It reached the UNC station at 00 UTC. This swell was further advected to the north, arriving at the HHN station with 10 seconds peak wave periods at 12 UTC. Six hours later it arrived the upper region of the Gulf.

Comparison of wave height and wave period time series at the HHN station is shown in Figure 4.6. In general, the modeled waves heights underestimate the observed wave heights especially in extreme case. This amount to an underestimation by as much as 20 %. The wave buoy reported the maximum of 4.06 m significant wave height, whereas the simulated value is approximately 3.2 meters at 06 UTC in November 3rd, 1997. Difference of nearly 1 meters wave height can be attributed to i) the limited "local" quality of the wind field (since the NOGAPS wind data correspond to a grid size of 1.0° resolution while the WAM model grid size is 0.25°) and ii) the enhanced energy dissipation due to the centered differences used in the model and the relatively close presence of a "diagonal" boundary. The comparison in term of the time series peak wave period also reveals that from the beginning of the simulation to 481 hours there were mainly sea waves. After this time the peak period increased to 6 s (Buoy data) and 7.4 s (WAM), denoting a clear effect of typhoon LINDA winds on swell waves.

In this study we also construct wave spectrum shown in Fig. 4.7. The rectangles areas are equal to the squares of the amplitudes, $A^2(f)$, of each component wave train are plotted against the average frequency, f, a “stairway” approximation to the spectrum is obtained. There was highest wave spectrum at UNC station.

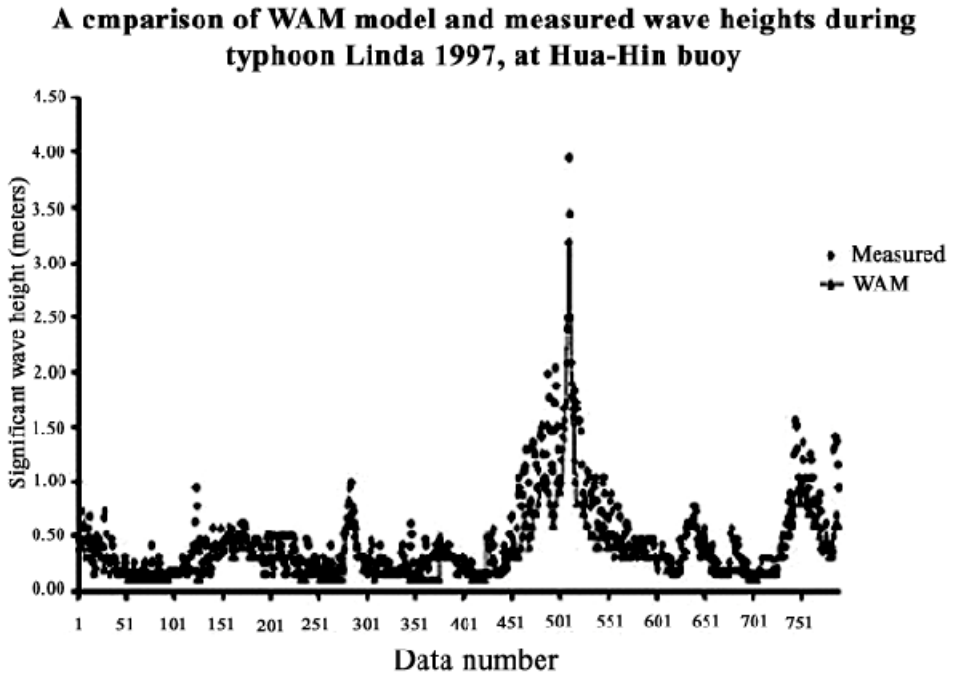

a) Wave height

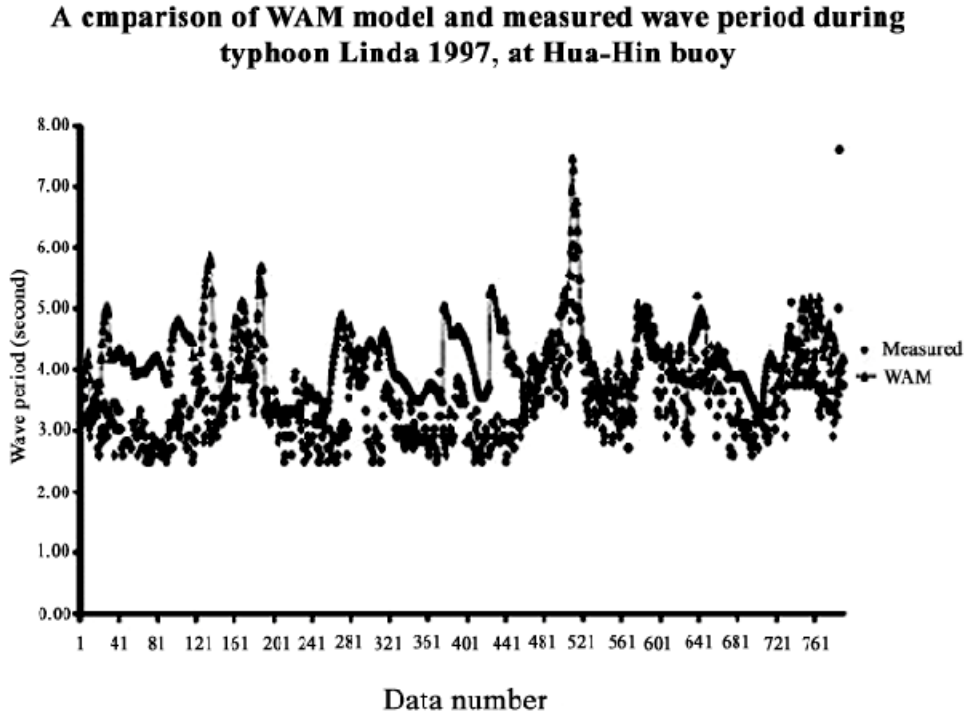

b) Peak wave period

Figure 4.6 A comparison of WAM model and measured at the HHN station

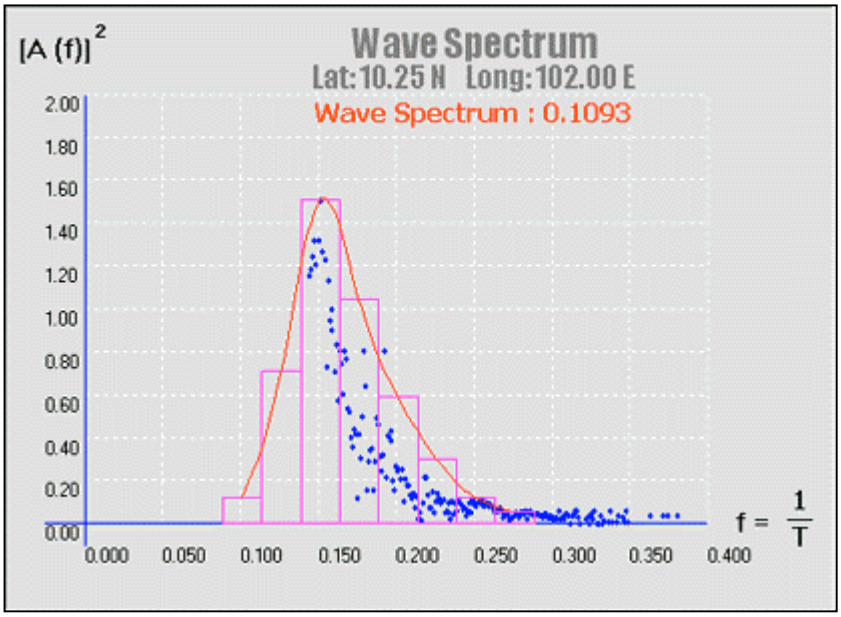

a) KCH station

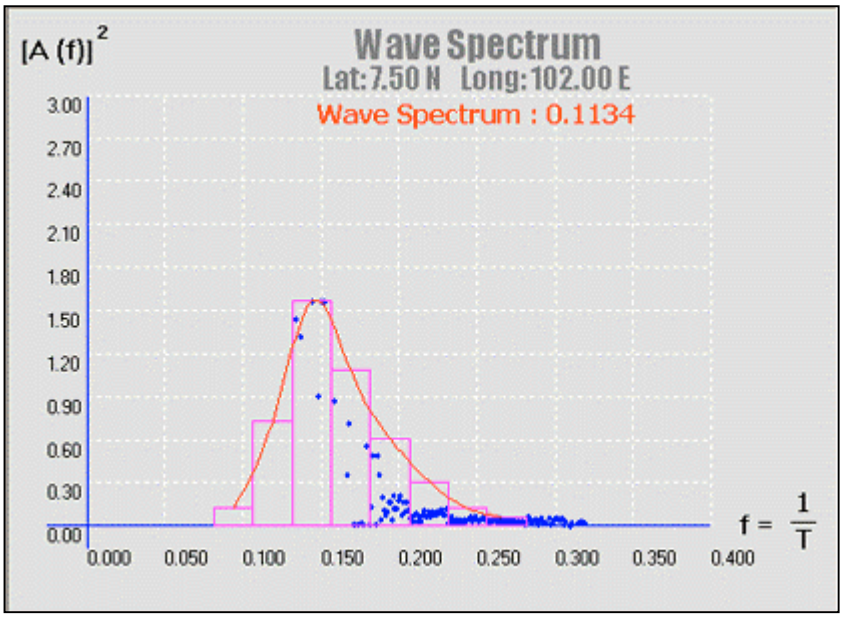

b) HHN station

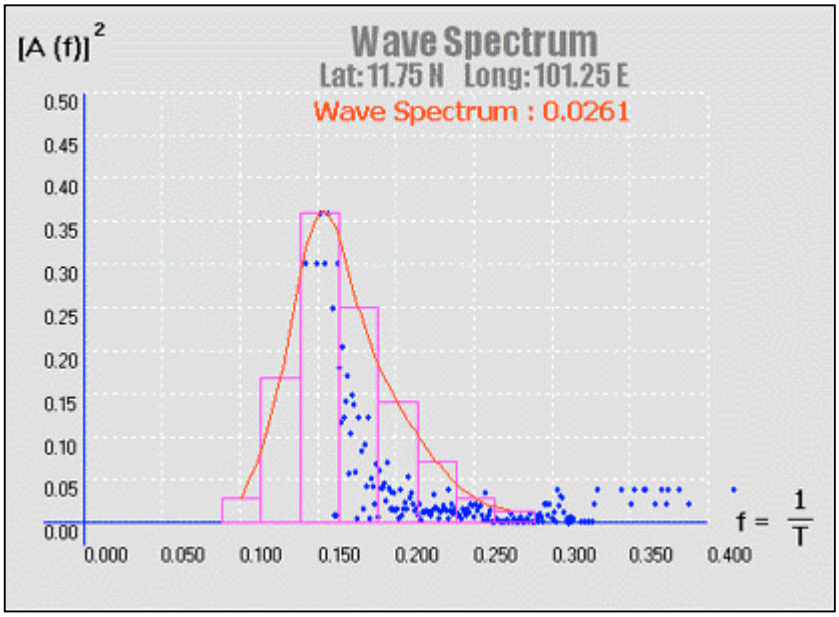

c) KSI station

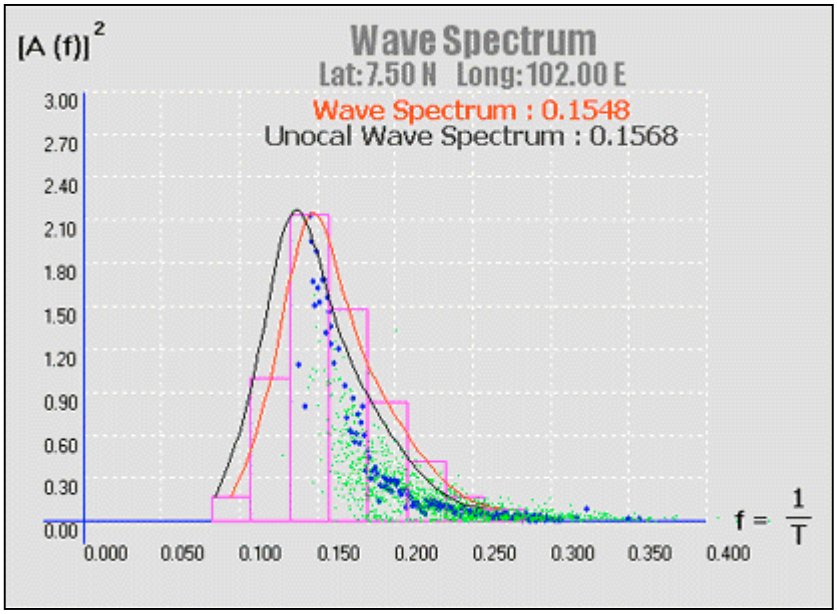

d) UNC station

Figure 4.7 “Stairway” approximation to the wave spectrum

For the GRNN, there are two models for prediction of the wave height and wave period, respectively. Each model was used to predict up to 24-hours leading time. The first model was constructed using the present values of wind velocity (U_{10}) and direction (θ_w), fetch length (F_L), significant wave height (H_s), and water depth (D_w) as inputs. The outputs are wave heights at leading time of 3, 6, 9, 12, and 24 hours. The second model was constructed in a similar way to the first model but using the wave periods instead of wave heights. There are 1,430 data patterns used in this study covering 4 wave stations. Each model was trained by using the cross-training technique (at every 2 data patterns). The results are shown in Fig. 4.8 to Fig. 4.11.

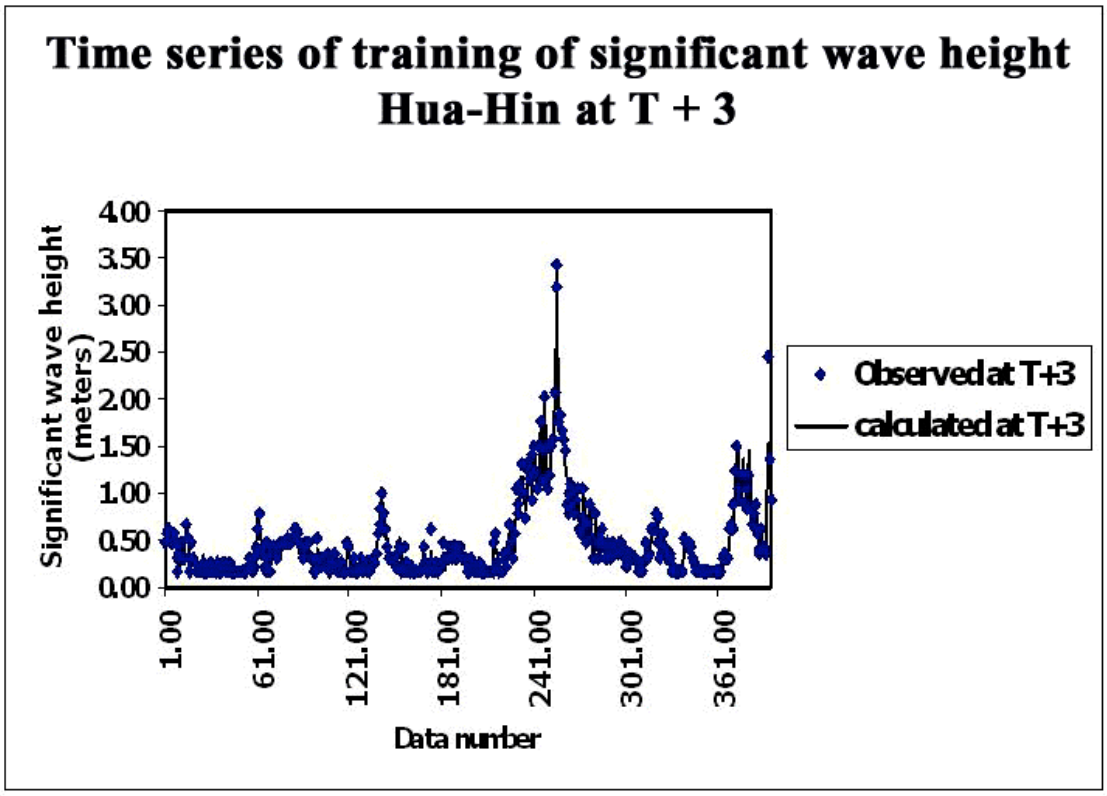
Time series of training of significant wave height
Hua-Hin at T + 3
Significant wave height (meters)
4.00
3.50
3.00
2.50
2.00
1.50
1.00
0.50
0.00
1.00
61.00
121.00
181.00
241.00
301.00
361.00
Data number
Observed at T+3
calculated at T+3

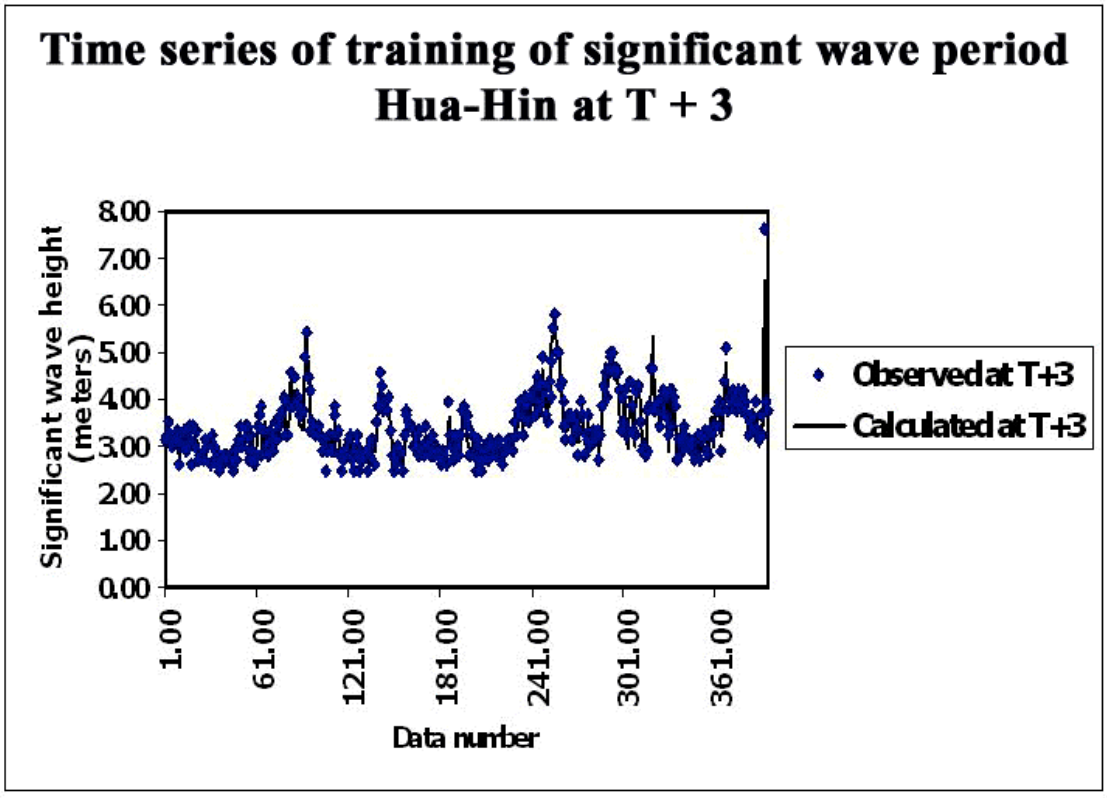
Time series of training of significant wave period
Hua-Hin at T + 3
Significant wave height (meters)
8.00
7.00
6.00
5.00
4.00
3.00
2.00
1.00
0.00
1.00
61.00
121.00
181.00
241.00
301.00
361.00
Data number
Observed at T+3
Calculated at T+3

a) T + 3

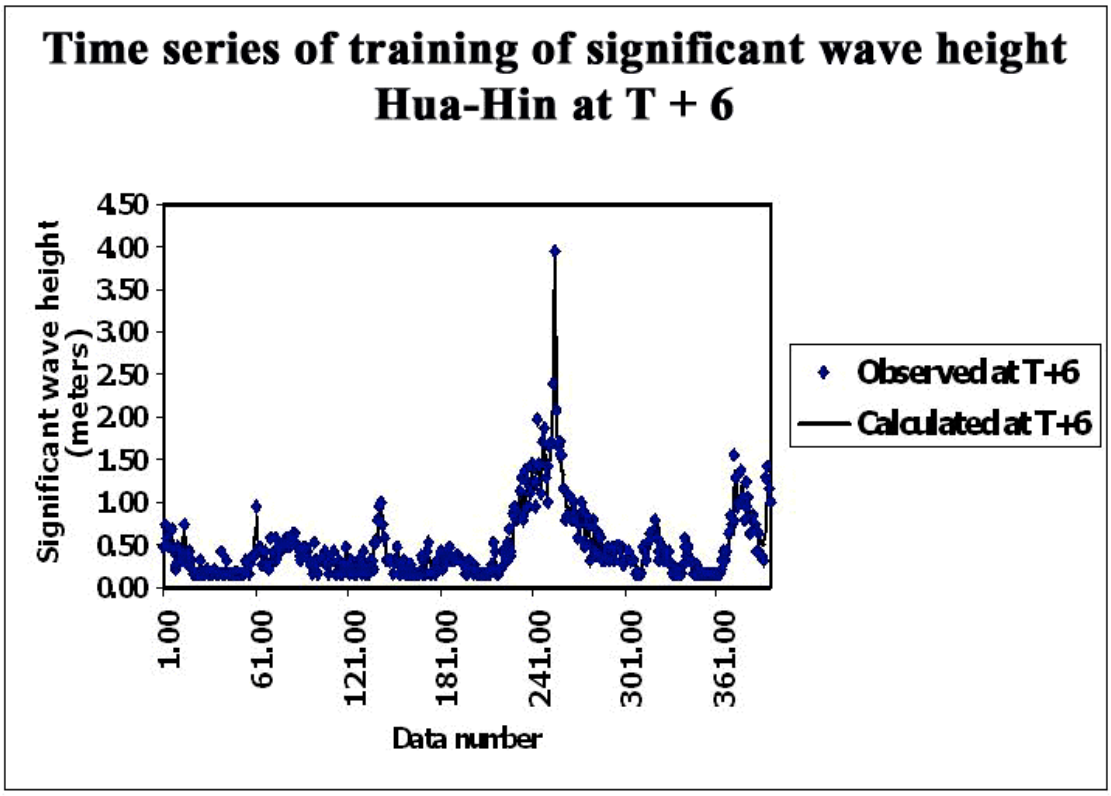
Time series of training of significant wave height
Hua-Hin at T + 6
Significant wave height (meters)
4.50
4.00
3.50
3.00
2.50
2.00
1.50
1.00
0.50
0.00
1.00
61.00
121.00
181.00
241.00
301.00
361.00
Data number
Observed at T+6
Calculated at T+6

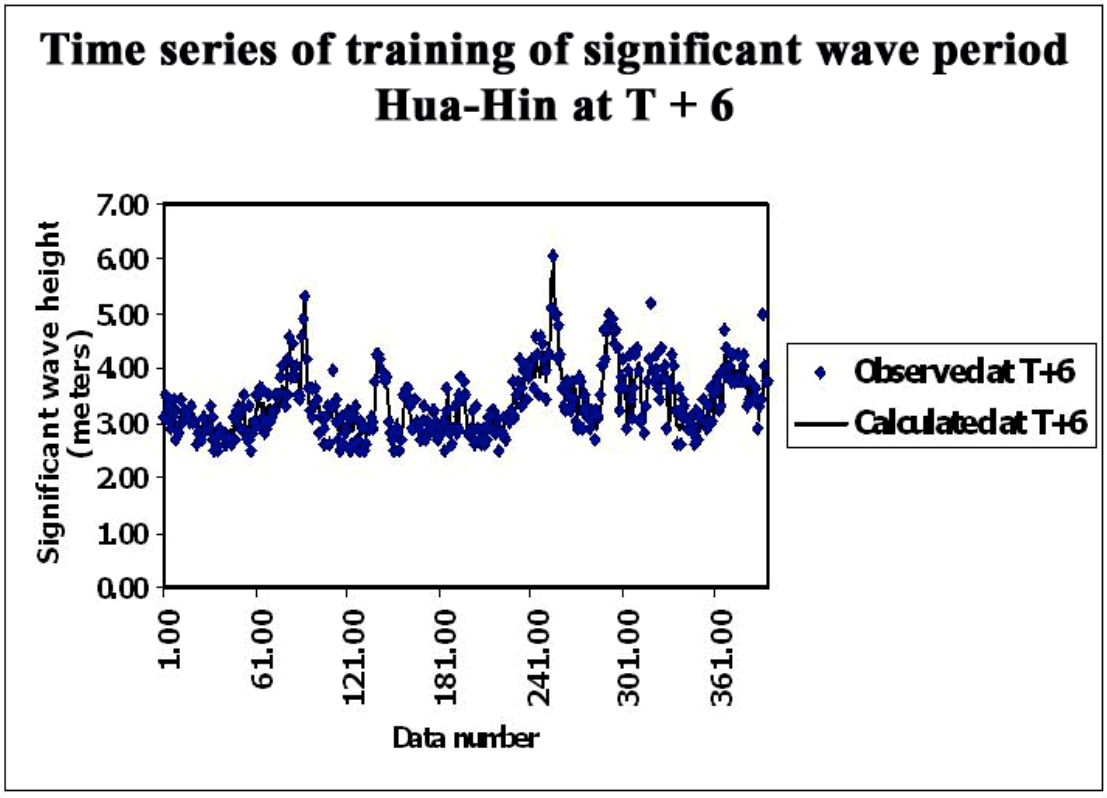
Time series of training of significant wave period
Hua-Hin at T + 6
Significant wave height (meters)
7.00
6.00
5.00
4.00
3.00
2.00
1.00
0.00
1.00
61.00
121.00
181.00
241.00
301.00
361.00
Data number
Observed at T+6
Calculated at T+6

b) T + 6

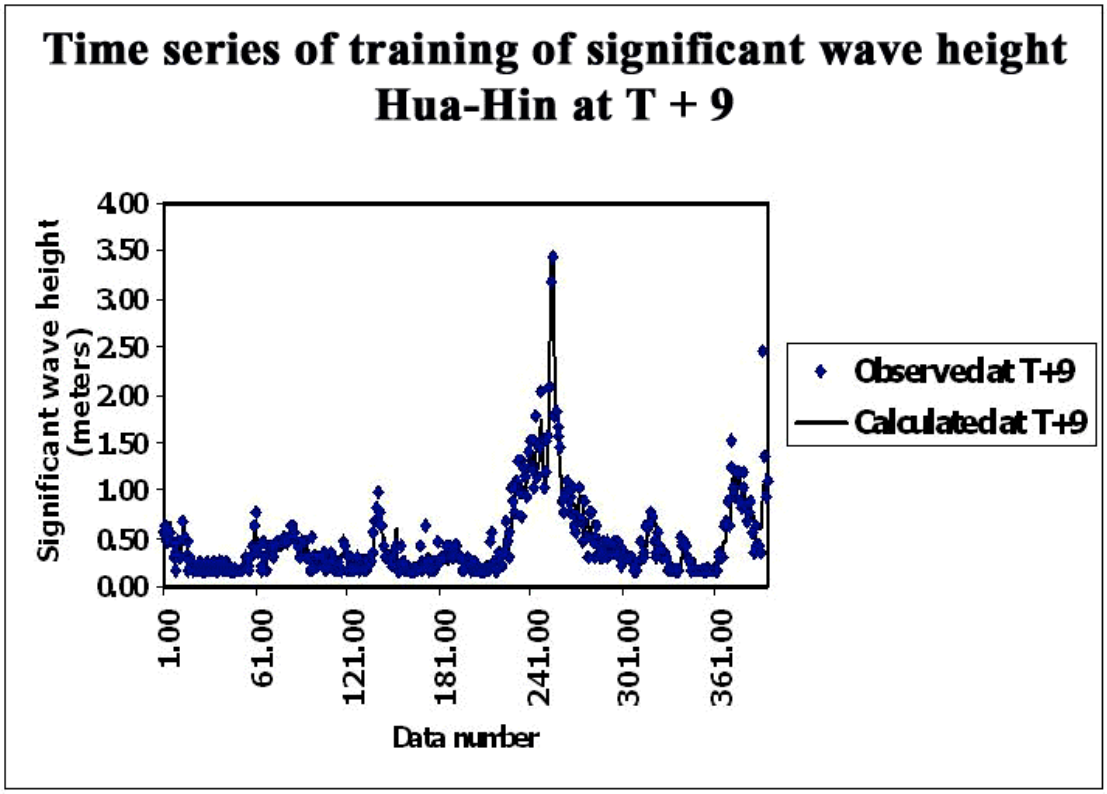
Time series of training of significant wave height
Hua-Hin at T + 9
Significant wave height (meters)
4.00
3.50
3.00
2.50
2.00
1.50
1.00
0.50
0.00
1.00
61.00
121.00
181.00
241.00
301.00
361.00
Data number
Observed at T+9
Calculated at T+9

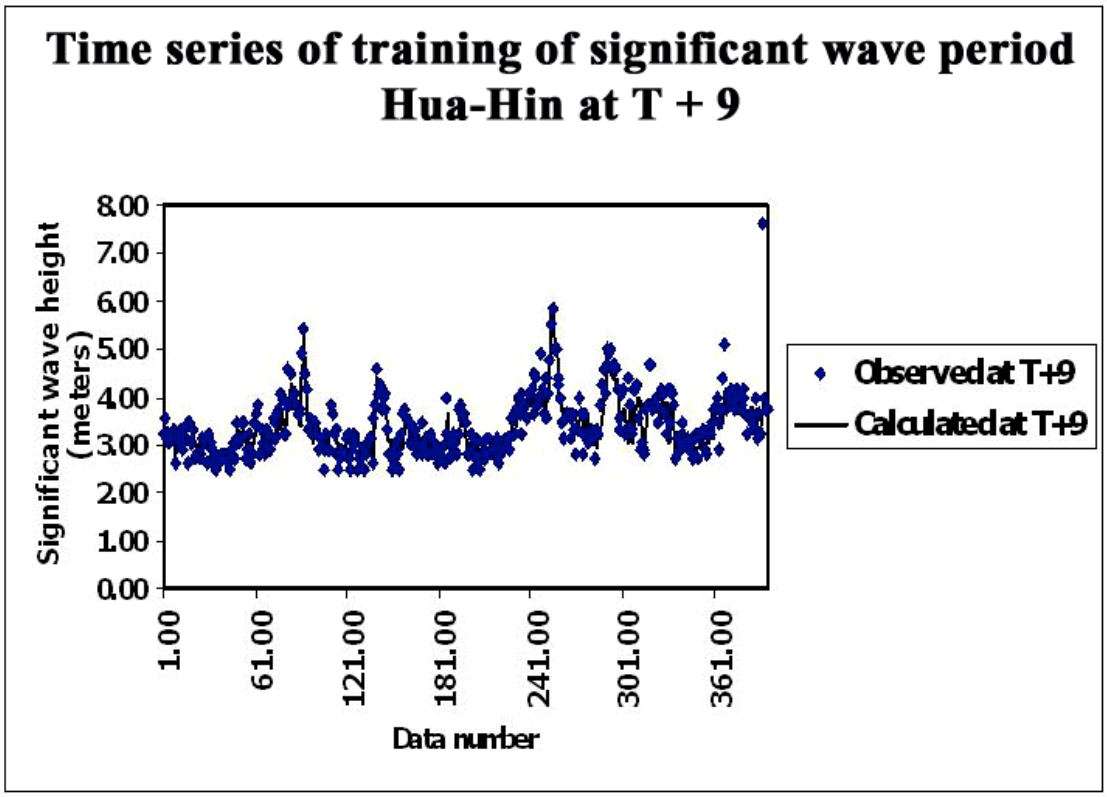
Time series of training of significant wave period
Hua-Hin at T + 9
Significant wave height (meters)
8.00
7.00
6.00
5.00
4.00
3.00
2.00
1.00
0.00
1.00
61.00
121.00
181.00
241.00
301.00
361.00
Data number
Observed at T+9
Calculated at T+9

c) T + 9

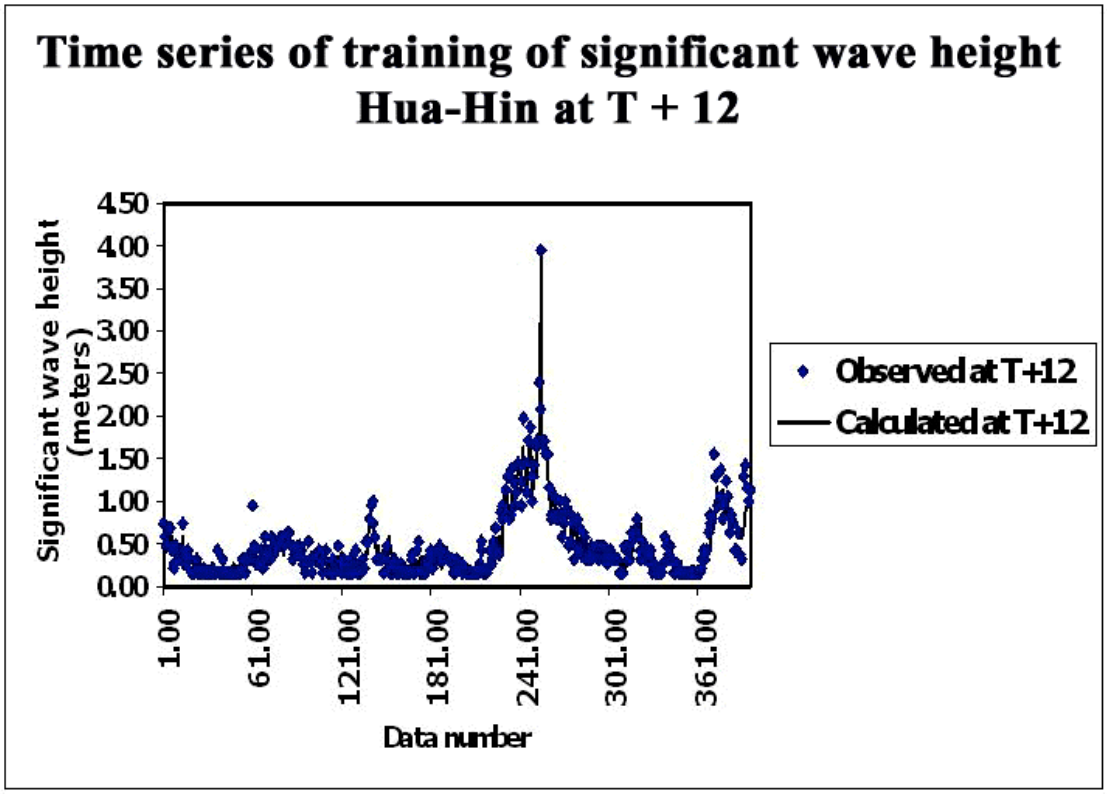
Time series of training of significant wave height
Hua-Hin at T + 12
Significant wave height (meters)
4.50
4.00
3.50
3.00
2.50
2.00
1.50
1.00
0.50
0.00
1.00
61.00
121.00
181.00
241.00
301.00
361.00
Data number
Observed at T+12
Calculated at T+12

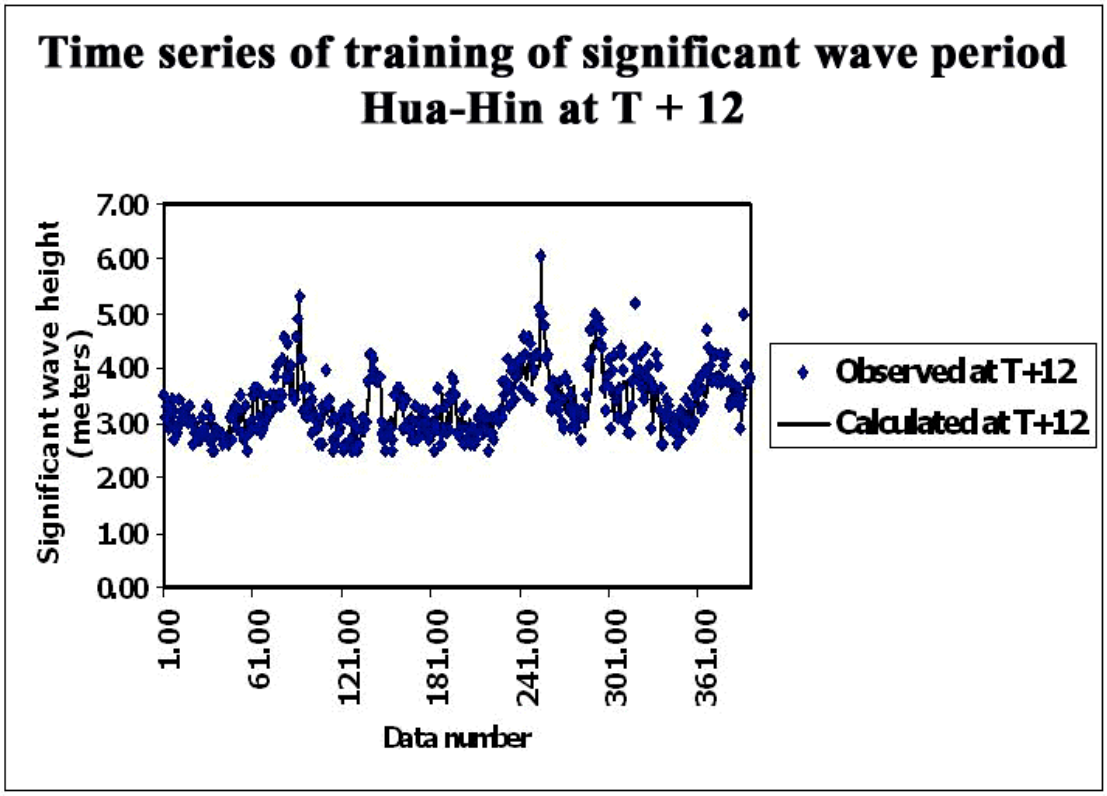
Time series of training of significant wave period
Hua-Hin at T + 12
Significant wave height (meters)
7.00
6.00
5.00
4.00
3.00
2.00
1.00
0.00
1.00
61.00
121.00
181.00
241.00
301.00
361.00
Data number
Observed at T+12
Calculated at T+12

d) T + 12

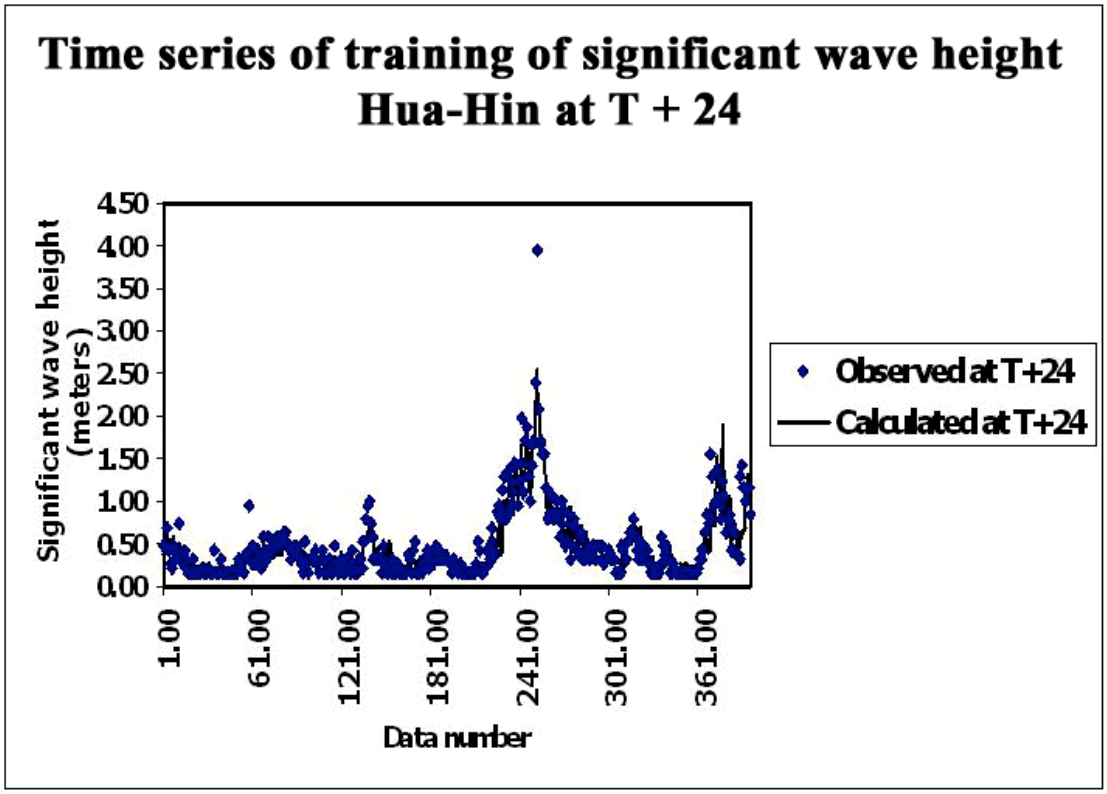

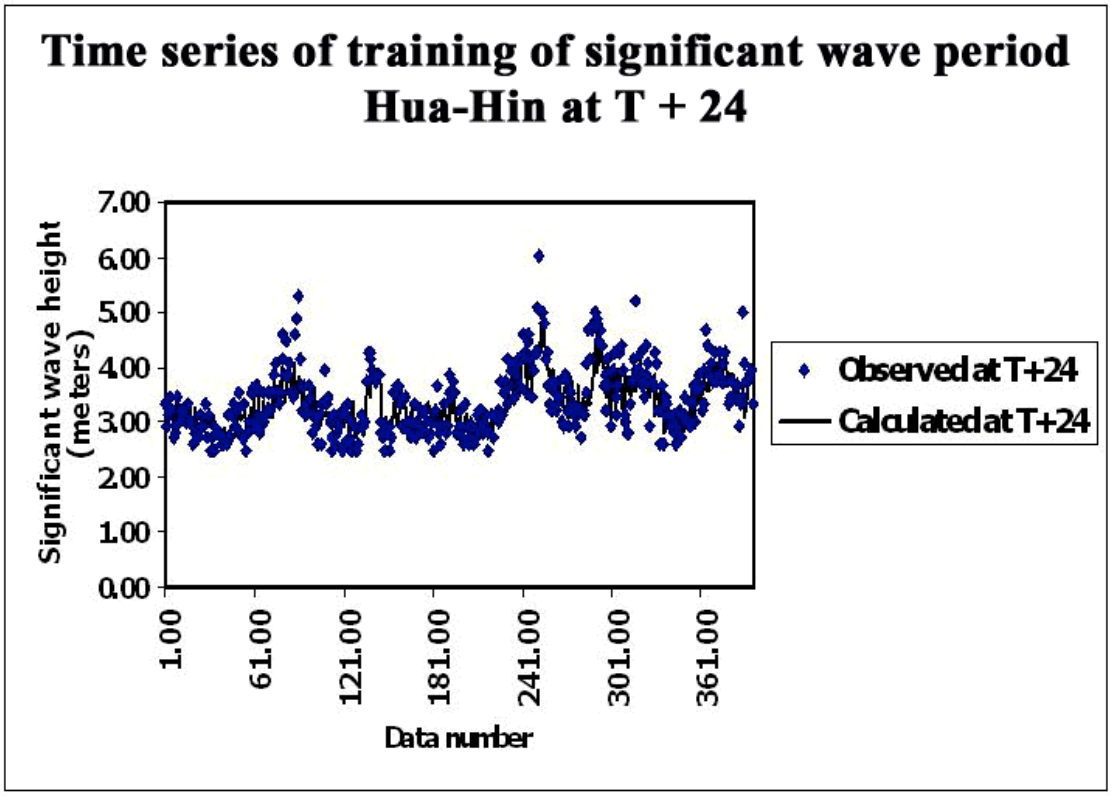

e) T + 24

Figure 4.8 Time series of wave parameters at HHN station

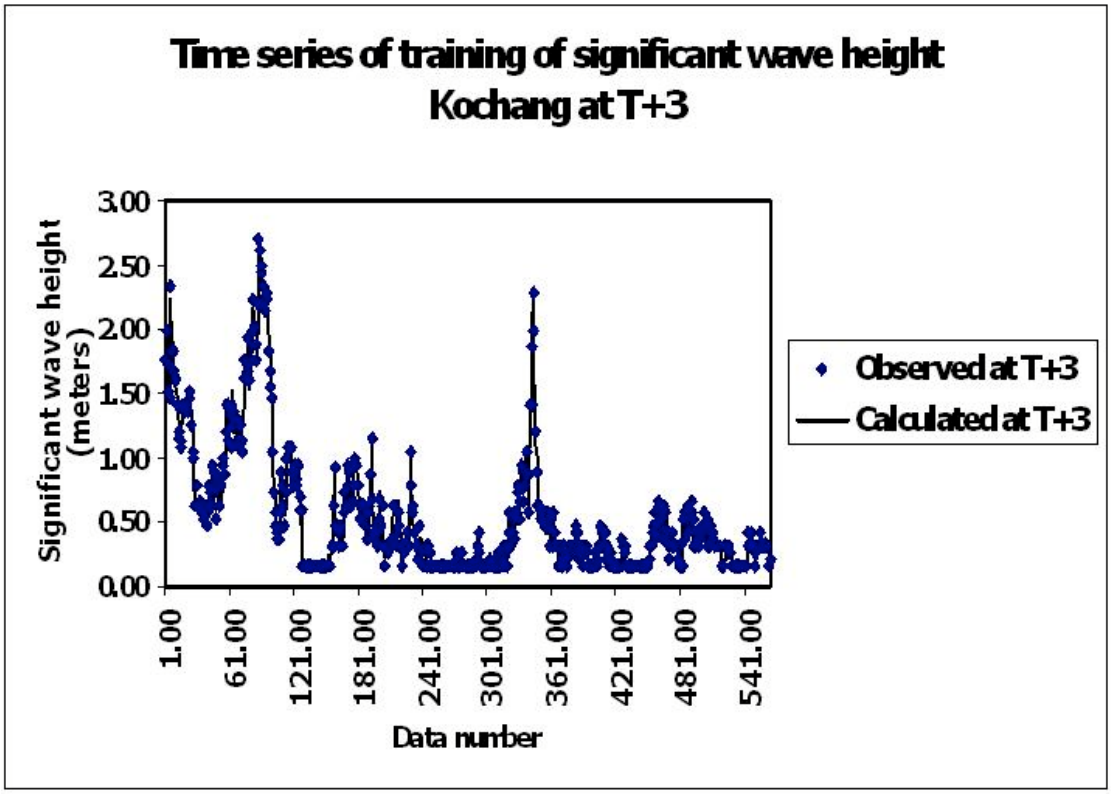
Time series of training of significant wave height
Kochang at T+3
Significant wave height (meters)
3.00
2.50
2.00
1.50
1.00
0.50
0.00
1.00
61.00
121.00
181.00
241.00
301.00
361.00
421.00
481.00
541.00
Data number
Observed at T+3
Calculated at T+3

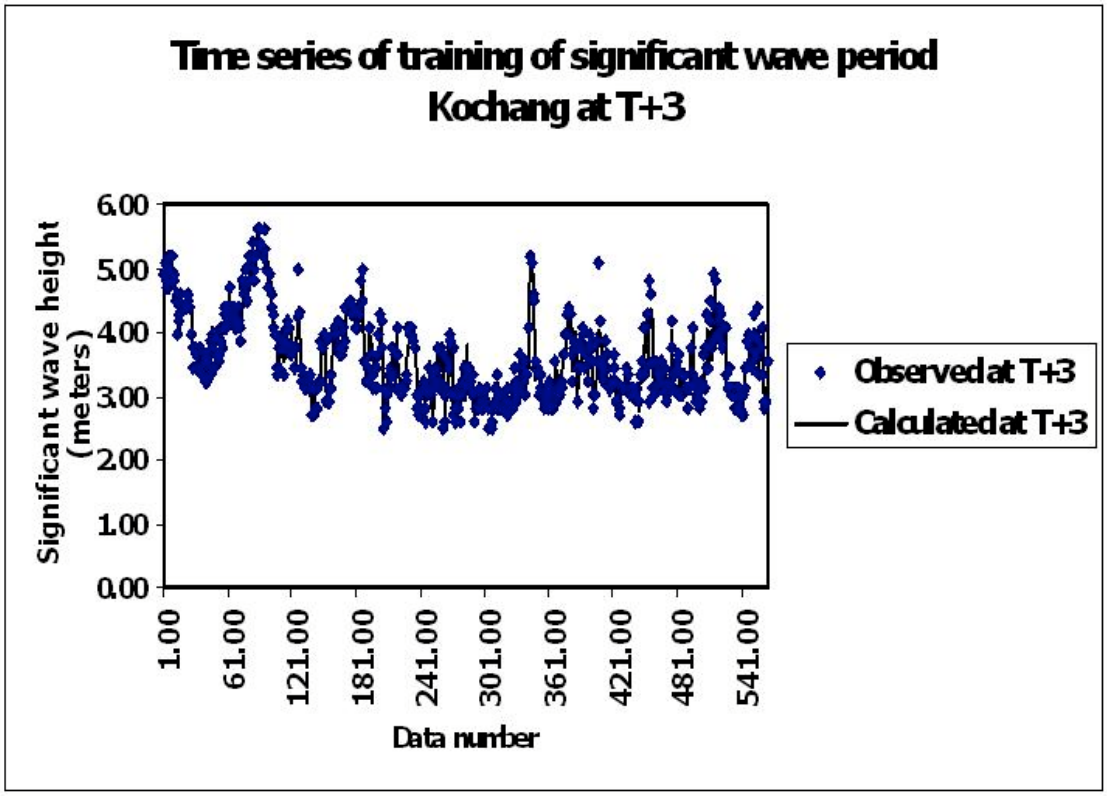
Time series of training of significant wave period
Kochang at T+3
Significant wave height (meters)
6.00
5.00
4.00
3.00
2.00
1.00
0.00
1.00
61.00
121.00
181.00
241.00
301.00
361.00
421.00
481.00
541.00
Data number
Observed at T+3
Calculated at T+3

a) T + 3

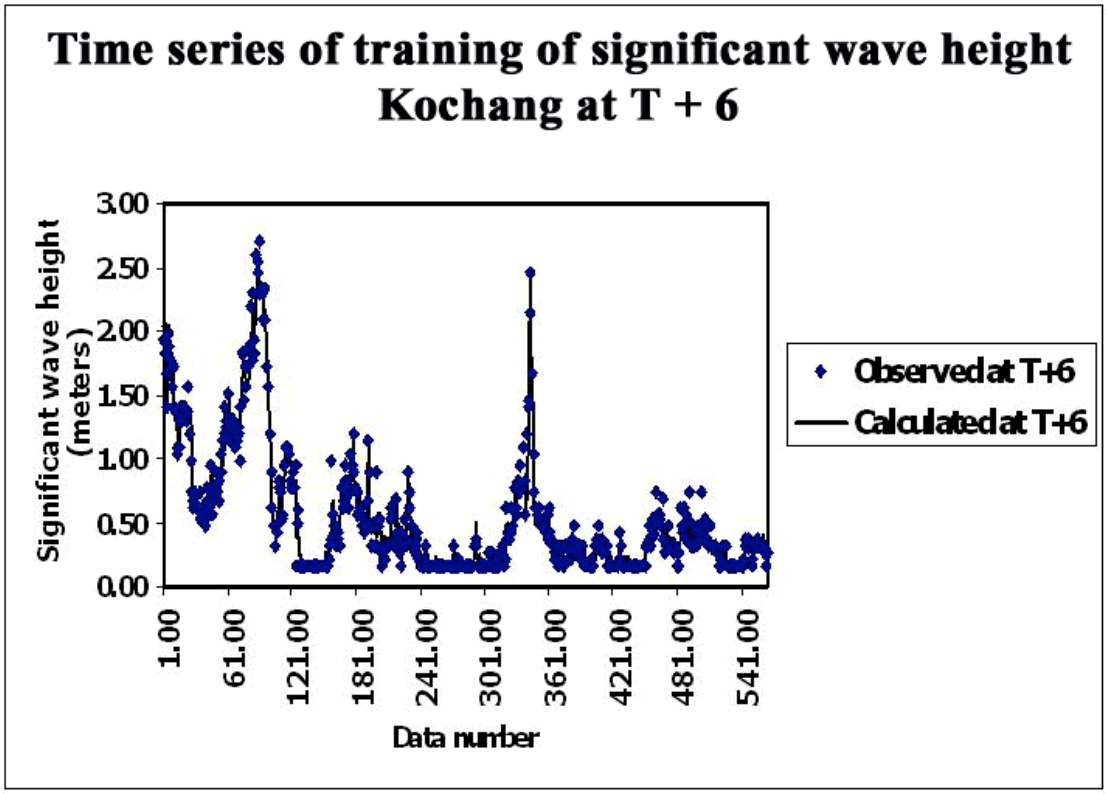
Time series of training of significant wave height
Kochang at T + 6
Significant wave height (meters)
3.00
2.50
2.00
1.50
1.00
0.50
0.00
1.00
61.00
121.00
181.00
241.00
301.00
361.00
421.00
481.00
541.00
Data number
Observed at T+6
Calculated at T+6

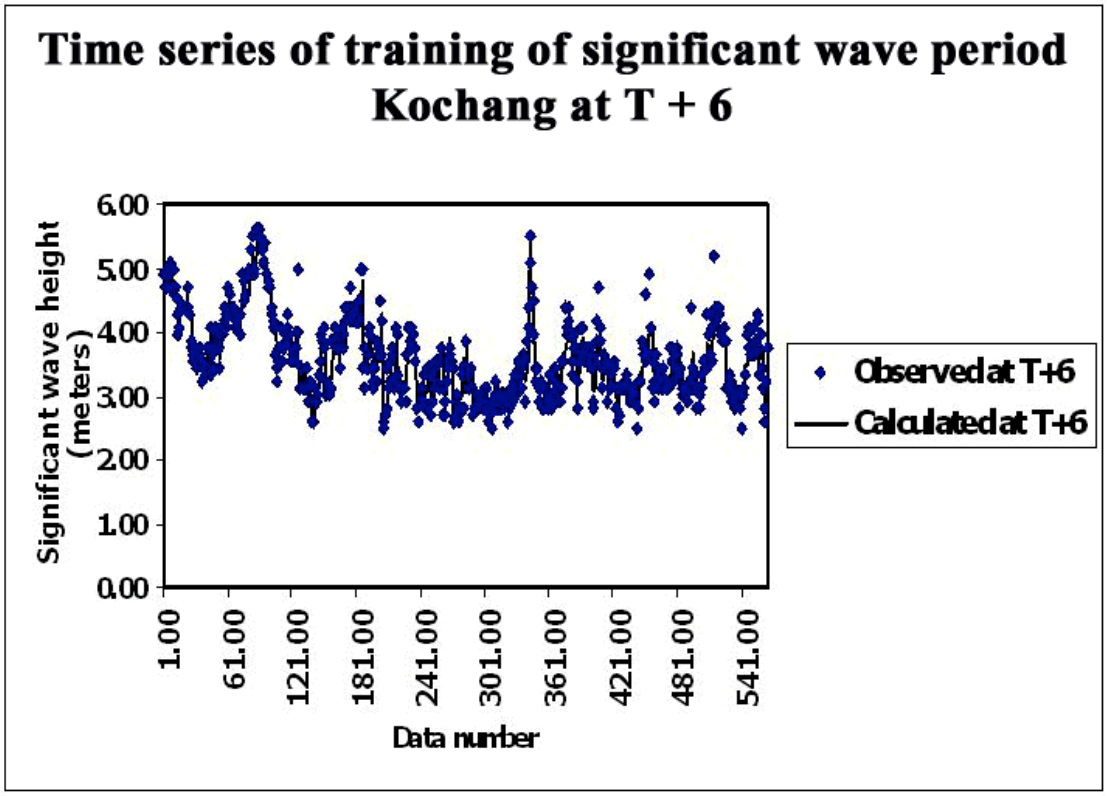
Time series of training of significant wave period
Kochang at T + 6
Significant wave height (meters)
6.00
5.00
4.00
3.00
2.00
1.00
0.00
1.00
61.00
121.00
181.00
241.00
301.00
361.00
421.00
481.00
541.00
Data number
Observed at T+6
Calculated at T+6

b) T + 6

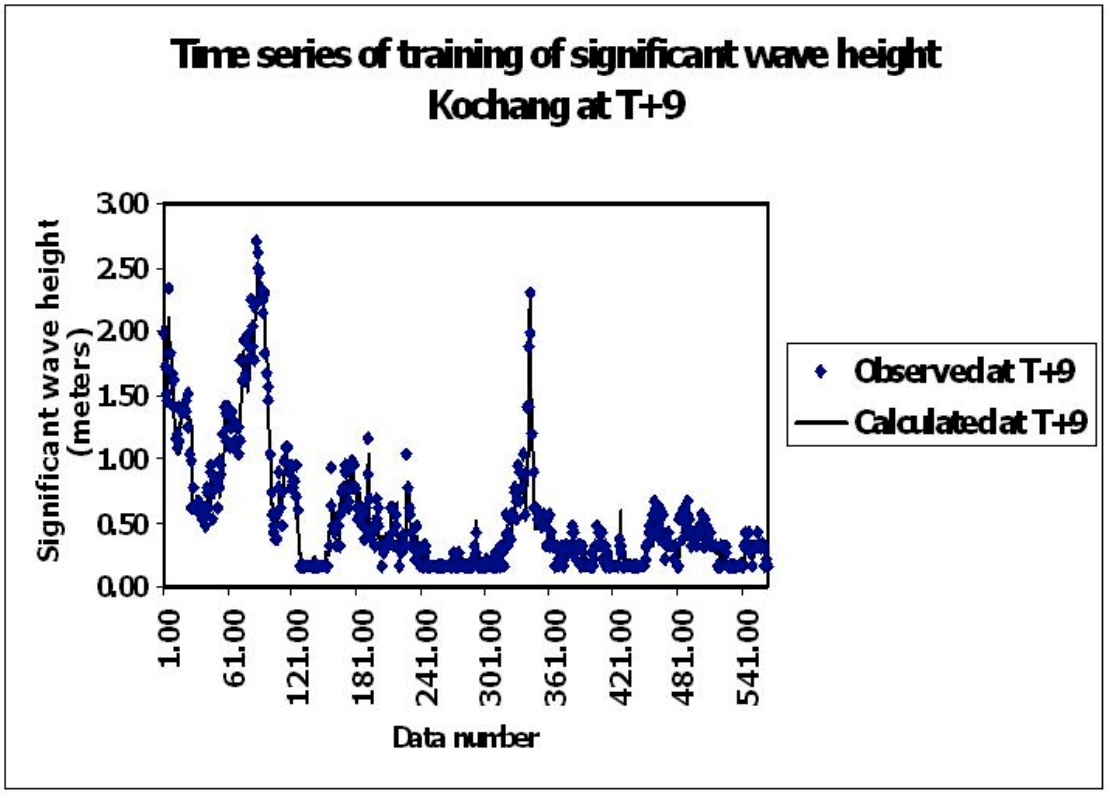
Time series of training of significant wave height
Kochang at T+9
Significant wave height (meters)
3.00
2.50
2.00
1.50
1.00
0.50
0.00
1.00
61.00
121.00
181.00
241.00
301.00
361.00
421.00
481.00
541.00
Data number
Observed at T+9
Calculated at T+9

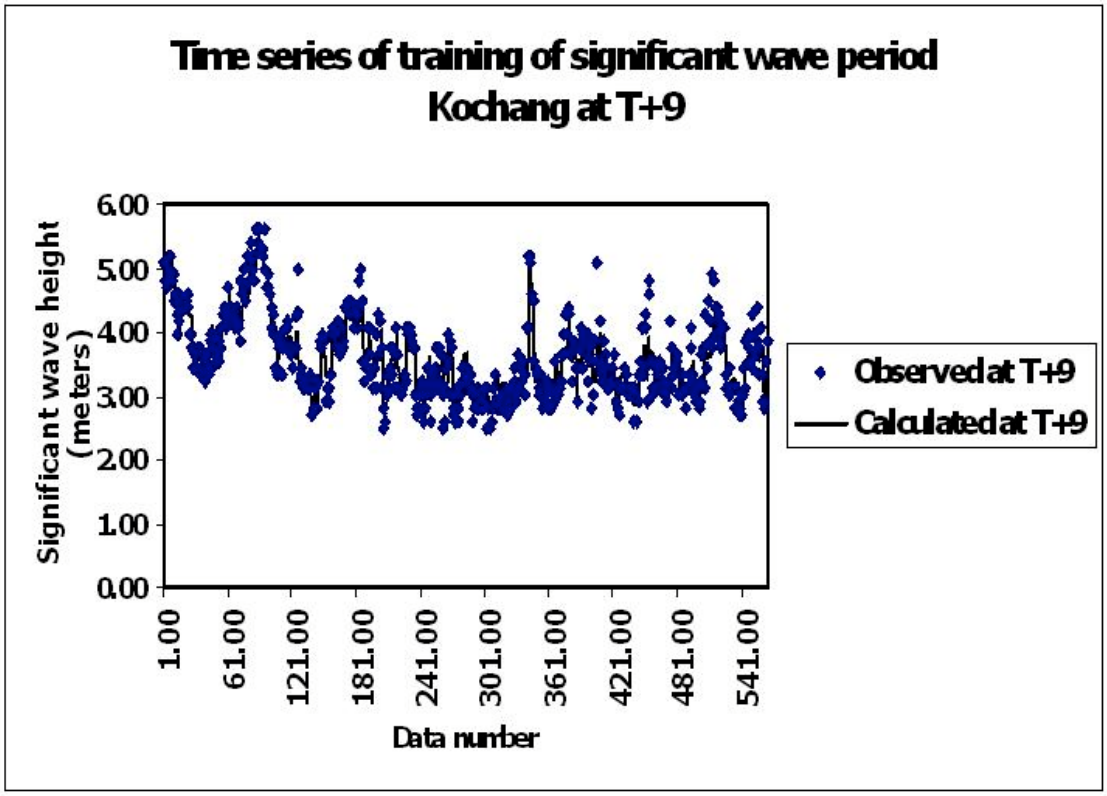
Time series of training of significant wave period
Kochang at T+9
Significant wave height (meters)
6.00
5.00
4.00
3.00
2.00
1.00
0.00
1.00
61.00
121.00
181.00
241.00
301.00
361.00
421.00
481.00
541.00
Data number
Observed at T+9
Calculated at T+9

c) T + 9

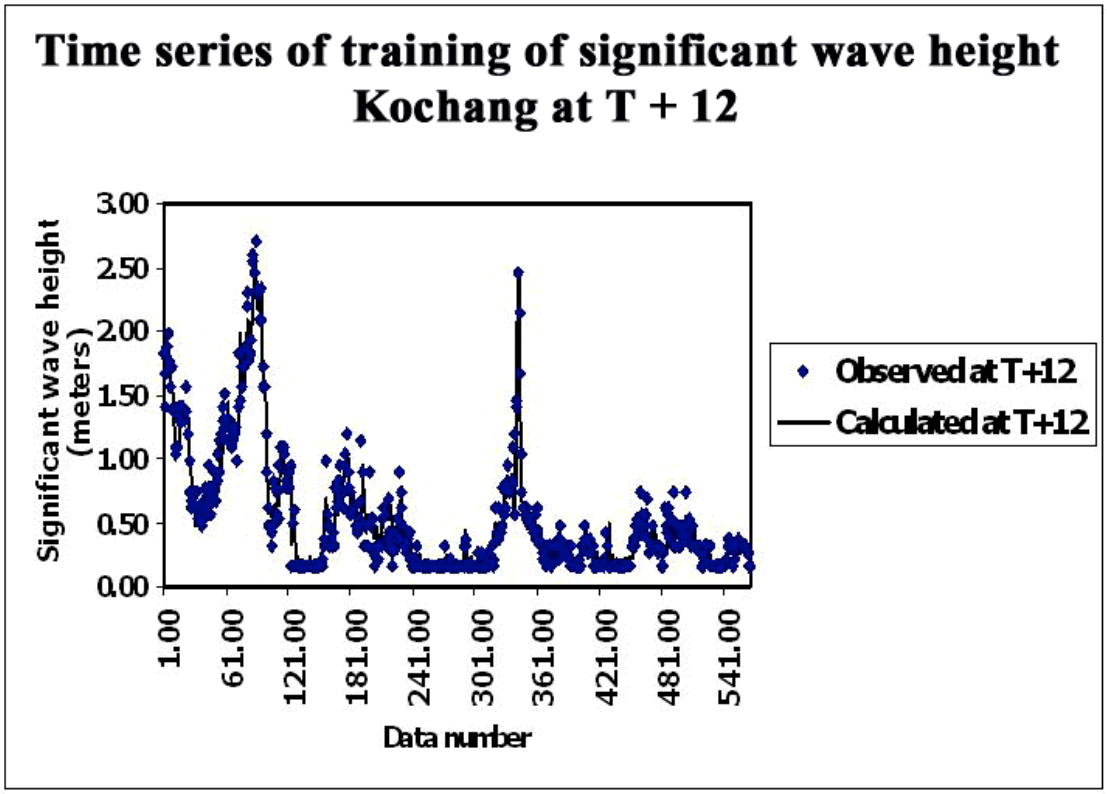
Time series of training of significant wave height
Kochang at T + 12
Significant wave height (meters)
3.00
2.50
2.00
1.50
1.00
0.50
0.00
1.00
61.00
121.00
181.00
241.00
301.00
361.00
421.00
481.00
541.00
Data number
Observed at T+12
Calculated at T+12

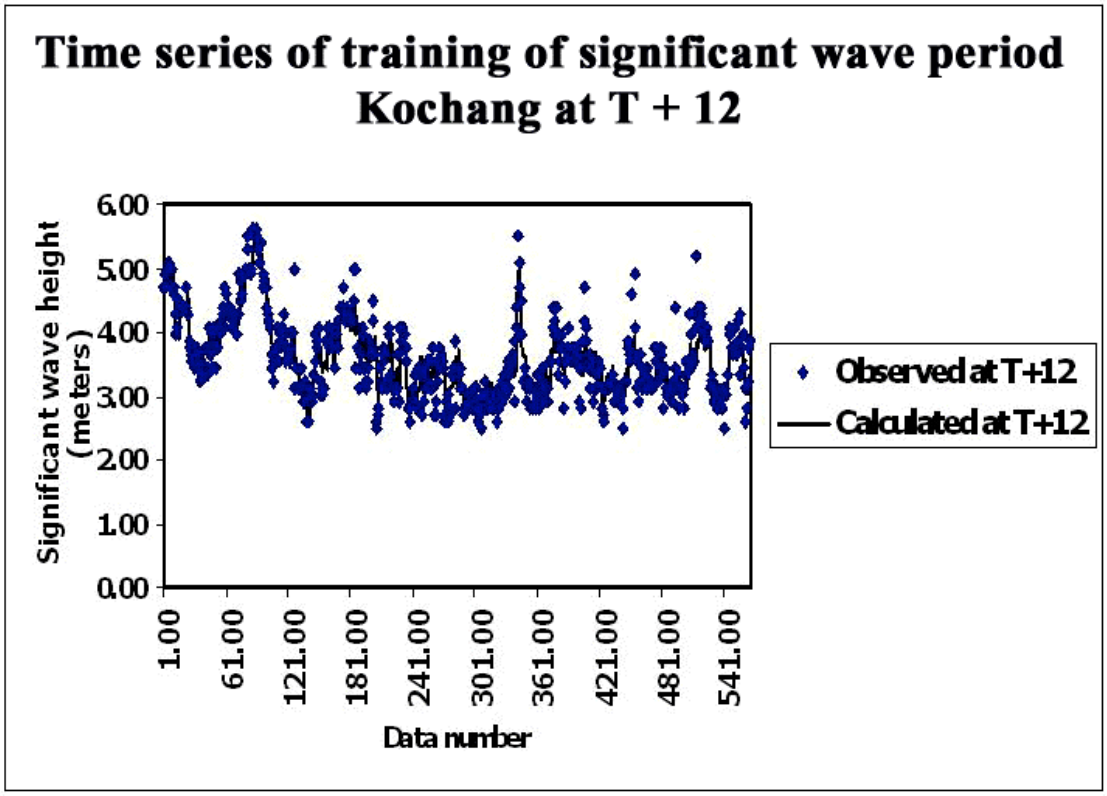
Time series of training of significant wave period
Kochang at T + 12
Significant wave height (meters)
6.00
5.00
4.00
3.00
2.00
1.00
0.00
1.00
61.00
121.00
181.00
241.00
301.00
361.00
421.00
481.00
541.00
Data number
Observed at T+12
Calculated at T+12

d) T + 12

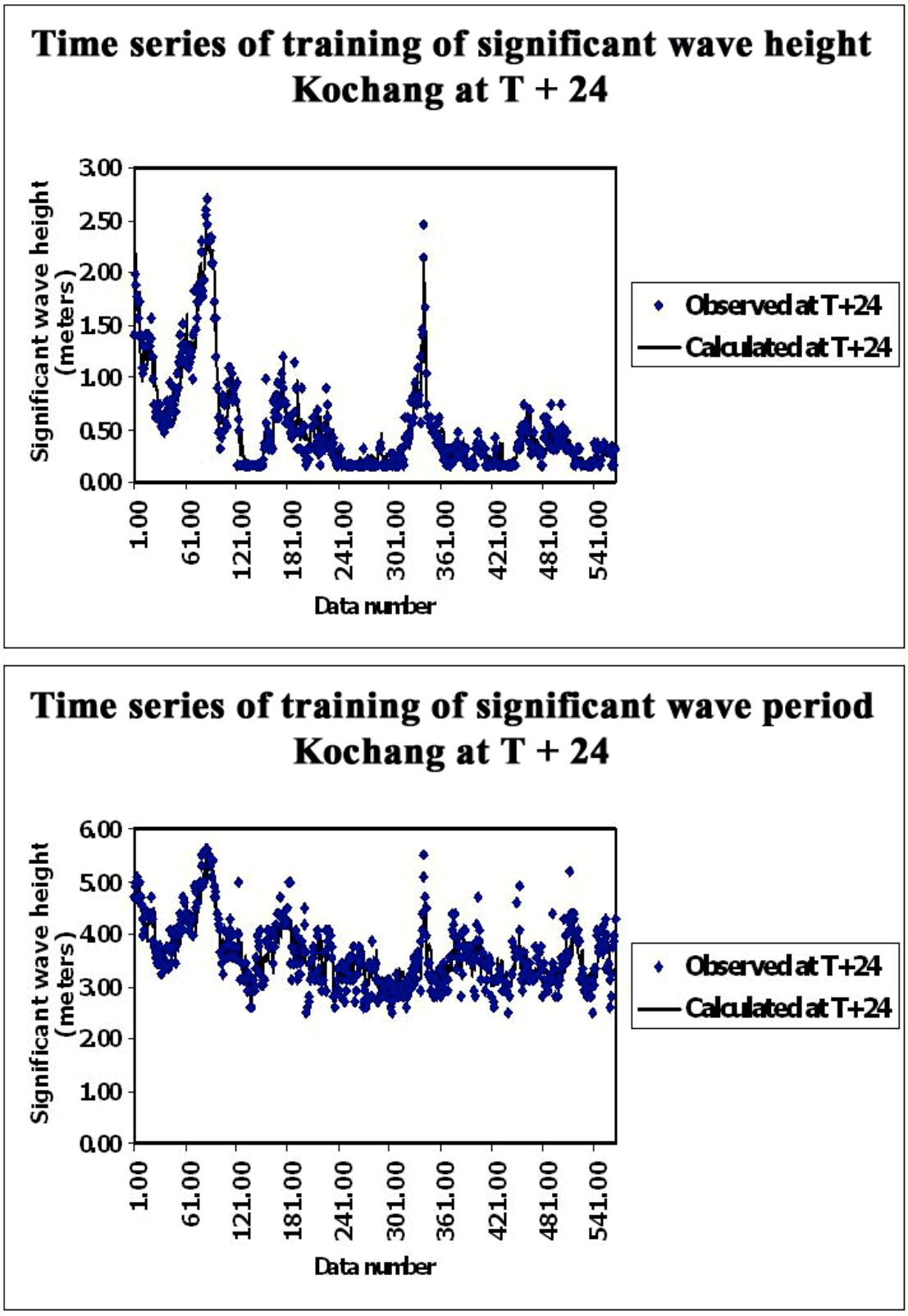

e) T + 24

Figure 4.9 Time series of wave parameters at KCH station

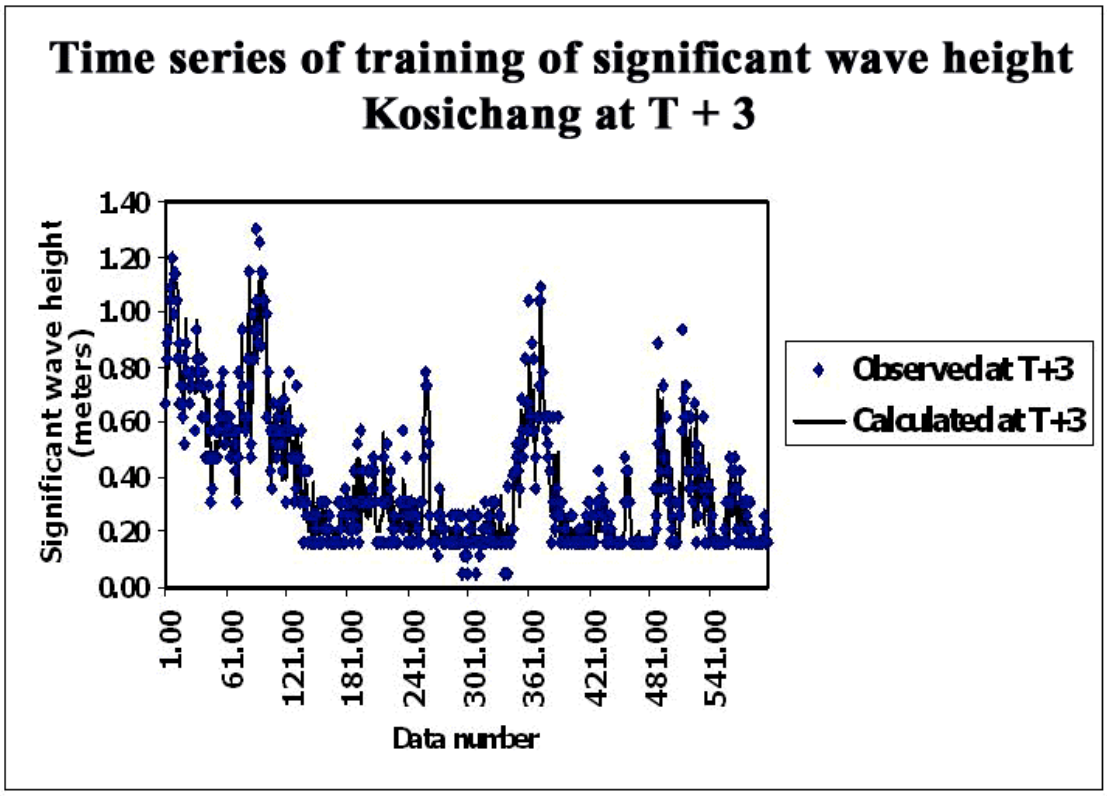
Time series of training of significant wave height
Kosichang at T + 3
Significant wave height (meters)
1.40
1.20
1.00
0.80
0.60
0.40
0.20
0.00
1.00
61.00
121.00
181.00
241.00
301.00
361.00
421.00
481.00
541.00
Data number
Observed at T+3
Calculated at T+3

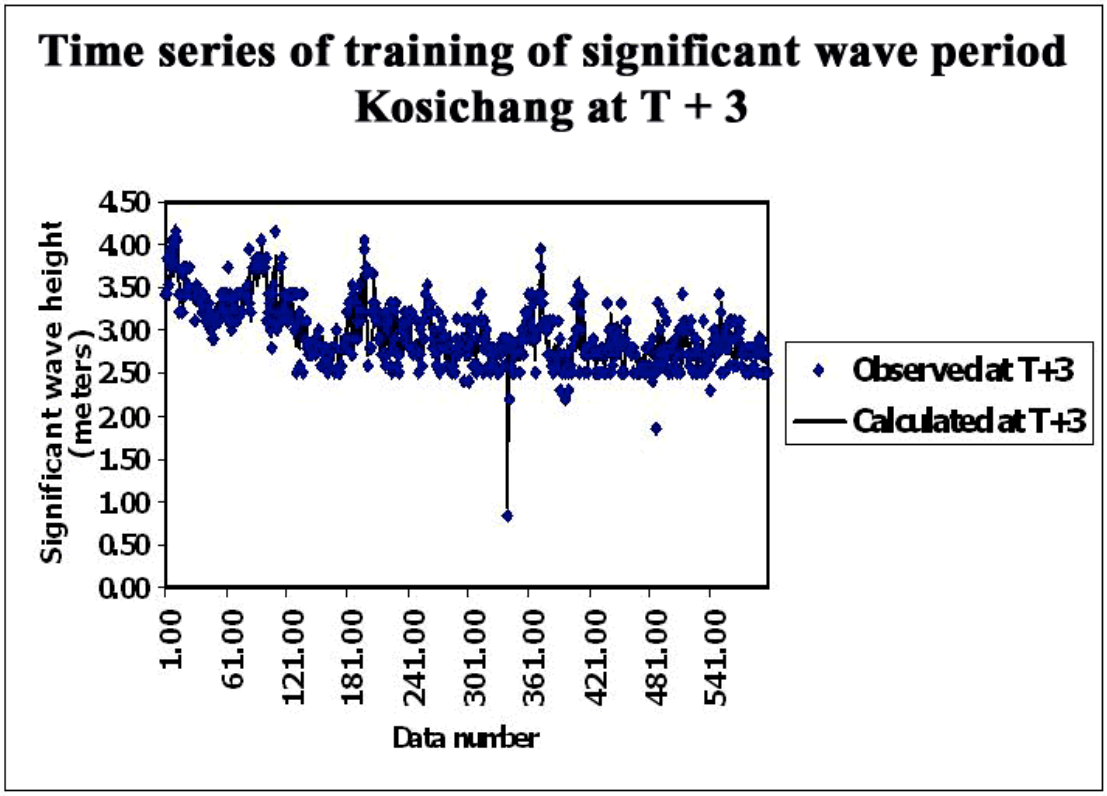
Time series of training of significant wave period
Kosichang at T + 3
Significant wave height (meters)
4.50
4.00
3.50
3.00
2.50
2.00
1.50
1.00
0.50
0.00
1.00
61.00
121.00
181.00
241.00
301.00
361.00
421.00
481.00
541.00
Data number
Observed at T+3
Calculated at T+3

a) T + 3

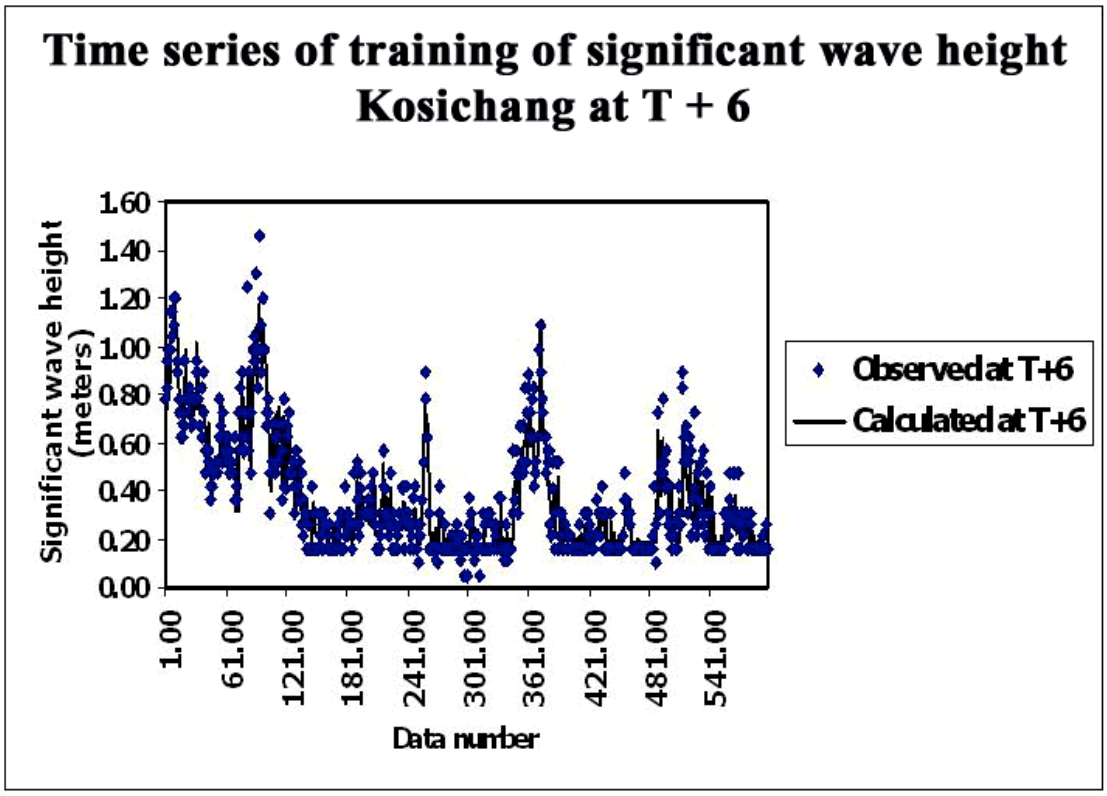
Time series of training of significant wave height
Kosichang at T + 6
Significant wave height (meters)
1.60
1.40
1.20
1.00
0.80
0.60
0.40
0.20
0.00
1.00
61.00
121.00
181.00
241.00
301.00
361.00
421.00
481.00
541.00
Data number
Observed at T+6
Calculated at T+6

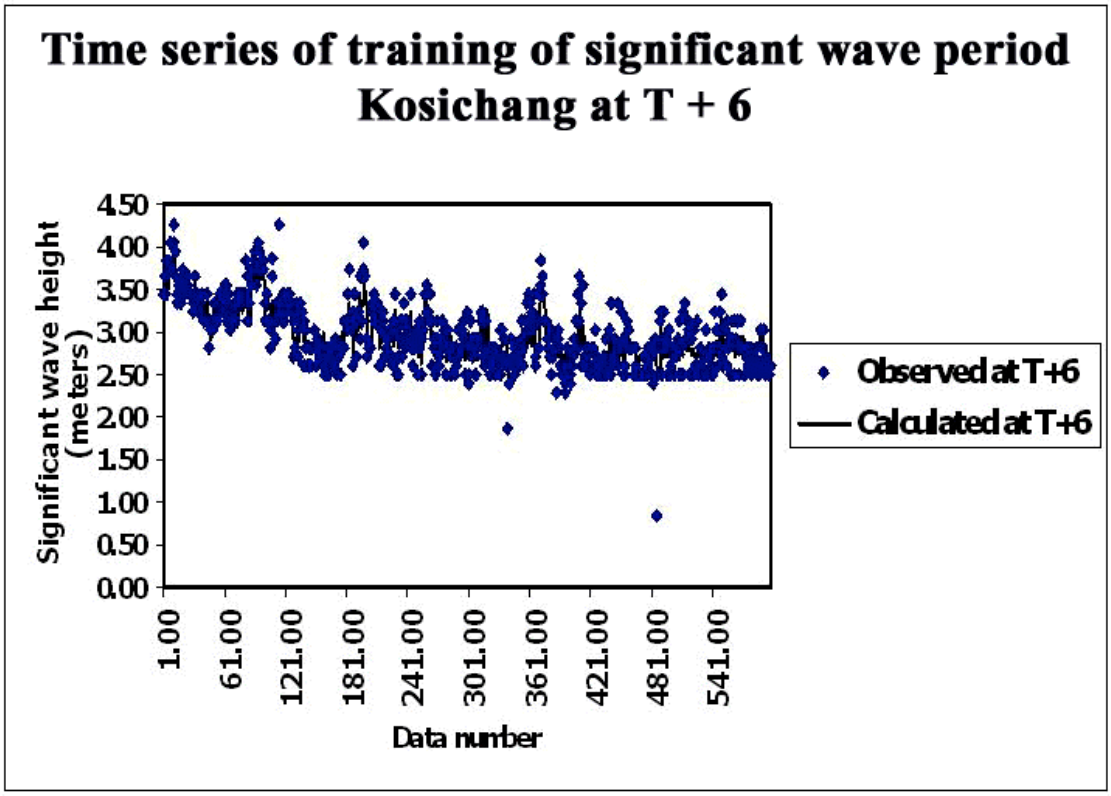
Time series of training of significant wave period
Kosichang at T + 6
Significant wave height (meters)
4.50
4.00
3.50
3.00
2.50
2.00
1.50
1.00
0.50
0.00
1.00
61.00
121.00
181.00
241.00
301.00
361.00
421.00
481.00
541.00
Data number
Observed at T+6
Calculated at T+6

b) T+ 6

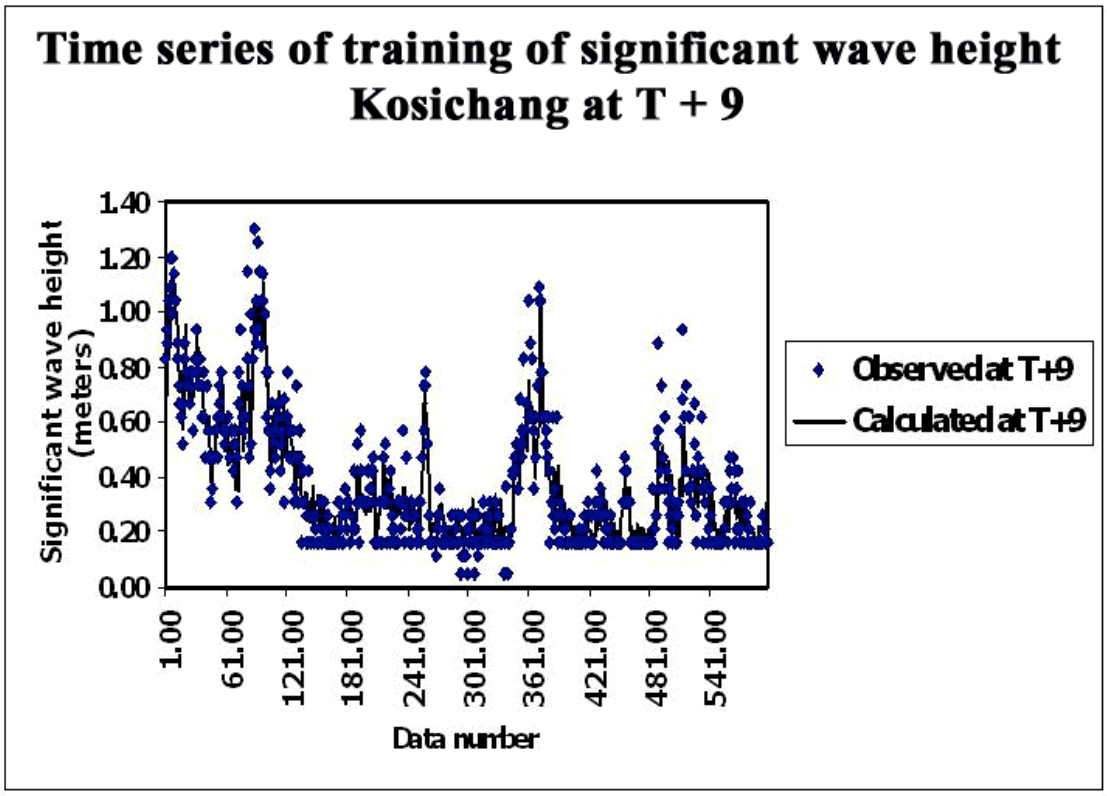
Time series of training of significant wave height
Kosichang at T + 9
Significant wave height (meters)
1.40
1.20
1.00
0.80
0.60
0.40
0.20
0.00
1.00
61.00
121.00
181.00
241.00
301.00
361.00
421.00
481.00
541.00
Data number
Observed at T+9
Calculated at T+9

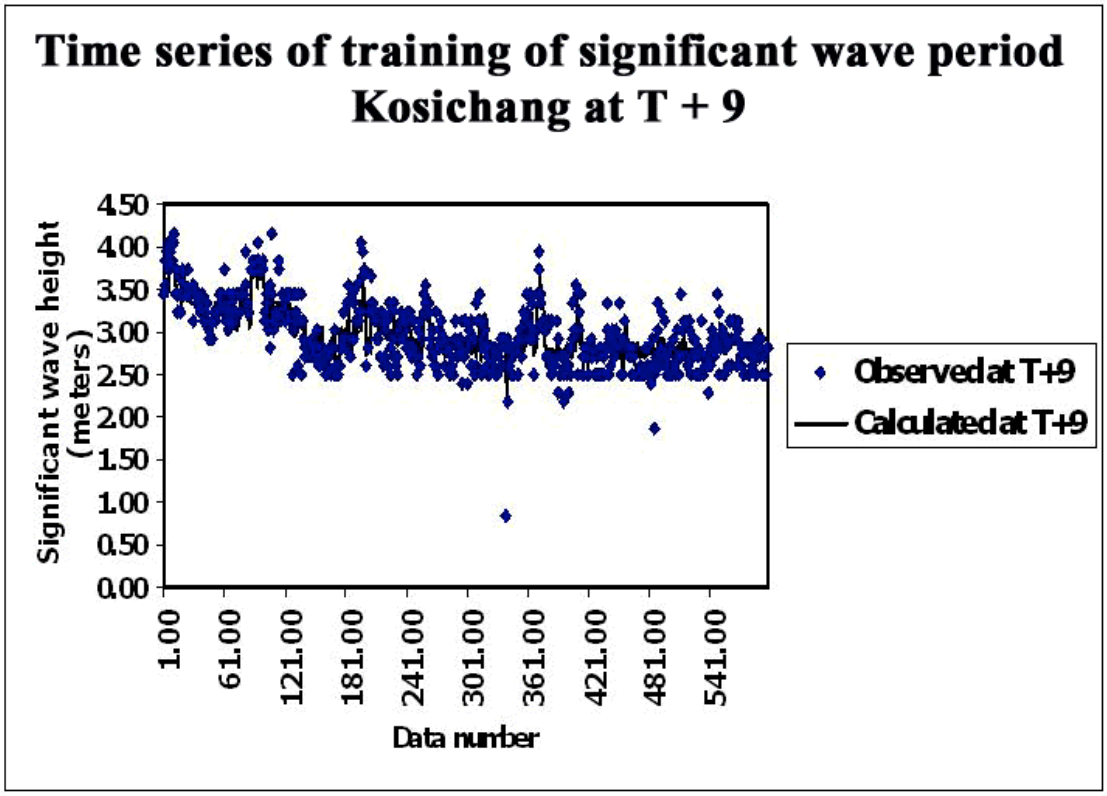
Time series of training of significant wave period
Kosichang at T + 9
Significant wave height (meters)
4.50
4.00
3.50
3.00
2.50
2.00
1.50
1.00
0.50
0.00
1.00
61.00
121.00
181.00
241.00
301.00
361.00
421.00
481.00
541.00
Data number
Observed at T+9
Calculated at T+9

c) T+ 9

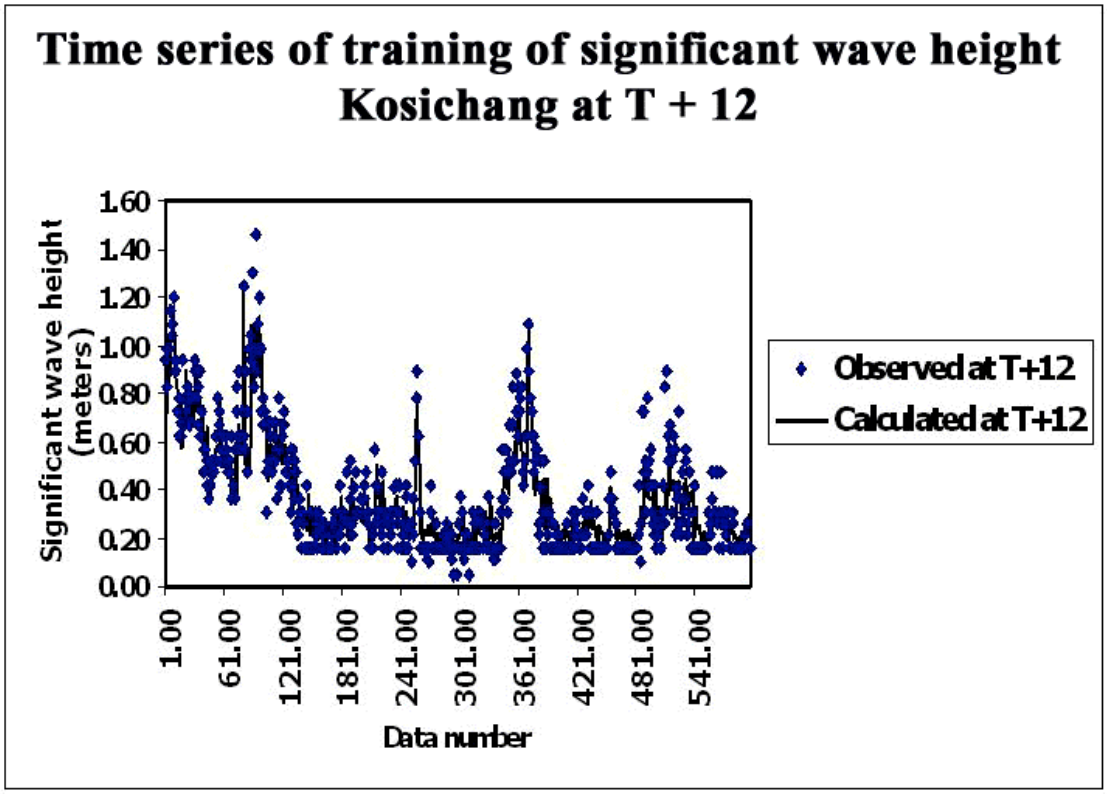
Time series of training of significant wave height
Kosichang at T + 12
Significant wave height (meters)
1.60
1.40
1.20
1.00
0.80
0.60
0.40
0.20
0.00
1.00
61.00
121.00
181.00
241.00
301.00
361.00
421.00
481.00
541.00
Data number
Observed at T+12
Calculated at T+12

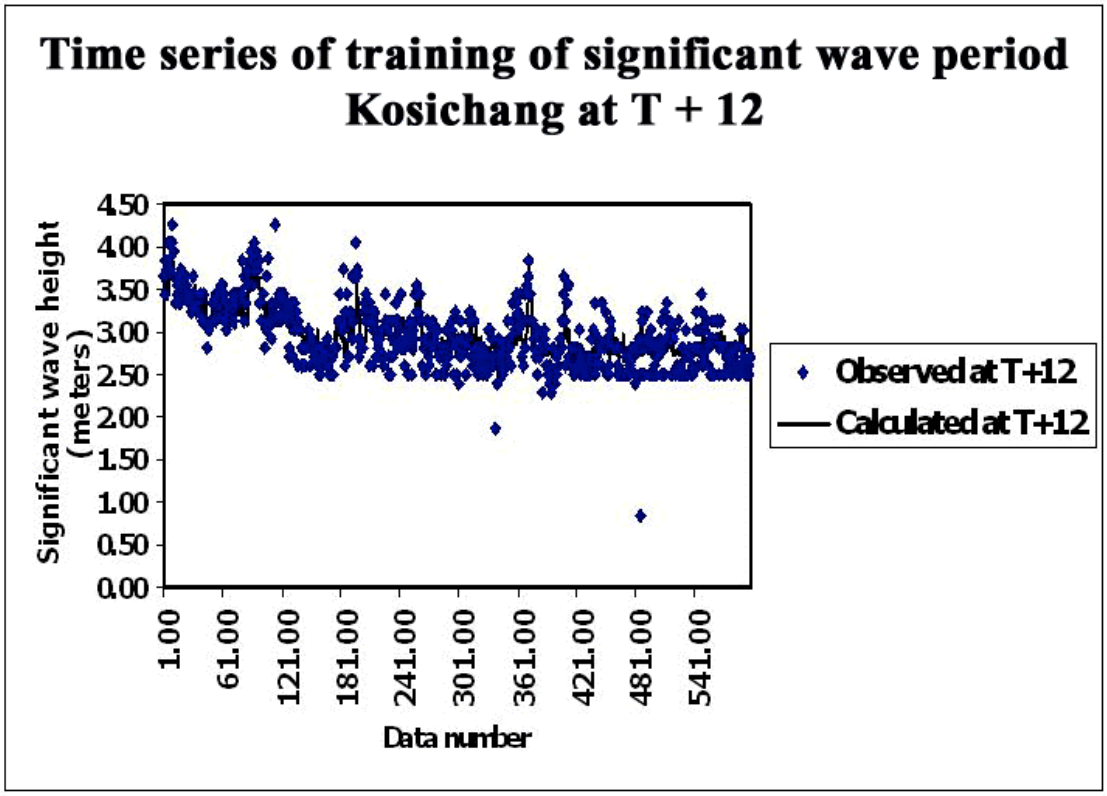
Time series of training of significant wave period
Kosichang at T + 12
Significant wave height (meters)
4.50
4.00
3.50
3.00
2.50
2.00
1.50
1.00
0.50
0.00
1.00
61.00
121.00
181.00
241.00
301.00
361.00
421.00
481.00
541.00
Data number
Observed at T+12
Calculated at T+12

d) T + 12

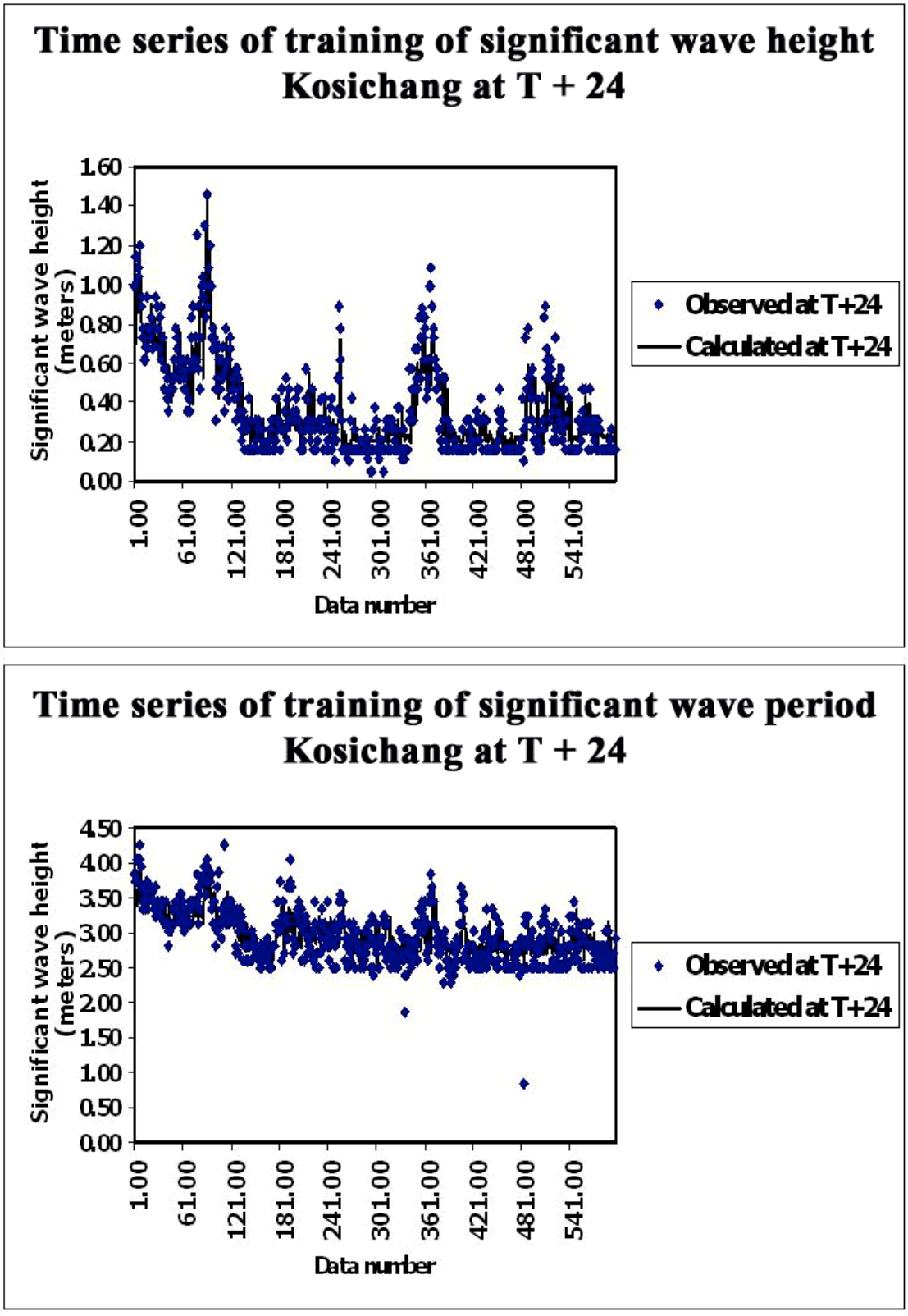

e) T + 24

Figure 4.10 Time series of wave parameters at KSI station

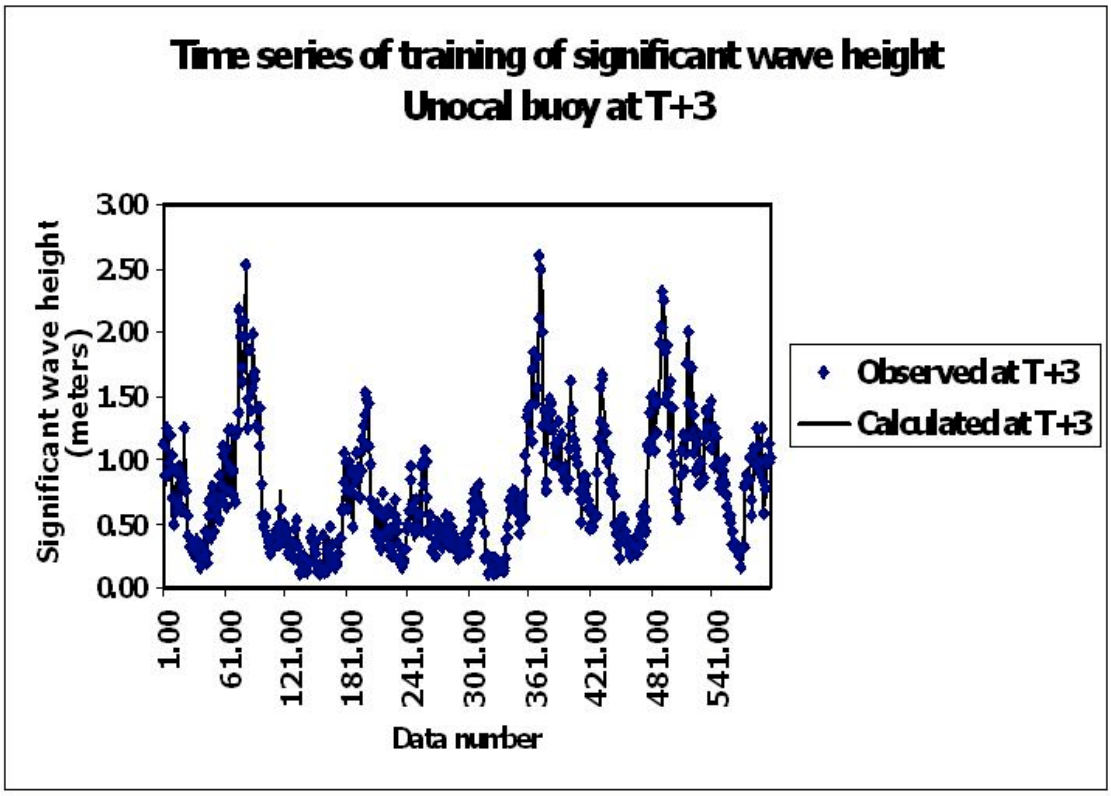
Time series of training of significant wave height
Unocal buoy at T+3
Significant wave height (meters)
3.00
2.50
2.00
1.50
1.00
0.50
0.00
1.00
61.00
121.00
181.00
241.00
301.00
361.00
421.00
481.00
541.00
Data number
Observed at T+3
Calculated at T+3

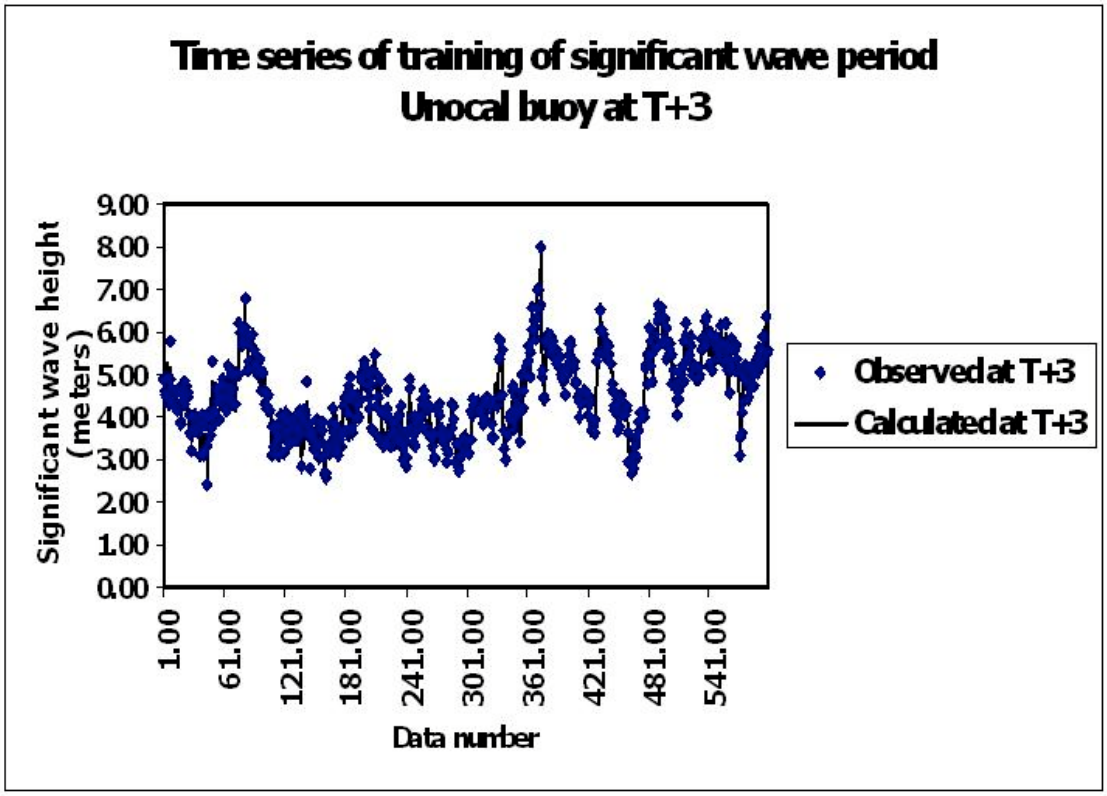
Time series of training of significant wave period
Unocal buoy at T+3
Significant wave height (meters)
9.00
8.00
7.00
6.00
5.00
4.00
3.00
2.00
1.00
0.00
1.00
61.00
121.00
181.00
241.00
301.00
361.00
421.00
481.00
541.00
Data number
Observed at T+3
Calculated at T+3

a) T + 3

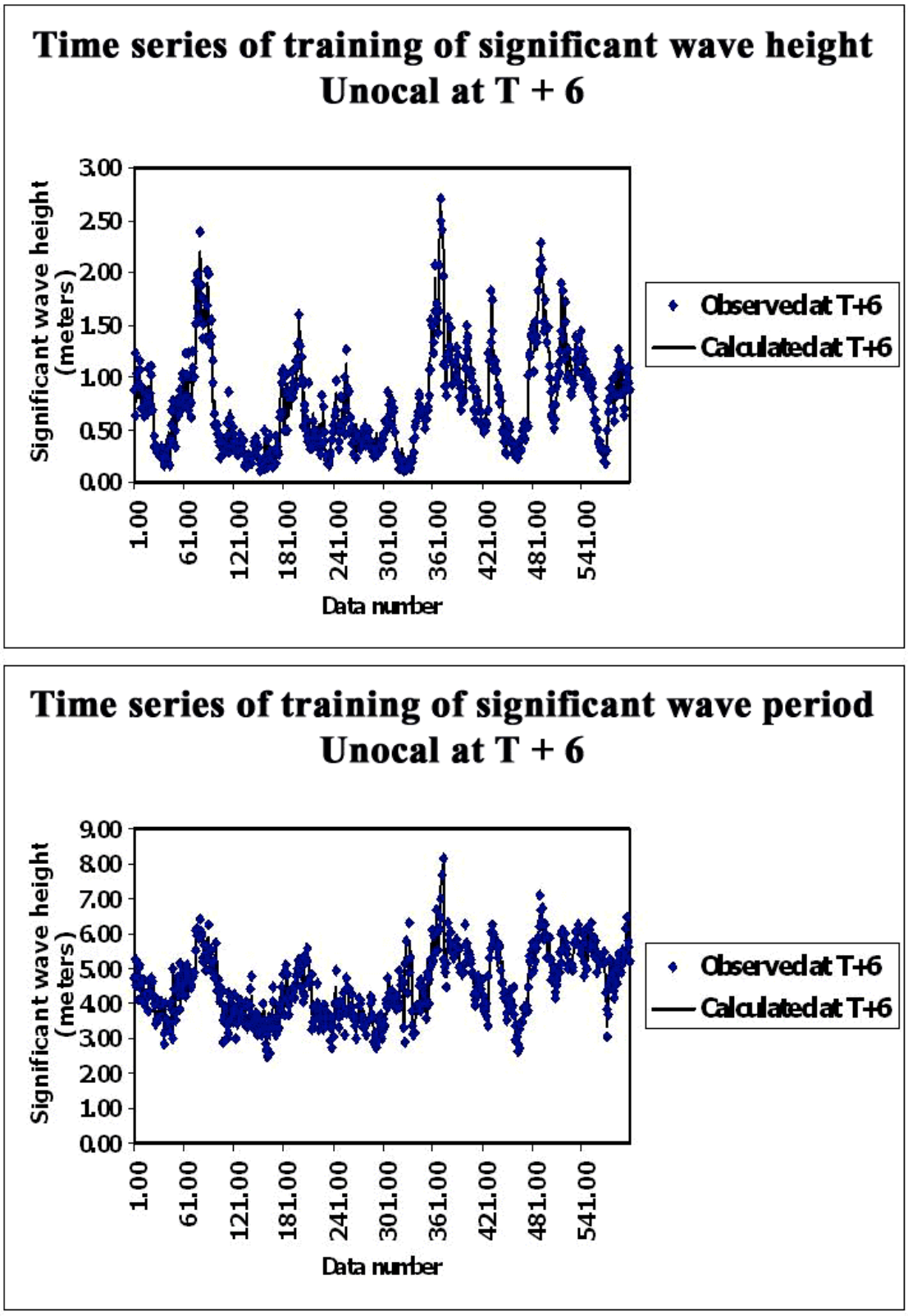
Time series of training of significant wave height
Unocal at T + 6
Significant wave height (meters)
3.00
2.50
2.00
1.50
1.00
0.50
0.00
1.00
61.00
121.00
181.00
241.00
301.00
361.00
421.00
481.00
541.00
Data number
Observed at T+6
Calculated at T+6
Time series of training of significant wave period
Unocal at T + 6
Significant wave height (meters)
9.00
8.00
7.00
6.00
5.00
4.00
3.00
2.00
1.00
0.00
1.00
61.00
121.00
181.00
241.00
301.00
361.00
421.00
481.00
541.00
Data number
Observed at T+6
Calculated at T+6

b) T + 6

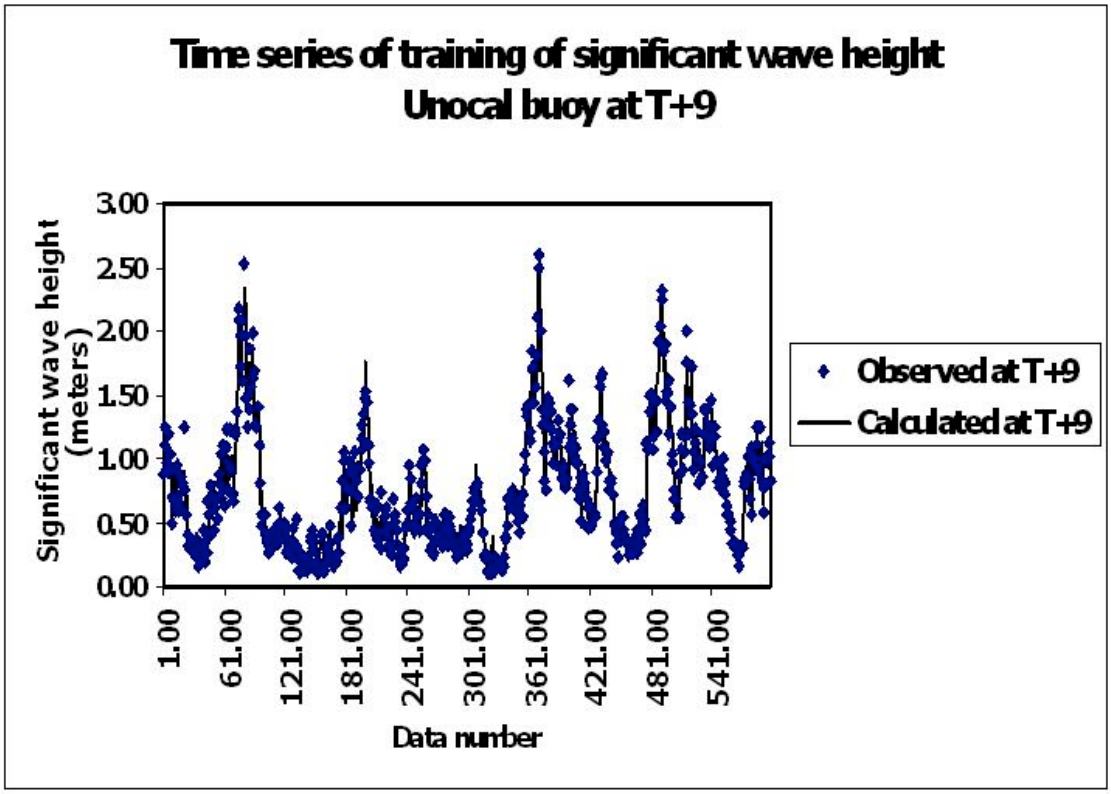
Time series of training of significant wave height
Unocal buoy at T+9
Significant wave height (meters)
3.00
2.50
2.00
1.50
1.00
0.50
0.00
1.00
61.00
121.00
181.00
241.00
301.00
361.00
421.00
481.00
541.00
Data number
Observed at T+9
Calculated at T+9

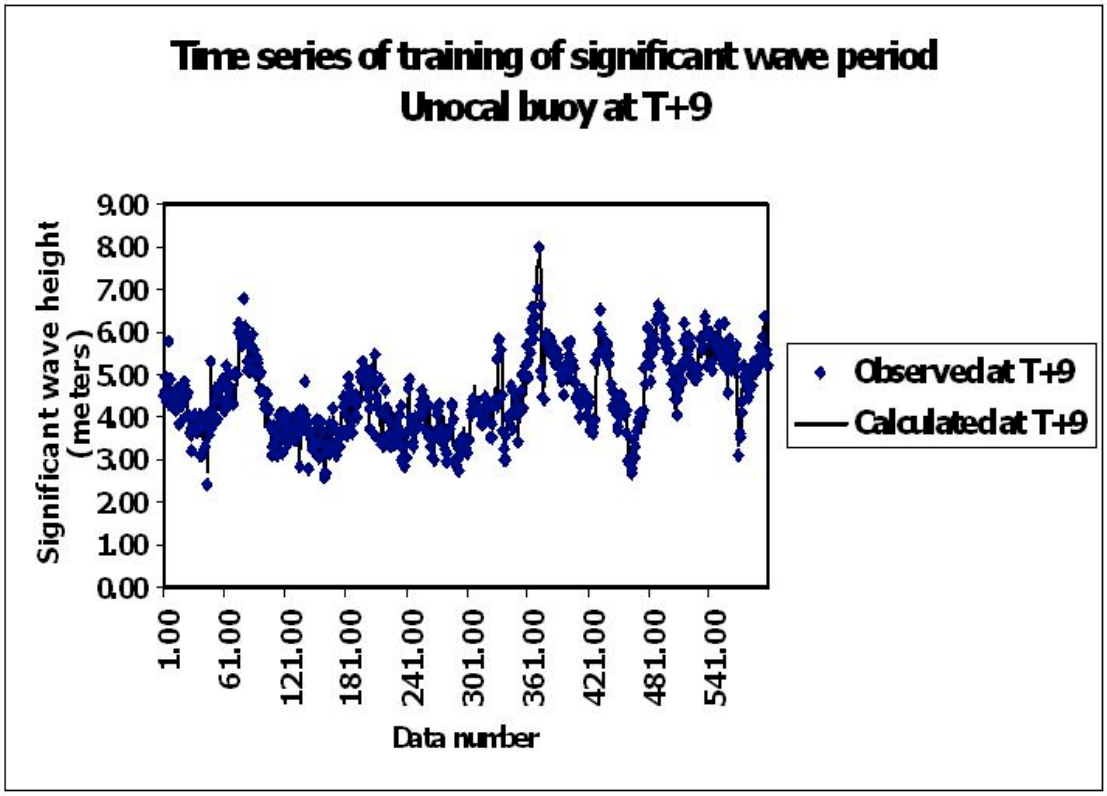
Time series of training of significant wave period
Unocal buoy at T+9
Significant wave height (meters)
9.00
8.00
7.00
6.00
5.00
4.00
3.00
2.00
1.00
0.00
1.00
61.00
121.00
181.00
241.00
301.00
361.00
421.00
481.00
541.00
Data number
Observed at T+9
Calculated at T+9

c) T + 9

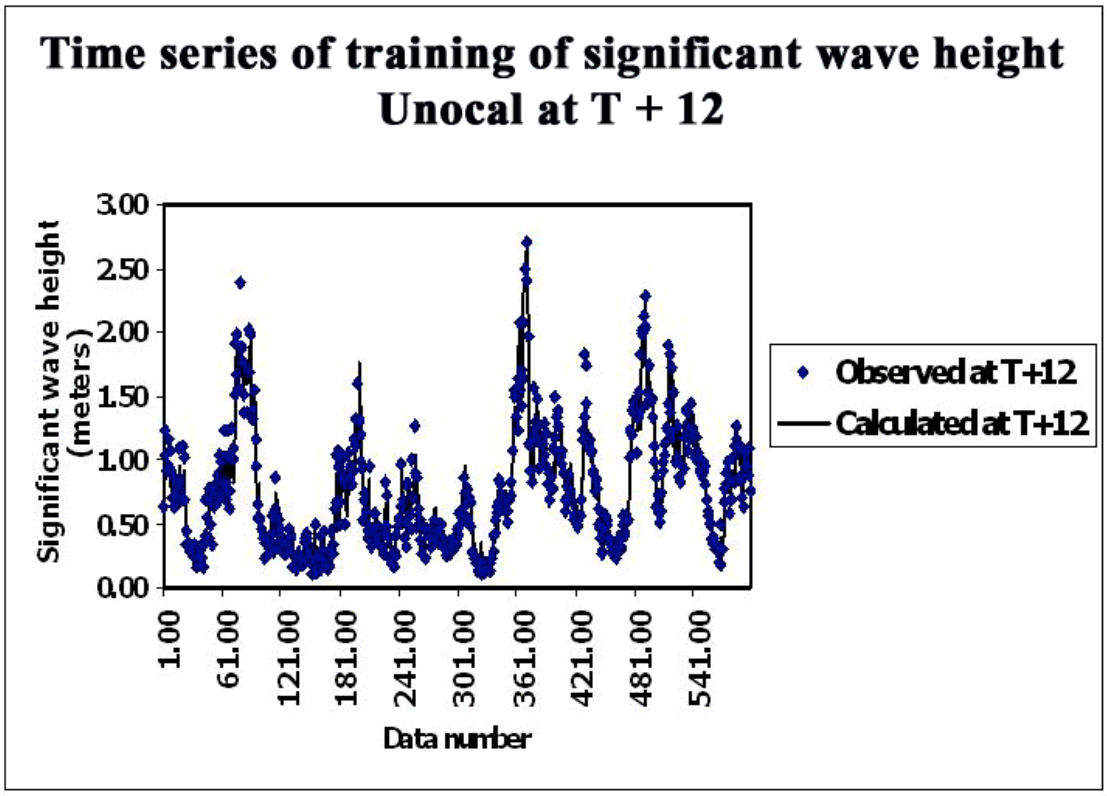
Time series of training of significant wave height
Unocal at T + 12
Significant wave height (meters)
3.00
2.50
2.00
1.50
1.00
0.50
0.00
1.00
61.00
121.00
181.00
241.00
301.00
361.00
421.00
481.00
541.00
Data number
Observed at T+12
Calculated at T+12

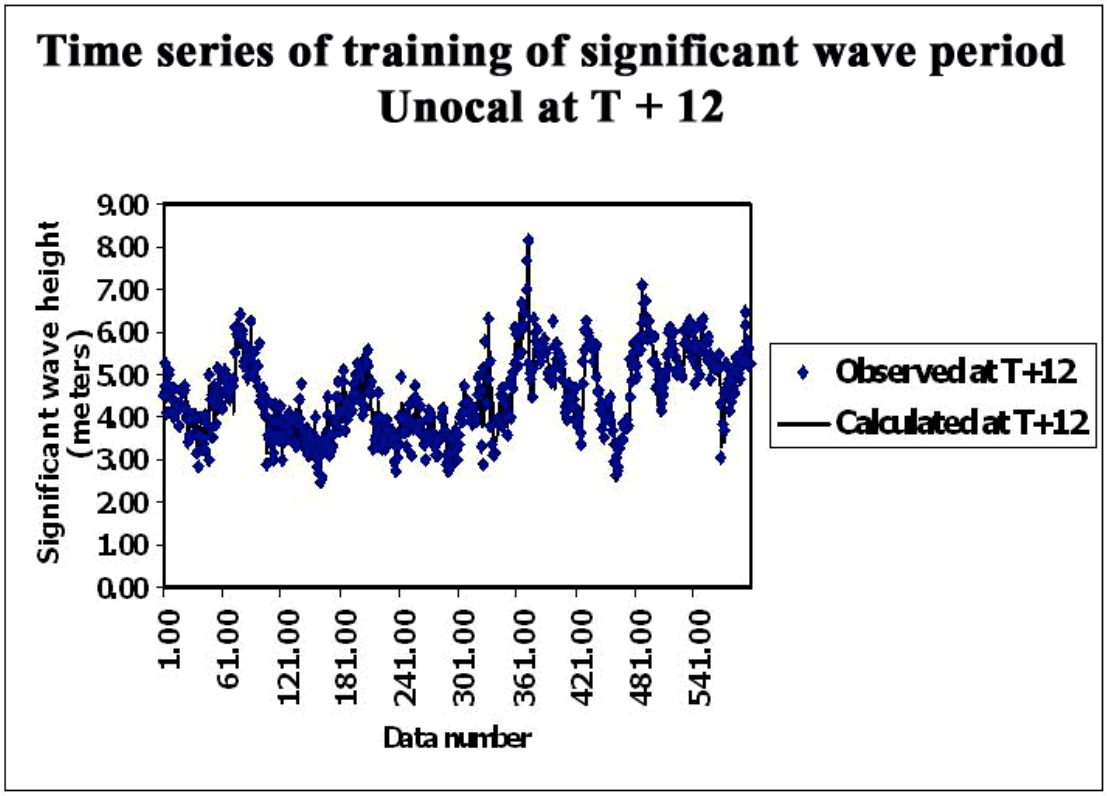
Time series of training of significant wave period
Unocal at T + 12
Significant wave height (meters)
9.00
8.00
7.00
6.00
5.00
4.00
3.00
2.00
1.00
0.00
1.00
61.00
121.00
181.00
241.00
301.00
361.00
421.00
481.00
541.00
Data number
Observed at T+12
Calculated at T+12

d) T + 12

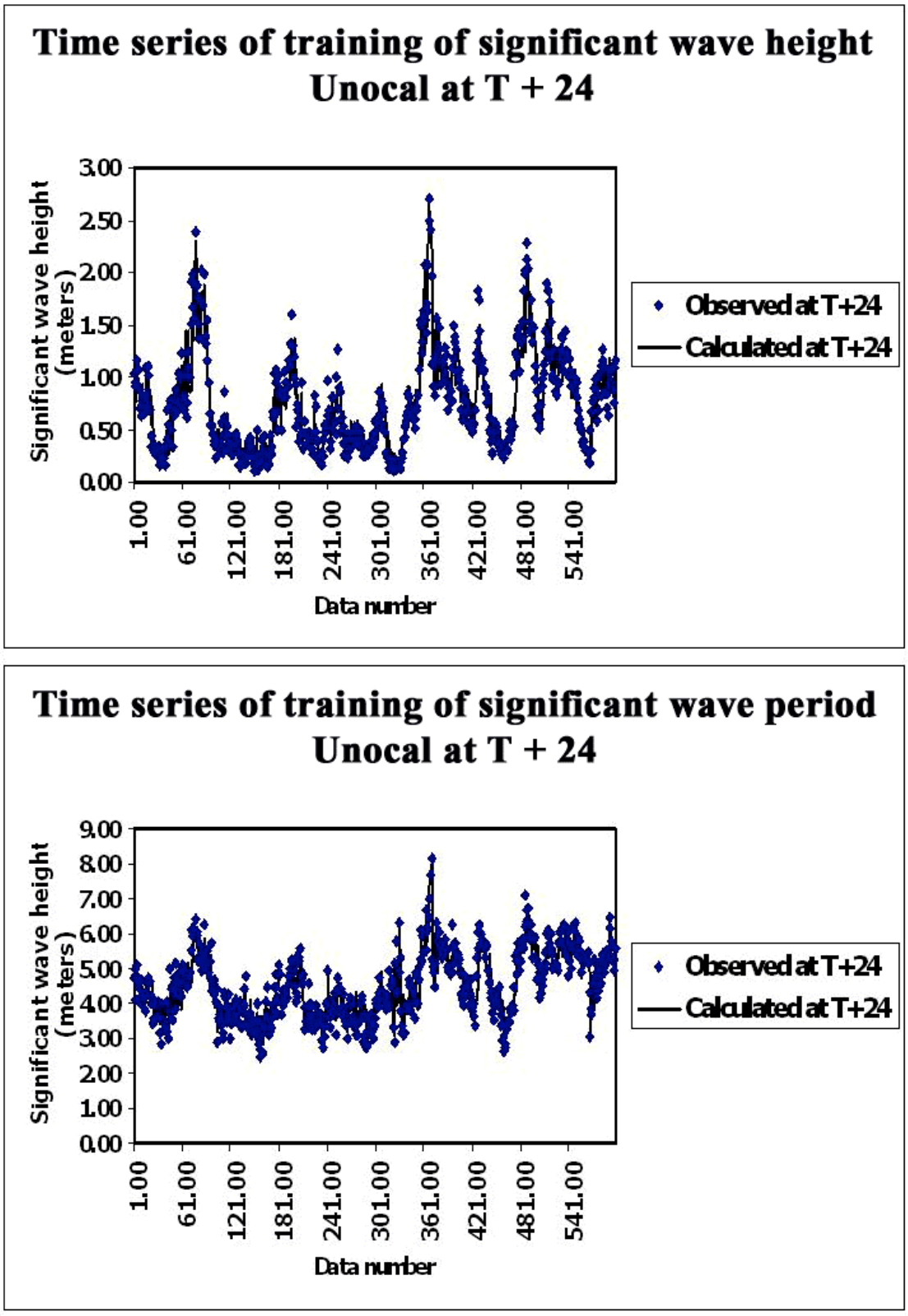

e) T + 24

Figure 4.11 Time series of wave parameters at UNC station

Results of simulations obtained from the GRNN are presented in Table 1. The verification statistics (by the root mean square error, RMSE and the efficiency index, EI) show that the wave heights were simulated very satisfactorily when short-term prediction of less than 12 hours are concerned. In addition, the predictions with leading time of 24 hours still exhibit fairly good results. The RMSE are less than or equal to 0.15 m; the MAD are less than or equal to 0.10 m; and the EI of these forecasts are higher than or equal to 0.85, except at the KSI station where effects of wave reflection and diffraction may contribute to the errors. The wave periods were simulated not so good as wave heights. The RMSE are less than or equal to 0.4 s; the MAD are less than or equal to 0.3 s; and the EI of these forecasts are higher than or equal to 0.6.

A global evaluation of the individual forecasts is provided by the scatter plots in Fig. 4.12 and Fig. 4.13, where the forecasts are compared with the observation on a one-to-one basis at the HHN station. Ideal forecasts should watch the observations exactly, and therefore all the points in the scatter plot should fall on a 1:1 line. Remarkably, this is practically the case for leading times < 24 hrs. The longer the predictions are performed, the more errors are observed. Figure 8 displays the time series of the wave heights and wave periods at the HHN wave stations. In general, the magnitude and phase can be simulated reasonably well. The maximum wave height obtained from the GRNN during the typhoon LINDA event was found to be 4 m, which is closer to the measured data than the WAM model results.

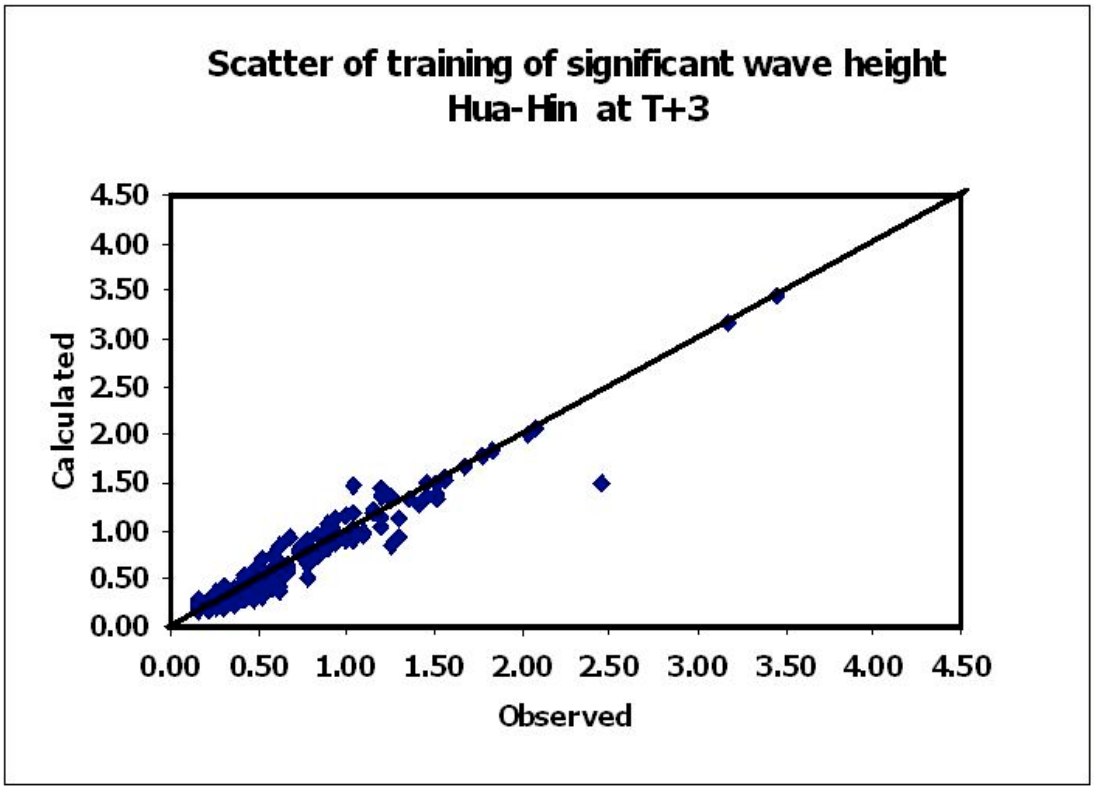
Scatter of training of significant wave height
Hua-Hin at T+3
Calculated
Observed
0.00
0.50
1.00
1.50
2.00
2.50
3.00
3.50
4.00
4.50

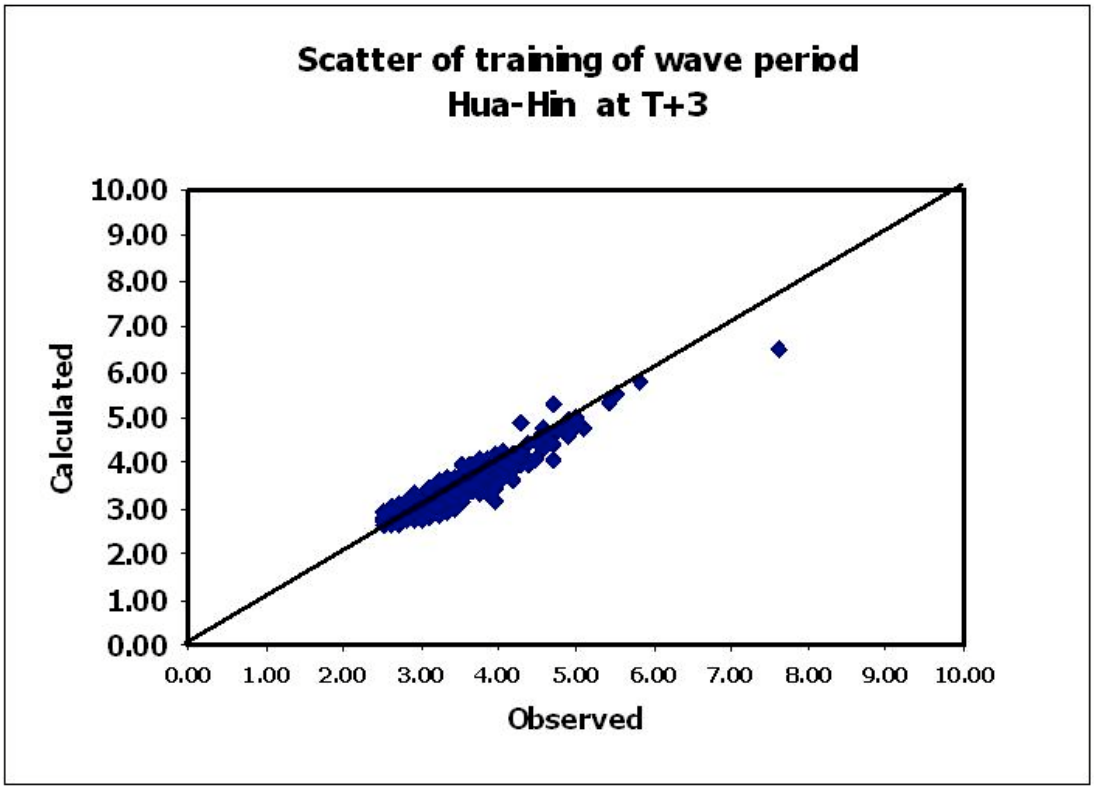
Scatter of training of wave period
Hua-Hin at T+3
Calculated
Observed
0.00
1.00
2.00
3.00
4.00
5.00
6.00
7.00
8.00
9.00
10.00

a) T + 3

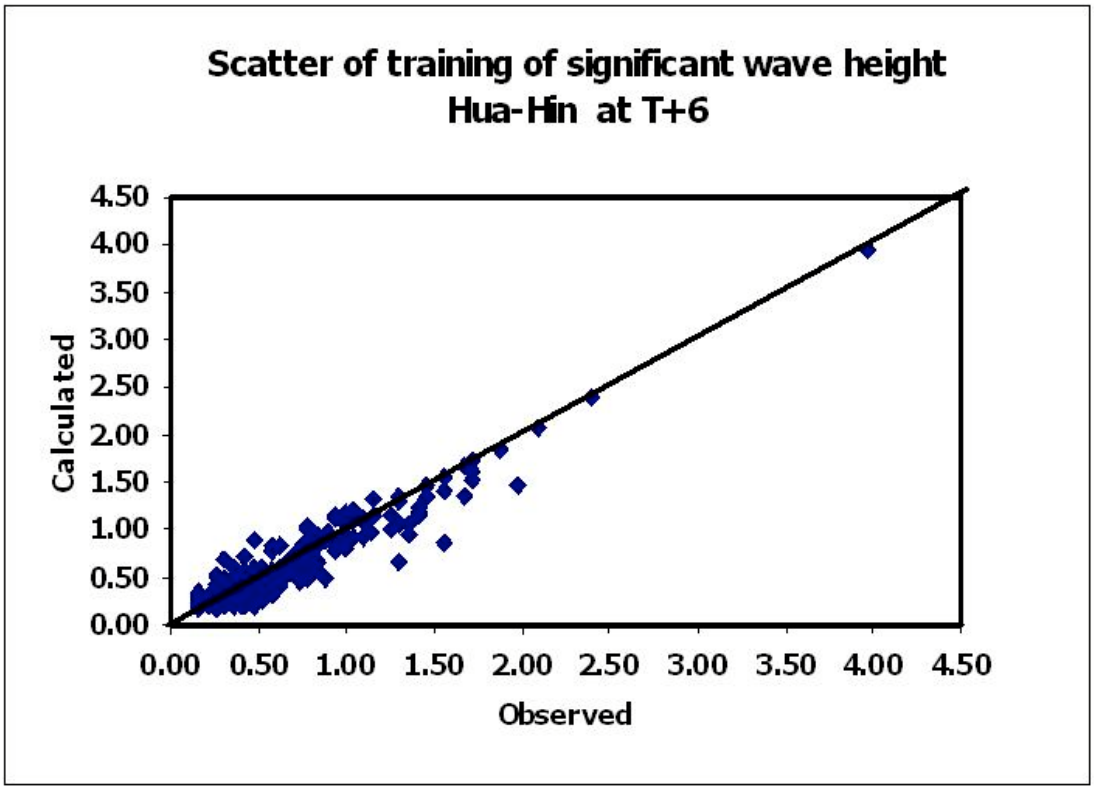
Scatter of training of significant wave height
Hua-Hin at T+6
Calculated
Observed
0.00
0.50
1.00
1.50
2.00
2.50
3.00
3.50
4.00
4.50

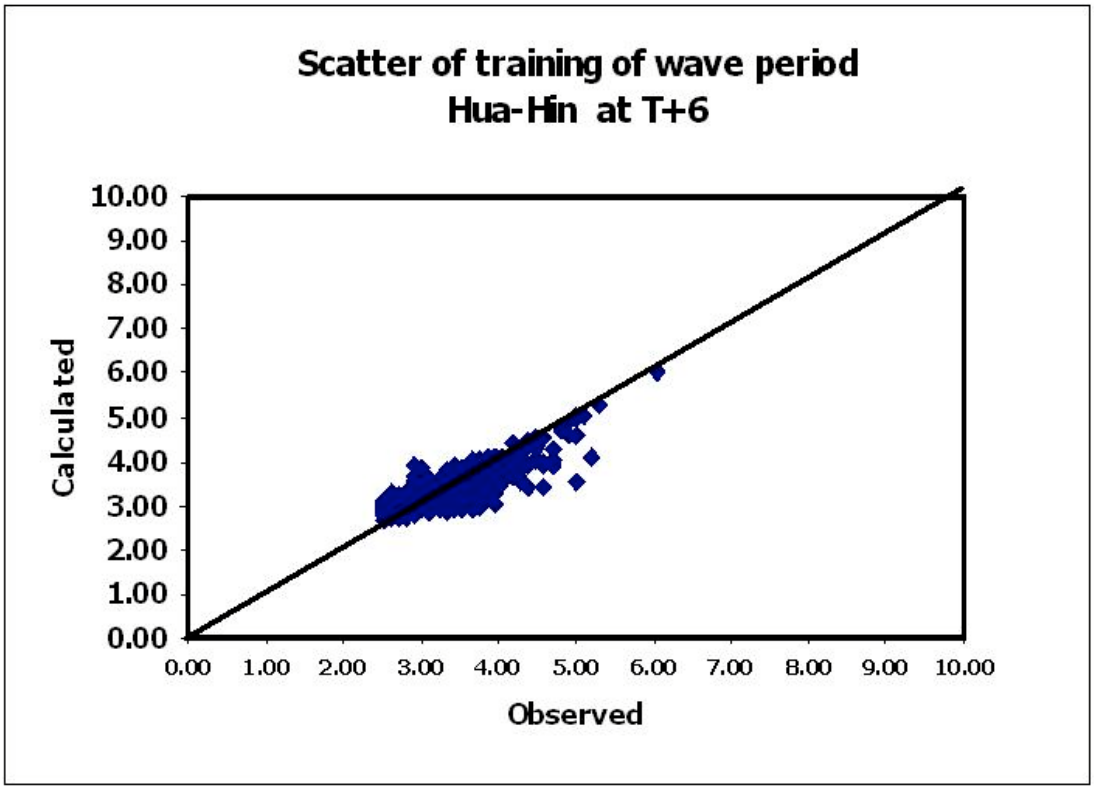
Scatter of training of wave period
Hua-Hin at T+6
Calculated
Observed
0.00
1.00
2.00
3.00
4.00
5.00
6.00
7.00
8.00
9.00
10.00

b) T + 6

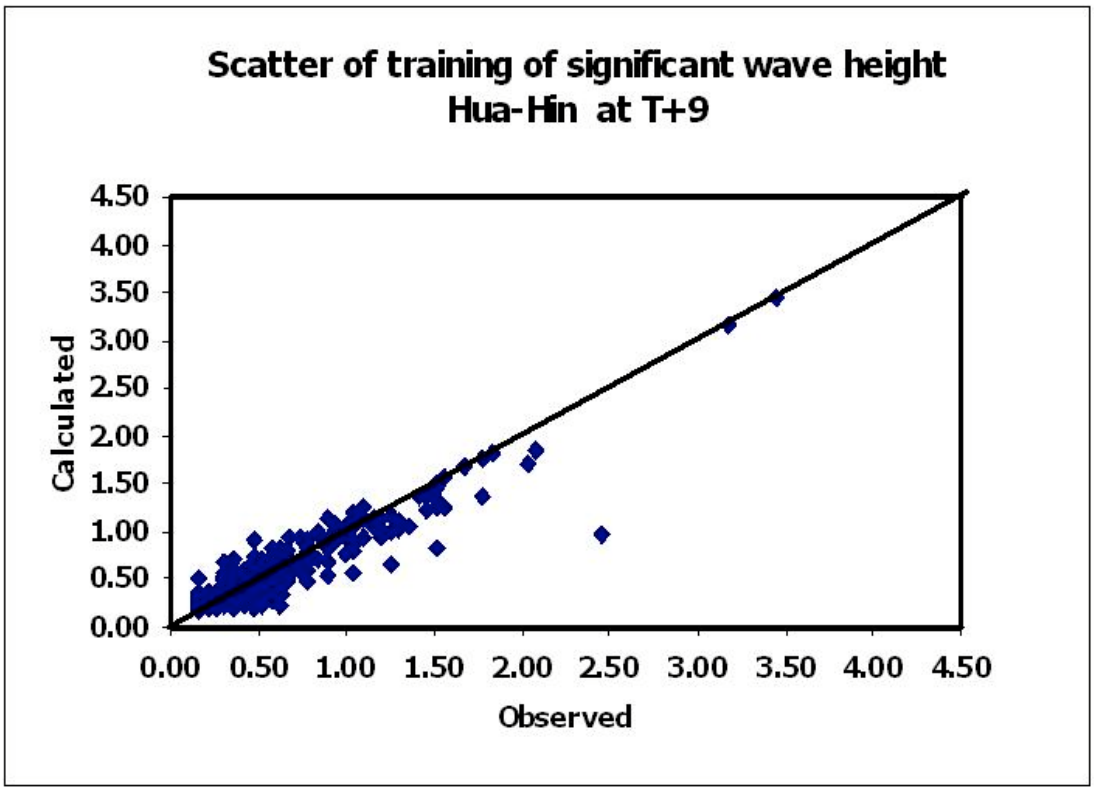
Scatter of training of significant wave height
Hua-Hin at T+9
Calculated
Observed
0.00
0.50
1.00
1.50
2.00
2.50
3.00
3.50
4.00
4.50

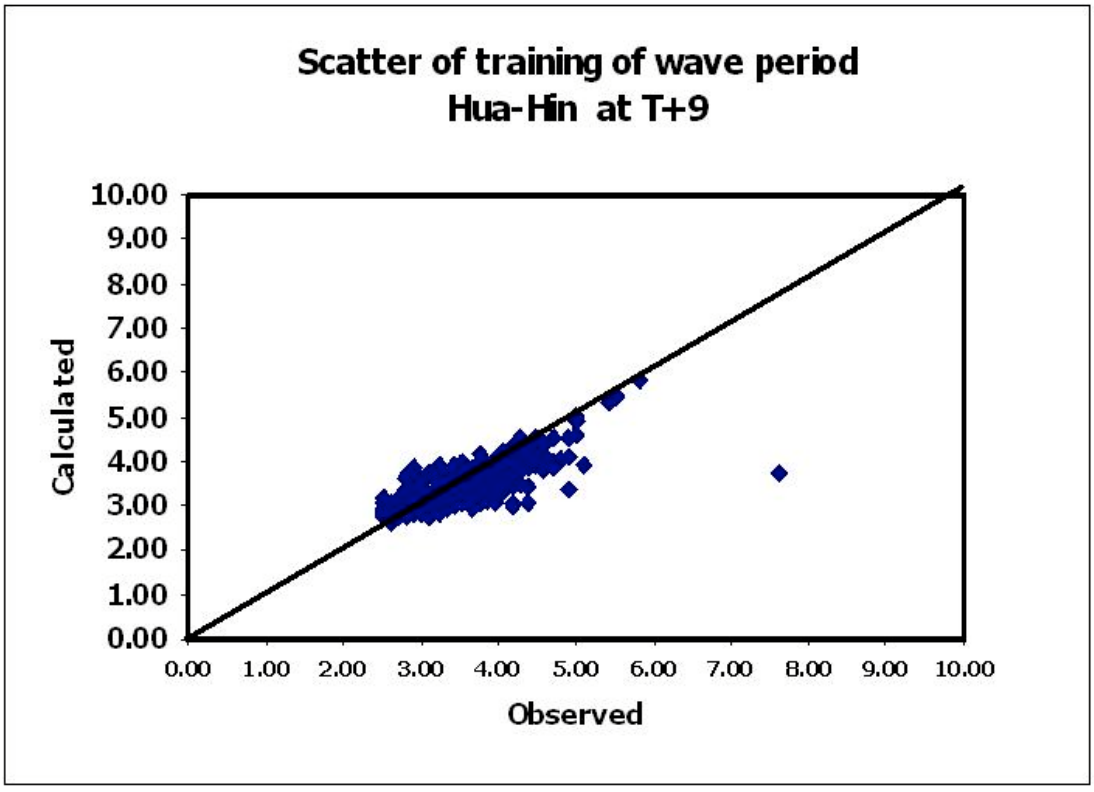
Scatter of training of wave period
Hua-Hin at T+9
Calculated
Observed
0.00
1.00
2.00
3.00
4.00
5.00
6.00
7.00
8.00
9.00
10.00

c) T + 9

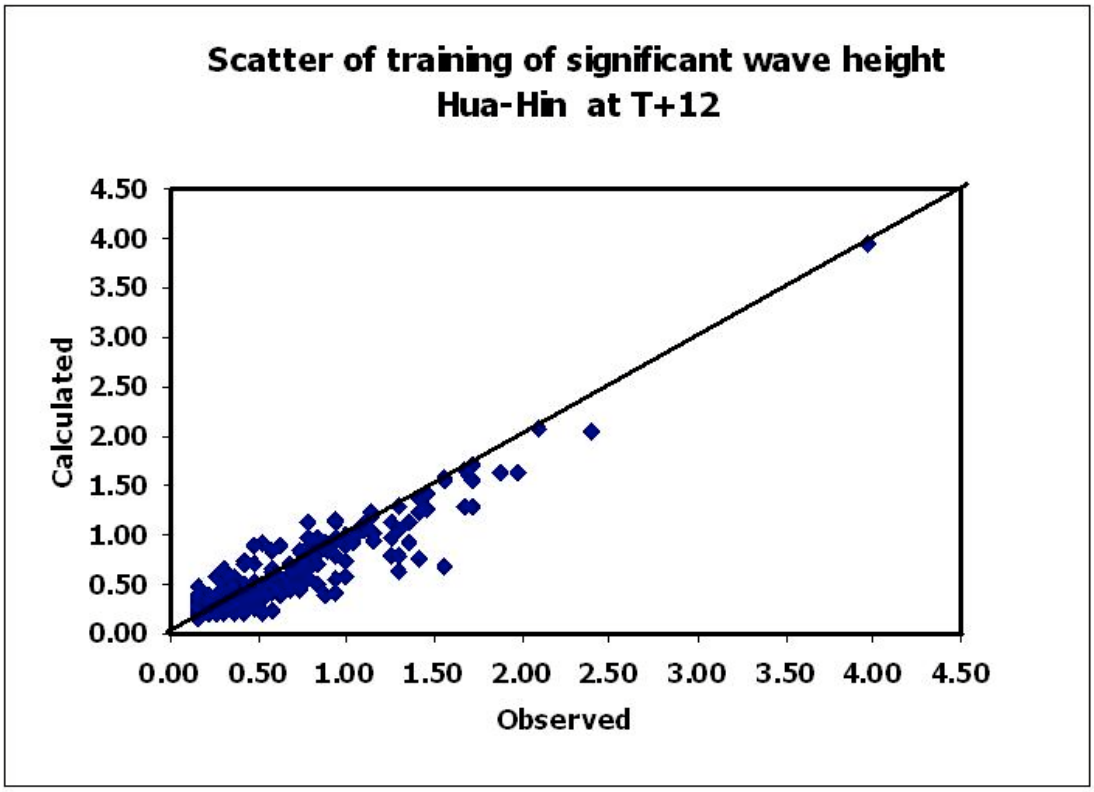
Scatter of training of significant wave height
Hua-Hin at T+12
Calculated
Observed
0.00
0.50
1.00
1.50
2.00
2.50
3.00
3.50
4.00
4.50

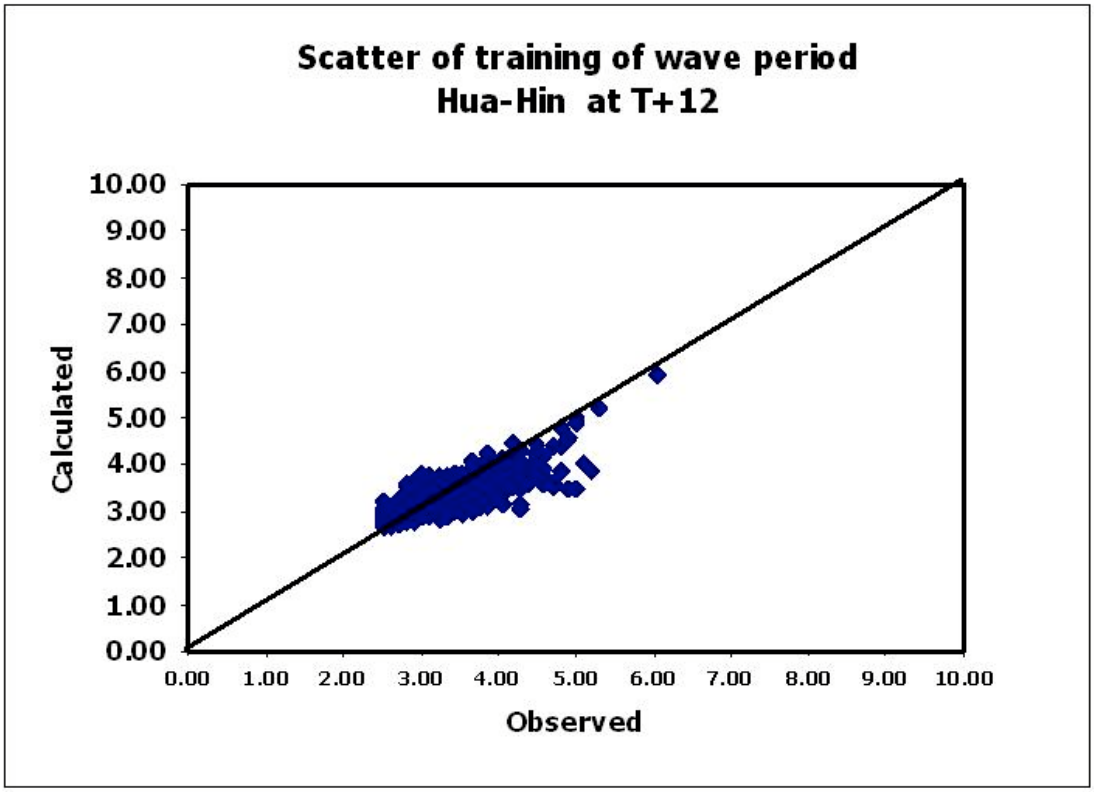
Scatter of training of wave period
Hua-Hin at T+12
Calculated
Observed
0.00
1.00
2.00
3.00
4.00
5.00
6.00
7.00
8.00
9.00
10.00

d) T +12

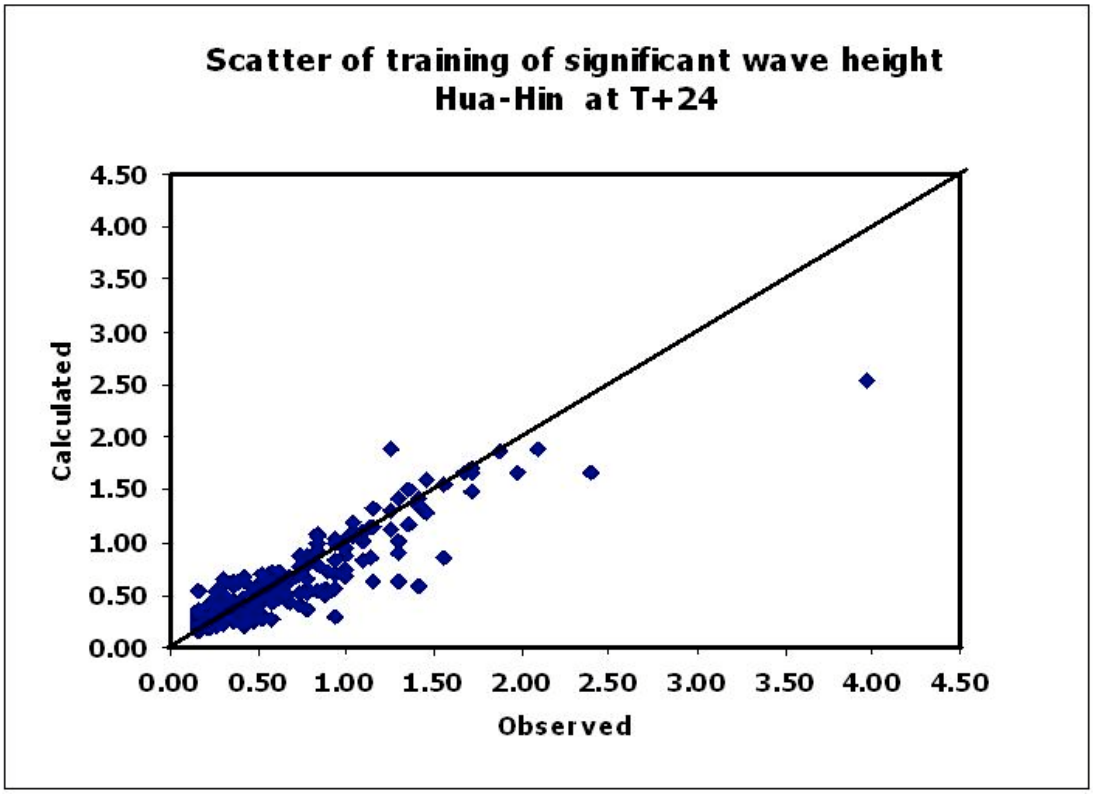

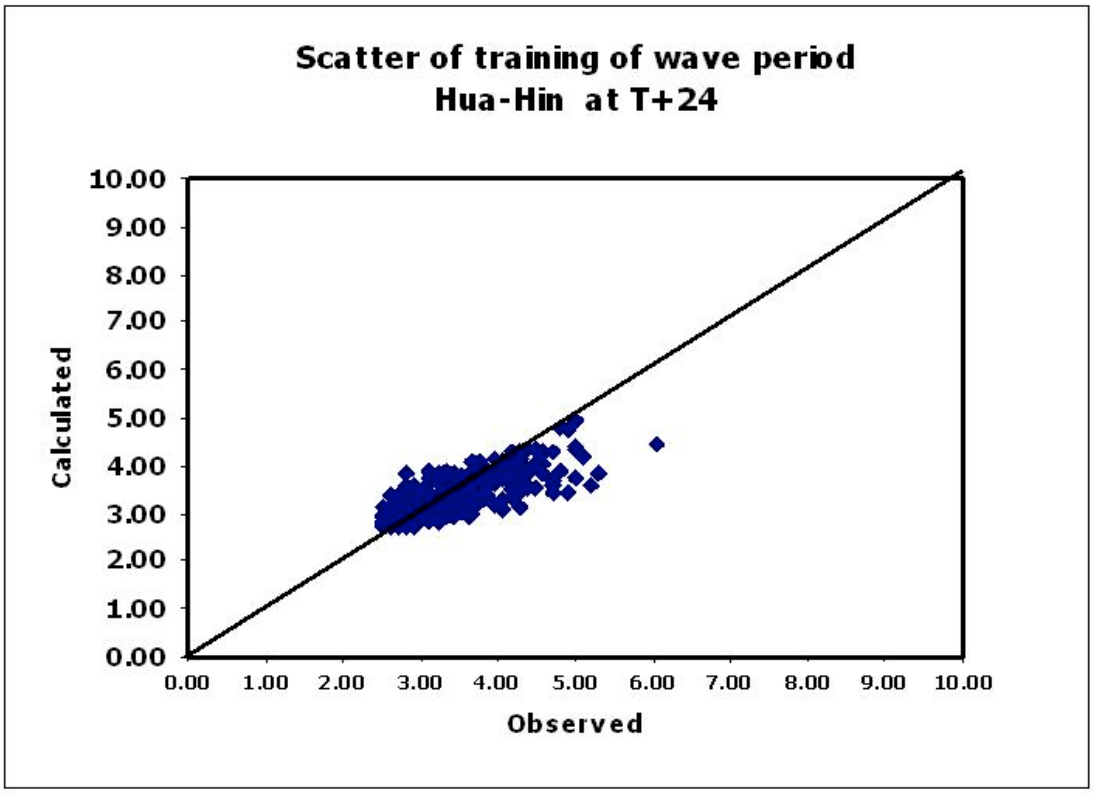

e) T + 24

Figure 4.12 Scatter plots of wave hights and wave periods at the HHN station

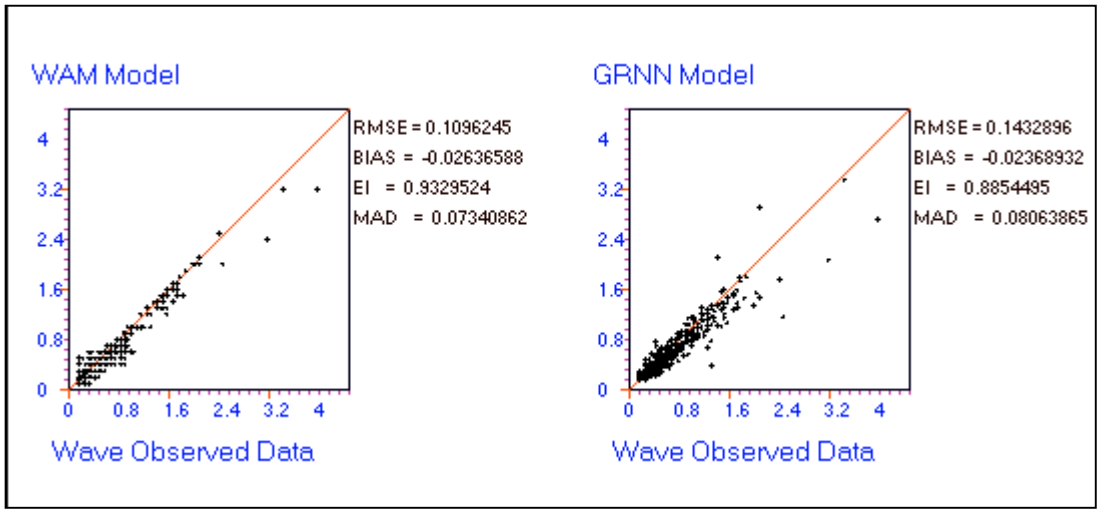

a) HHN station

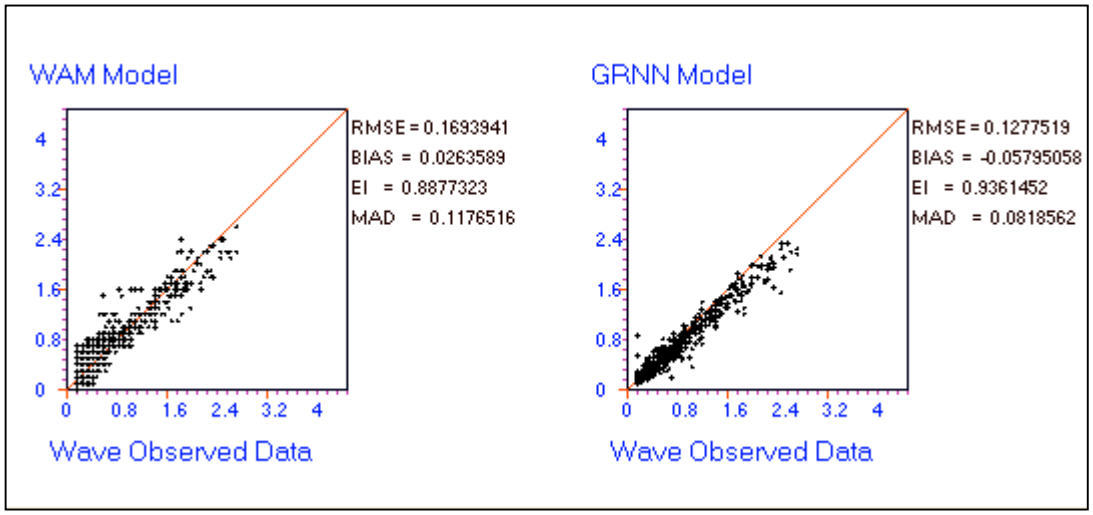

b) KCH station

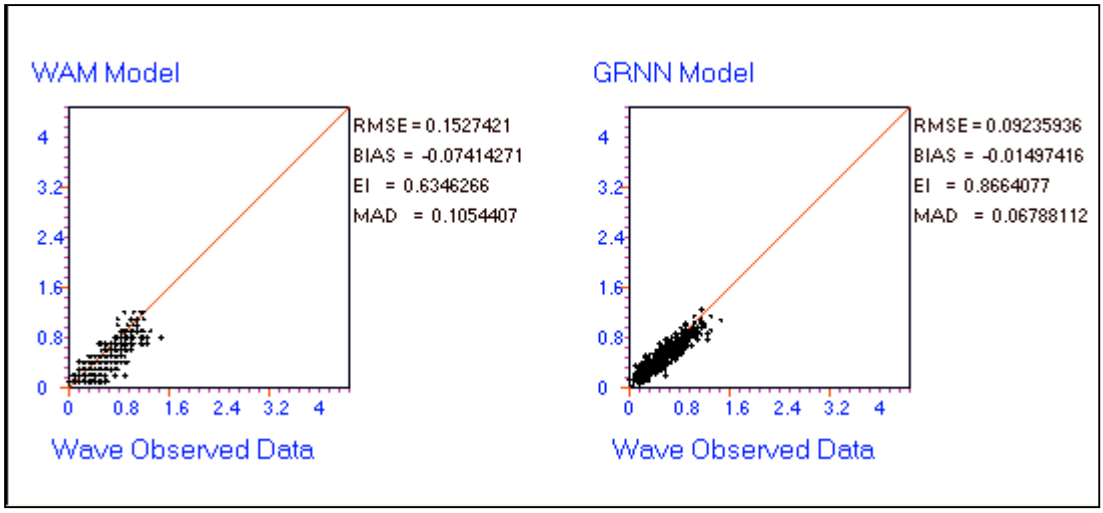

c) KSI station

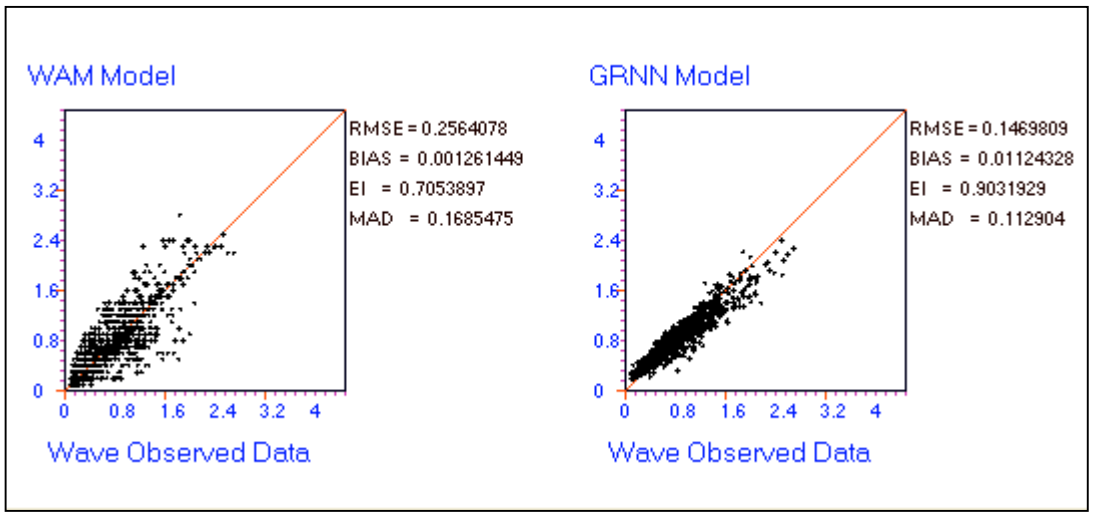

d) UNC station

Figure 4.13 Scatter plots of wave height of WAM and GRNN

Table 4.1 Results of GRNN wave parameters predictions

Stations	Parameters	Wave height					Wave period				
		Leading time (hrs.)					Leading time (hrs.)				
		t+3	t+6	t+9	t+12	t+24	t+3	t+6	t+9	t+12	t+24
HHN	RMSE	0.09	0.12	0.13	0.15	0.15	0.21	0.31	0.33	0.35	0.35
	MAD	0.06	0.08	0.09	0.10	0.10	0.16	0.23	0.25	0.26	0.25
	EI	0.95	0.92	0.90	0.87	0.85	0.89	0.74	0.70	0.66	0.64
KCH	RMSE	0.06	0.09	0.11	0.12	0.14	0.19	0.26	0.30	0.30	0.33
	MAD	0.04	0.06	0.07	0.08	0.09	0.13	0.18	0.22	0.22	0.25
	EI	0.99	0.96	0.95	0.95	0.92	0.91	0.85	0.79	0.79	0.73
KSI	RMSE	0.07	0.10	0.11	0.12	0.12	0.17	0.22	0.24	0.25	0.25
	MAD	0.05	0.07	0.08	0.09	0.08	0.13	0.18	0.19	0.19	0.19
	EI	0.92	0.84	0.80	0.77	0.77	0.80	0.66	0.59	0.57	0.56
UNC	RMSE	0.06	0.09	0.10	0.11	0.14	0.17	0.24	0.26	0.30	0.34
	MAD	0.04	0.06	0.07	0.07	0.09	0.12	0.17	0.18	0.21	0.24
	EI	0.98	0.96	0.96	0.94	0.91	0.97	0.94	0.93	0.90	0.87

Table 4.2 Verification statistics of WAM and GRNN

Parameters	HHN				KCH				KSI				UNC			
	Wave height		Wave period		Wave height		Wave period		Wave height		Wave period		Wave height		Wave period	
	WAM	GRNN	WAM	GRNN	WAM	GRNN	WAM	GRNN	WAM	GRNN	WAM	GRNN	WAM	GRNN	WAM	GRNN
RMSE	0.23	0.15	0.68	0.35	0.18	0.14	0.47	0.33	0.21	0.12	0.67	0.25	0.26	0.14	0.53	0.34
MAD	0.16	0.10	0.19	0.25	0.13	0.09	0.36	0.25	0.16	0.08	0.16	0.19	0.19	0.09	0.42	0.24
EI	0.68	0.85	0.58	0.64	0.87	0.92	0.46	0.73	0.28	0.77	0.58	0.56	0.69	0.91	0.67	0.87

Comparisons of wave heights and wave periods are made between the WAM and GRNN at lead times of 24 hours in Table 2. It is clearly observed that the GRNN shows better verification statistics than the WAM. Therefore, for the short-term predictions of wave parameters within 24 hours, the GRNN which is based on the concept of learning from experiences is recommended. In addition, it is also observed that the simulated results at the KSI station are not so good as the other stations.

CHAPTER V

SUMMARY AND CONCLUSIONS

5.1 Concluding Remarks

The project focuses on the turbulent effect of typhoon LINDA in 1997 to the wave field in the Gulf of Thailand. The investigation were based on two well known models, WAM and GRNN models. The wave propagation providing information of the wave heights and wave periods distribution on the computational domain was simulated using the hard computing approach for the WAM and the soft computing approach for the GRNN model. Comparison the results between two models was investigated. The proposed model and computational technique was verified by using data from the 4 wave stations. The results and conclusions gained from the research may be summarized as the following.

5.1.1 The WAM model underestimates the wave heights. The result indicated that the root mean square errors (RMSE) and the mean absolute deviations (MAD) for all 4 wave stations are 0.18 –0.26 m and 0.13-0.18 m, respectively. These differences between buoy data and simulated wave parameters may be due to the low spatial resolution of the employed wind fields and to the coastal boundary damping effect. The use of an analysis global wind model should improve the hindcasted waves.

5.1.2 The wind data set provided by the NRLMRY allows more accurate simulations with nested domains. In addition, diffraction, triad-wave interactions, depth-induced breaking and bottom friction effect, are important processes in coastal regions and are not considered in WAM cycle 4.0 model. This should be an interesting alternative to reproduce wind waves in very shallow water.

5.1.3 The prediction accuracy of the GRNN for short lead times is quite high (RMSE < 0.15 m and MAD < 0.10 m). The magnitude and phase of wave heights and wave periods can be simulated reasonably well. However, the simulated wave periods are not so good as wave heights. The network results are also found to be more accurate than those based on the WAM model. The maximum wave height simulated by the GRNN model during the typhoon LINDA event was found to be 4.0 m which is closer to the measured wave buoy data than the WAM model results. This indicates that for short-term prediction within 24 hrs, the data-driven model such as the GRNN should be viewed as a strong alternative in operational forecasting.

5.2 Further Works

The work of this study is linked to the evaluation of coastal processes and to assessing the wider uses of ocean environments, particularly through the use of data incorporated into coastal. The work requires the development of validation procedures before wind field data obtained from a numerical weather prediction model as high resolution limited area model can be incorporated into ocean wave model, together with the further validation of the wave data outputs. This validation though is inherently difficult because of the limited sources of good quality and readily available observational data from the offshore zone.

Together with further validation, future work hopes to include comparative studies with numerical wave models, and the compilation of significant wave height and wave period climatologies, in order to study the geographical, seasonal/annual variability and wave spectrum of the ocean wave field.

The propagative effects of water waves are quantified by noting that the local rate of change of energy is equal to the net rate of energy flow to or from that locality, i.e. the divergence of energy density flux. The practical problem encountered in computer modelling is to find a numerical scheme for calculating this. In manual

models, propagation is only considered outside the generation area and attention is focused on the dispersion and spreading of waves as they propagate.

REFERENCES

1. Albrecht Schmidt. 1996. A Modular Neural Network Architecture with Additional Generalization Abilities for High Dimensional Input Vectors. Master Thesis, Manchester Metropolitan University, UK. Available from: http://www.teco.uni-karlsruhe.de/~albrecht/neuro/html/report.html [Accessed 2003 Aug 2].
2. ASCE Task Committee on Application of Artificial Neural Networks in Hydrology : 2000a, Artificial neural networks in hydrology I : Preliminary concepts, J. Hydrologic Engrg., ASCE, 5(2), 115-123.
3. ASCE Task Committee on Application of Artificial Neural Networks in Hydrology : 2000b, Artificial neural networks in hydrology II : Hydrologic applications, J. Hydrologic Engrg., ASCE, 5(2), 124-137.
4. Barnett, T. P. (1968). “On the generation, dissipation, and prediction of wind waves.” J. Geophys. Res. 73, 647-656.
5. Barnett, T. P., and Wilkerson, J. C. (1967). “On the generation of wind waves as inferred from air-borne measurements of fetch-limited spectra.” J. Marine Research, 25, 292-328.
6. Borgman, L. E. 1967. “Spectral Analysis of Ocean Wave Forces on Piling,” ASCE Jour. Waterw., Port,Coastal and Ocean Engr., Vol 93, pp 129-156.
7. Borgman, L. E. 1969. “Ocean wave Simulation for Engineering Design,” ASCE Jour. Waterw., Port,Coastal and Ocean Engr., Vol 95, pp 557-583.
8. Borgman, L. E. 1990. “Irregular Ocean waves: Kinematics and Forces,” The Sea, B. Le Mhaut and D. M. Hanes, ed., Part A, Vol 9, pp 121-168.
9. Bouws, E., Gunther, H., Rorenthal, W., and Vincent, C. L. 1984. “Similarity of the Wind Wave Spectrum in Finite Depth Water, Part I-Spectral Form,” Jour. Geophys. Res., Vol 89, No. C1, pp 975-986.

10. Bouws, E., Gunther, H., and Vincent, C. L. 1985. “Similarity of Wind Wave Spectrum in Finite-Depth Water, Part I: Spectral Form,” J. Geophys. Res., Vol 85, No. C3, pp 1524-1530.
11. Bowden, K.F., 1983: Physical Oceanography of Coastal Waters, Ellis Horwood Ltd., England, pp.302 .
12. Bretschneider, C. 1952. “Revised Wave Forecasting Relationships,” Proceedings of the 2nd Coastal Engineering Conference, American Society of Civil Engineers, pp 1-5.
13. Bretschneider, C. L. 1959. “Wave Variability and Wave Spectra for Wind-Generated Gravity Waves,” U.S. Army Corps of Engrs., Beach Erosion Board, Tech. Memo. No. 118.
14. Bretschneider, C. 1990. “Tropical Cyclones,” Handbook of Coastal and Ocean Engineering, Vol 1, J. B. Herbich, ed., pp 249-270.
15. Briggs, M. J., Thompson, E. F., Green, D. R., and Lillycrop, L. S. 1993. “Laboratory Description of Harbor Idealized Tests,” Vol 1, U.S. Army Engineer Waterways Experiment Station, CERC-93-1, Vicksburg, MS.
16. Burgers. G. (1990). “A guide to the Nedwam wave model.” Koninklijk Nederlans Meteorlogish Instituut, KNMI Report No. WR-90-04, DeBiIt. The Netherlands.
17. Cacoullos, T. (1966). “Estimation of a multivariable density.” Ann. Inst. Statist. Math., Tokyo, Japan, 18(2), 179-189.
18. Campolo, M., Andreussi, P., and Soldati, A.: 1999, River flood forecasting with a neural network model, Water Resour. Res., 35, 1191-1197.
19. Cardone, V. J., Pierson, W. J., and Ward, E. Cl. (1976). “Hindcasting the directional spectra of hurricane generated winds.” J. Petroleum Technology, 28, 385-394.
20. Cardone. V. J., Graber, H. C., Jensen, R. E., Hasselmann, S., and Caruso, M. J. (1994). “In search of the true surface wind field: ocean wave modelling perspective.” (In preparation).
21. Chakrabarti, S. K. 1987. “Hydrodynamics of Offshore Structures,” WIT Press, Southampton, UK.

22. Clancy, R. M., Kaitala, J. E., and Zambresky, L. F. (1986). “The Fleet Numerical Oceanography Centre Global Spectral Ocean Wave Model.” Bull. Amer. Meteor. Society, 67, No. 5, 498-512.

23. Cooley, J. W. and Tukey, J. W. 1965. “An Algorithm for the Machine Computation of Complex Fourier Series,” Math. Comp., Vol 19, pp 297-301.

24. Dean, R. G. and Dalrymple, R. A. 1991. Water Wave Mechanics for Engineers and Scientists, World Scientific Pub. Co., Teaneck, NJ.

25. Demirbilek, Z. and Halvorsen, T. 1985. “Hydrodynamic Forces on Multitube Production Risers Exposed to Currents and Waves,” Trans. ASME, J. Energy Resources Technology, Vol 107, No. 2, pp 226-234.

26. Demirbilek, Z., Moe, G., and Yttervoll, P. 1987. “Morison’s Formula: Relative Velocity versus Independent Flow Fields Formulations for a Case Representing Fluid Damping,” Proc. Intl. Symposium on Offshore Mech. and Arctic Engineering, Vol II, pp 25-32, Houston, TX.

27. Demirbilek, Z. 1988. “Forces on Marine Risers in a Coexisting Environment,” J. Waterway, Port, Coastal,and Ocean Engineering, Vol 114, No. 3, pp 346-362.

28. Demirbilek, Z. 1989. Tension Leg Platform: A State-Of-The-Art Review, New York, pp 335.

29. Deo, M.C., Naidu, C. Srihar: 1999, Real time wave forecasting using neural networks, Journal of Ocean Engineering 26, 191-203.

30. Donelan, M. A., Hamilton, J., and Hu, W. H. 1982. “Directions Spectra of Wind-Generated Waves,” Unpublished manuscript, Canada Centre for Inland Waters.

31. Elgar, S. et al. 1985. “Wave Group Statistics from Numerical Simulation of a Random Sea,” Jour. Applied Ocean Res., Vol 7, pp 93-96.

32. Ewing, J. A. (1971). “A numerical wave prediction method for the North Atlantic Ocean.” Deutsche Hydrographtische Zeit. 24, 241-261.

33. Faltinsen, O. M., and Demirbilek, Z. 1989. “Hydrodynamics of Tension Leg Platforms - TLP’s,” Tension Leg Platform: A State-of-the-art Review, Z. Demirbilek, ed., ASCE Publ., New York.

34. Flood, I., and Kartam, N.: 1994, Neural networks in civil engineering –I Principles and understanding, J. Computing in Civil Engrg., ASCE, 8 (2), 131-148.

35. French, M.N., Krajewski, W.F., and Cuykendall, R.R.: 1992, Rainfall forecasting in space and time using a neural network, J. Hydro.137, 1-31.

36. Funke, E. R. and Mansard, E. P. D. 1980. “On the Synthesis of Realistic Sea State,” Proc. 17th Coastal Engr. Conf., Vol 2, pp 2974-2991.

37. Goda, Y. 1974. “Estimation of wave Statistics from Spectra Information,” Proc. Intl. Symp. on Ocean Wave Meas. and Anal., ASCE, Vol 1, pp 320-337.

38. Goda, Y. 1976. “On Wave Groups,” Proc. BOSS’76, Vol 1, pp 115-128.

39. Goda, Y. and Suzuki, Y. 1976. “Estimation of Incident and Reflected Waves in Random Wave Experiments,” Proc. 15th Coastal Engr. Conf., Vol 1, pp 828-845.

40. Goda, Y. 1985a. “Numerical Examination of Several Statistical Parameters of Sea Waves,” Rept. Port and Harbor Res. Inst., Vol 24, No. 4, pp 65-102.

41. Goda, Y. 1985b. Random Seas and Design of Maritime Structures, Univ. of Tokyo Press, Tokyo, Japan.

42. Goda, Y. 1987. “Statistical Variability of Sea State Parameters as a Function of Wave Spectrum,” Proc.IAHR Seminar on Wave Anal. and Gen. in Lab. Basins, Lausanne, Switzerland.

43. Graber, H. C., Caruso, M. J., and Jensen, R. E. (1991). “Surface wave simulations during the October storm in SWADE.” Proc. MTS ‘91 Conf. Marine Technology Society, Washington, DC, 159-164.

44. Guide to Wave Analysis and Forecasting. 1998 (second edition). World Meteorological Organization. WMO – No. 702. Geneva. Switzerland. 159 p.

45. Gunther, H., S. Hasselmann and P.A.E.M. Janssen : 1991, Wamodel cycle 4. DKRZ report no. 4, Hamburg.

46. Gunther, H., Lionello, P., and Hansen, B. (1993). 'The impact of ERS-1 altimeter on the wave analysis and forecast." GKSS 93/E/44 GKSS-Forschungsxentrum Geesthacht GmbH , Geesthacht, Germany.

47. Helmholtz, H. 1888. "Uber Atmospharische Bewwgungen," S. Ber. Preuss. Akad. Wiss. Berlin, Mathem.Physik Kl.

48. Hasselmann, K. (1962). "On the non-linear energy transfer in a gravity-wave spectrum - Part 1." J. Fluid Mech. 12, 481-500.

49. Hasselmann, K. (1963a). . "On the non-linear energy transfer in a gravity-wave spectrum - Part 2." J. Fluid Mech. 15, 273-281.

50. Hasselmann, K. (1963a). "On the non-linear energy transfer in a gravity-wave spectrum - Part 3." .J. Fluid Mech. 15, 385-398.

51. Hasselmann, K., Barnett, T.P., Bouws, E., Carlson, H., Cartwright, D.E., Enke, K., Ewing, J.A., Gienapp, H., Hasselmann. D.E., Kruseman, P., Meerburg, A., Muller, P., Olbers, K.J., Richter, K., Sell, W., and Walden, W.H. (1973). "Measurements of wind-wave growth and swell decay during the Joint North Sea Wave Project (JONSWAP)." Deutsche Hydrograph, Zeit., Erganzung-self Reihe A 8(12).

52. Hasselmann, K. : 1974, On the characterization of ocean waves due to white capping; Boundary-Layer Meteorology, Vol. 6, pp. 107-127.

53. Hasselmann, K. et al. 1976. "A Parametric Wave Prediction Model," Jour. Phys. Ocean., Vol 6, pp 200-228.

54. Hasselmann, S., and Hasselmann, K. (1981). "A symmetrical method of computing the nonlinear transfer in a gravity-wave spectrum." Hanb. Geophys. Einzelschriften, Reihe A: Wiss. Abhand. 52.

55. Hasselmann, S.and Hasselmann, K. : 1985, Computations and parameterizations of the nonlinear energy transfer in a gravity wave spectrum. Part I: A new method for efficient computations of the exact nonlinear transfer integral; J. Phys. Oceanogr., Vol. 15, No. 11, pp. 1369-1377.

56. Hasselmann, S., Hasselmann, K., Allender, J.H. and Barnett, T.P. : 1985, Computations and parameterizations of the nonlinear energy transfer in a gravity wave spectrum. Part II: Parameterizations of the nonlinear energy transfer for application in wave models; J. Phys. Oceanogr., Vol. 15, No. 11, pp. 1378-1391.

57. Holthuijsen, L. H. 1983. “Observation of the Directional Distribution of Ocean-Wave Energy in Fetch-Limited Conditions,” Jour. Phys. Ocean., Vol 13, No. 2, pp 191-207.

58. Hsieh, B.B. and Pratt, T.C. : 2001, Field data recovery in tidal system using artificial neural networks(ANNs), Coastal and Hydraulic Engineering Technical note CHETN-IV-38, U.S. Army Engineer Research and Development Center, Vicksburg, MS.

59. Hsu, K., Gupta, H.V., and Sorooshian, S.: 1995, Artificial neural networks modeling of the rainfall-runoff process, Water Resour. Res., 31(10), 2517-2530.

60. Hu, T.S., Lam, K.C., and NG, S.T.: 2001, River flow time series prediction with a range-dependent neural network, Hydrol. Sci. J. 46(5), 729-745.

61. ISSC 1964. Proceedings of the Second International Ship Structures Congress, Delft, The Netherlands.

62. ITTC 1966. “Recommendations of the 11th International Towing Tank Conference,” Proc. 11th ITTC,Tokyo, Japan.

63. Janssen, P. A. E. M. : 1989, Wave-induced stress and the drag of air flow over sea waves; J. Phys. Oceanogr., Vol. 19, pp. 745-754.

64. Janssen, P. A. E. M.: 1991, Quasi-Linear theory of wind wave generation applied to wave forecasting; J. Phys. Oceanogr., Vo. 21, pp. 1631-1642.

65. Jeffreys, J. (1924). “On the formation of waves by wind.” Proc. R. Soc. London Ser. A 107, 189-205.

66. Jeffreys, H. 1925. “On the Formation of Waves by Wind,” *Proc. Roy. Soc. Lon*d., Ser. A., Vol 110, pp 341-347.

67. Jensen, R. E., Graber, H. C., and Caruso, M. J. (1991). “A wind-wave forecast for the Surface Wave Dynamics Experiment.” Proc. MTS ‘91 Conf. Marine Technology Society, Washington, DC, 147-153.

68. Kelvin, Lord, 1887. “On the Waves Produced by a Single Impulse in Water of Any Depth or in a Dispersive Medium,” *Mathematical and Physical Papers,* Vol IV, London, Cambridge University Press, 1910, pp 303-306.

69. Khandekar, M. L. (1989). “Operational analysis and prediction of ocean wind waves.” Coastal and Estuarine Studies, Springer-Verlag Press, New York, NY.

70. Khandekar, M .L., Lalbeharry , R., and Cardone, V. J. (1994). “The performance of the Canadian Spectral Ocean Wave Model (CSWOM) during the Grand Banks ERS-1 SAR wave spectra validation experiment.” 1. At.-Ocean. 32, (in press).

71. Kimura, A. 1980. “Statistical Properties of Random Wave Groups,” *Proc. 1th Coastal Engr. Conf.,* Vol 2, pp 2955-2973.

72. Kinsman, B. 1965. Wind Waves, Prentice-Hall, Englewood Cliffs, NJ.

73. Kitaigorodskii, S. A. 1962. “Application of the Theory of Similarity to the Analysis of Wind Generated Wave Motion as a Stochastic Process,” *Bull. Acad. Sci*., USSR Ser. Geophys., Vol 1, No.1, pp 105-117.

74. Kitaigorodoskii, S. A. et al. 1975. “On Phillips’ Theory of equilibrium Range in the Spectra of Wind-Generated Gravity Waves,” *Jour. Phys. Ocean.,* Vol 5, No. 3, pp 410-420.

75. Kitaigorodskii, S. A. 1983. “On the Theory of the Equilibrium Range in the Spectrum of Wind-Generated Gravity Waves,” *J. Phys. Oceanogr.,* Vol 13, pp 816-827.

76. Komen, G. J., S. Hasselmann and K. Hasselmann, 1984: On the existence of a fully developed windsea spectrum; J. Phys. Oceanogr. , 14, 1271-1285.

77. Komen, G. J., Cavaleri, L., Donelan, M., Hasselmann, K., Hasselmann, S. and Janssen, P.A.E.M. : 1994, Dynamics and Modelling of Ocean Waves, Cambridge University Press, 532 pp.

78. Lee, H.S. and Tanaka, H.: 2002, Prediction of water level in a river mouth using neural network approach, Proc. 13th IAHR-APD, 669-674.

79. Liong, S.Y., Lim, W.H., and Paudyal, G.N. : 2000, River stage forecasting in Bangladesh: Neural Network Approach, J. Comp. in Civ. Engrg., ASCE,8(2), 201-220.

80. Liu, P. C. 1971. “Normalized and Equilibrium Spectra of Wind-Wave in Lake Michigan,” Jour. Phys.Ocean., Vol 1 No. 4, pp 249-257.

81. Liu, P.-L. F. 1984. “Wave-Current Interactions on a Slowly Varying Topography,” Journal of Geophysical Research, Vol 88, pp 4421-4426.

82. Longuet-Higgins, M.S. 1952. “On the Statistical Distribution of the Wave Heights of Sea Waves,” Jour.Marine Res., Vol 11, pp 245-266.

83. Longuet-Higgins, M.S. 1962. “The Distribution of Intervals Between Zeros of Random Function,” Phil.Trans. Roy. Soc. London, Series A, Vol 254, pp 557-599.

84. Longuet-Higgins, M. S. 1984. “Statistical Properties of Wave Groups in a Random Sea State,” Phil. Trans.Roy. Soc. London, Series A, Vol 310, pp 219-250.

85. McCulloch, W. S. and Pitts, W. H. (1943). A logical calculus of the ideas immanent in nervous activity. Bulletin of Mathematical Biophysics, 5:115-133.

86. Miles, J. W. 1957. “On the Generation of Surface Waves by Shear Flows,” Journal of Fluid Mechanics, Vol3, pp185-204.

87. Mitsuyasu, H. (1968). “On the growth of the spectrum of wind-generated waves 1.” Rep. Res. Inst. Appl. Mech., Kyushu University, 16, 459-465.

88. Mitsuyasu, H. et al. 1975. “Observations of the Directional spectrum of Ocean Waves Using a Cloverleaf Buoy,” Jour. Phys. Ocean., Vol 5, pp 750-760.

89. Mitsuyasu, H. 1972. “The One-Dimensional Wave Spectra at Limited Fetch,” Proc. 13th Coastal Engr. Conf., Vol 1, pp 289-306.

90. Monbaliu, J., Padilla, R., Osuna, P., Flather, R., Hargreaves, J., Carretero, J.C., Espinar, S. and Gunther, H. : 1998, *WAM Shallow waters version 1.00, Code changes to WAM cycle 4.0 documentation*.

91. Myers, Raymond H. 1986. Classical and Modern Regression with Applications. Duxbery Press, Boston, Massachusetts, USA.

92. Nash, J.E. and Sutcliffee, J.V.(1970) River Flow Forecasting through Conceptual Models, *Journal of Hydrology*, Vol.10, pp.282-290.

93. Ochi, M. K. and Hubble, E. N. 1976. "Six Parameter Wave Spectra," *Proc. 15th Coastal Engr. Conf.*, Vol 1, pp 301-328.

94. Page, G.F., Gomm J.B. 1993, and Williams D. Application of Neural Networks to Modelling and Control. Chapman & Hall, London, UK.

95. Parzen, E. (1962). "On estimation of a probability density function and mode." Annals of Math. Statistics, 33, 1065 – 1076.

96. Patrick, Lynett. 2001. Coastal Engineering Manual 2001, Part II-Chapter2.

97. Phillips, O. M. (1957). "On the generation of waves by turbulent wind." J. Fluid Mech., 2, 417-445.

98. Phillips, O. M. 1958. "The Equilibrium Range in the Spectrum of Wind-Generated Waves," *Journal of Fluid Mechanic*s, Vol 4, pp 426-434.

99. Phillips, O. M. 1977. The Dynamics of the Upper Ocean, 2nd ed., Cambridge University Press.

100. Pierson, W. J. (1982). "The Spectral Ocean Wave Model (SWOM), a northern hemisphere computer model for specifying and forecasting ocean wave spectra." Final Report No. DlNSRDC-82/11, U. S. Naval Oceanography Command Detachment, Asheville, NC.

101. Pierson, W. J., and Moskowitz, L. 1964. "A Proposed Spectral Form for Fully Developed Wind Seas Based in the Similarity Theory of S. A. Kitiagorodskii," *J Geophys. Res.*, Vol 9, pp 5181-5190.

102. Pierson, W. J., Neuman, G., and James, R. W. 1955. "Observing and Forecasting Oceanwaves by Means of Wave Spectra and Statistics," U.S. Navy Hydrographic Office Pub. No. 60.

103. Resio, D. T. (1981). "The estimation of wind-wave generation in a discrete spectral model." J. Geophys. Res. ll, SlO-525.

104. Resio, D. T. (1993). ‘FuIl Boltzmann discrete spectral wave model, implementation and nondimensional tests.” ConrraCt Report CLXC-93-1 U.S. Army Engineer Waterways Experiment Station, Vicksburg, MS.

105. Resio, D. T., and Perrie, W. (1989). “Implications of an f -4 equilibrium range for wind-generated waves. ” J. Whys. Oceanogr. 19, 193-204.

106. Resio, D. T., and Perrie, W. (1991). “A numerical study of nonlinear energy fluxes due to wave-wave interactions - Part 1.” J. Fluid Mech. 223,603629.

107. Rice, S. O. 1944-1945. “Mathematical Analysis of Random Noise,” *Bell System Tech. Jour.*, Vol 23, pp 282-332.; Vol 24, pp 45-156.

108. Rumelhart D.E., Hinton G.E. andWilliams R.J., 1986 : *Learning internal representations by error propagation*, in Parallel Distributed Processing: Explorations in the Microstructures of Cognition, Vol.I, MIT Press, pp. 318–362

109. Ryan, Thomas P. 1997. Modern Regression Methods. New York: Wiley, USA.

110. Scott, J. R. 1965. “A Sea Spectrum for Model Tests and Long-Term Ship Prediction,” Jour. Ship Res., Vol 9, pp 145-152.

111. Smith, F. G. W., 1973: The Seas in Motion, Thomas Y. Crowell Co., New York, pp.248.

112. Snyder, R. L., and Cox, C. S. 1966. “A Field Study of the Wind Generation of Ocean Waves,” J. Mar. Res., Vol 24, p 141.

113. Snyder, R.L., F.W. Dobson, J.A. Elliott and R.B. Long: 1981, Array measurements of atmospheric pressure fluctuations above surface gravity waves. J. Fluid Mech. 102, 1-59.

114. Specht, D.F. : 1990, “Probabilistic neural network.” IEEE trans. Neural Networks, 3(1), 109-118.

115. Specht, D.F. : 1991, A general regression neural network, IEEE trans. Neural Networks, 2(6), 568-892.

116. St. Denis, M., and Pierson, W. J. 1953. “On the Motion of Ships in Confused Seas,” *Trans. SNAME*, Vol 61, pp 280-357.

117. Su, M.-Y. 1984. “Characteristics of Extreme Wave Groups,” *Oceans’84 Conf.*, Washington, DC.

118. Supharatid, S.: 2003, Tidal-level forecasting and filtering by neural network model, Coastal Engineering Journal 45(1), 119-138.

119. Sverdrup, H. U., and Munk, W. H. 1947. “Wind, Sea, and Swell: Theory of Relations for Forecasting.” Pub. No. 601, U.S. Navy Hydrographic Office, Washington, DC.

120. Tayfun, A. 1983a. “Effects of Spectrum Bandwidth on the Distribution of Wave Heights and Periods,” Intl. Jour. Ocean Engr., Vol 10, pp 107-118.

121. Tayfun, A. 1983b. “Nonlinear Effects on the Distribution of Crest-to-Trough Wave Heights,” Intl. Jour. Ocean Engr., Vol 10, pp 97-106.

122. The SWAMP Group (1985). “Sea wave modelling project (SWAMP). An intercomparison study of wind wave prediction models, Part 1: Principal results and conclusions.” Ocean Wave Modeling, Plenum Press.

123. Thirumalaiah,K. and Deo, M.: 1998, River stage forecasting using artificial neural networks, J. Hydrol. Engng 3(1), 26-32.

124. Thompson, E. F., and Cardone, V. J. 1996. “Practical Modeling of Hurricane Surface Wind Fields,” Journal of Waterway, Port, Coastal, and Ocean Engineering, Vol 122, No. 4, pp 195-205.

125. Thompson, E. F., and Vincent, C. L. 1985. “Significant wave Height for Shallow Water Design,” ASCE Jour. Waterw., Port, Coastal and *Ocean Engr.*, Vol 111, pp 828-842.

126. Toba, Y. (1973). “Local balance in the air-sea boundary processes, III. On the spectrum of wind waves.” J. Oceanogr. Sot. Japan 29, 209-220.

127. Tolman, H. L. (1989). “The numerical model WAVEWATCH: a third generation model for the hindcasting for wind waves on tides in shelf seas.” Communications on Hydraulic and Geotechnical Engineering, Delft Univ. of Techn. Rep. No. 89-2.

128. Tolman, H. L., 1990: Wind wave propagation in tidal seas. Doctoral Thesis, Delft Univ. Tech.

129. Tolman, H. L., 1994: Wind-waves and moveable-bed bottom-friction. J. Phys. Oceanogr., 24(5), 994.

130. Tsai, C.P. and Lee, T.L.: 1999, Back-propagation neural network in tidal-level forecasting, J. Wtrwy., Port, Coast., and Oc. Engrg., ASCE, 125(4), 195-202.

131. Tucker, M. J., et al. 1984. “Numerical Simulation of a Random Sea: A Common Error and Its Effect Upon Wave Group Statistics,” Jour. Applied Ocean Res., Vol 6, pp 118-122.

132. Vaziri, M. : 1997, Prediction of Caspian sea surface water level by ANN and ARIMA models, J. Wtrwy., Port, Coast., and Oc. Engrg., ASCE, 123 (4), 158-162.

133. WAMDI group : S. Hasselmann, K. Hasselmann, E. Bauer, P.A.E.M. Janssen, G.J. Komen, L. Bertotti, P. Lionello, A. Guillaume, V.C. Cardone, J.A. Greenwood, M. Reistad, L. Zambresky and J.A. Ewing : 1988, The WAM Model, A third generation ocean wave prediction model, *J.* Phys. Oceanogr. 18, 1775-1810.

134. Wittmann, P. A. (1992). “A comparison of GSWOM and global WAM predictions with buoy observations.” Models Department Technical Note 2-92, Fleet Numerical Oceanography Center, Monterey, CA.

135. Wittmann. P. A., and Clancy, R. M. (1991). “Predictions from the GSOWM during LEWEX.” Directional Ocean Wave Spectra, ed. R. C. Beal, Johns Hopkins University Press, 147-151.

136. WMO; 1995: Guide to Wave Analysis and Forecasting. Revised edition, draft for final reviews.

137. Zambresky. L. (1989). “A verification study of the global WAM model December 1987-November 1988.” ECMWT Tech. Rep. 63 European Centre for Medium-Range Weather Forecasting, Reading, England.

BIOGRAPHY

NAME	Mr. Wattana Kanbua
DATE OF BIRTH	25 April 1965
PLACE OF BIRTH	Pathumthani, Thailand
INSTITUTIONS ATTENDED	Ramkamhaeng University, 1984-1988: Bachelor of Science (Mathematics) Mahidol University, 1991-1994: Master of Science (Applied Mathematics) Mahidol University, 2001-2004: Doctor of Philosophy (Mathematics)
FELLOWSHIP / RREASEARCH GRANTS	The Royal Golden Jubilee Ph.D. Program scholarship from the Thailand Research Fund. (2001-2004)